



## Master Thesis

# CFD Simulation of Cold Spray Nozzle Optimization and Reduction of Clogging Effect

Supervised by: Prof. Dr.-Ing. Erwin Buerk

Co-supervised by: Braun Thomas, M.Sc

Submitted on: 30-04-2022

Submitted by:  
Dinesh Poluru Baskar  
smart systems  
264374  
Hochschule Furtwangen



## **Abstract**

Cold spray (CS) is a solid-state method that deposits spray particles via supersonic velocity impact at temperatures well below the spray material's melting point. This work aims in developing a suitable thermodynamic model and implementing the model in Ansys Fluent to generate a physically feasible simulation result and also to develop a particle simulation using ESSS Rocky in the interest of studying the particle properties by coupling with flow simulation. This thesis work provides a detailed study of geometry, meshing, simulation setup, and also recommendations for choosing the best physical models and boundary conditions that will aid in the simulation setup. A numerical simulation has been performed and compared with KSS (Kinetic Spray Solutions) to prove the existence of shock diamonds for a particular geometry and the creation of bow shock near the surface. The simulation setup provided in this thesis work generated a 0.8% error when compared with the numerical solution and showed improved flow properties compared to KSS. In addition, particle simulation has been made with the help of ESSS Rocky software in the interest of studying the properties of a particle at the substrate region and diverging section of the nozzle in the presence of fluid. The simulation results prove that the particle reaches a maximum velocity of 536 m/s near the substrate, exceeding the critical velocity of the copper particle of 328 m/s. Furthermore, future recommendations for two-way simulation have been provided in the interest of studying the clogging effect that occurs inside the nozzle.



## Zusammenfassung

Kaltgasspritzen (CS) ist eine Festkörpermethode, bei der Spritzpartikel durch Aufprall mit Überschallgeschwindigkeit bei Temperaturen weit unterhalb des Schmelzpunkts des Spritzmaterials abgeschieden werden. Diese Arbeit zielt darauf ab, ein geeignetes thermodynamisches Modell zu entwickeln und das Modell in Ansys Fluent zu implementieren, um ein physikalisch machbares Simulationsergebnis zu erzeugen. Außerdem soll eine Partikelsimulation mit ESSS Rocky entwickelt werden, um die Partikeleigenschaften durch Kopplung mit der Strömungssimulation zu untersuchen. Diese Arbeit bietet eine detaillierte Untersuchung der Geometrie, der Vernetzung und des Simulationsaufbaus sowie Empfehlungen für die Auswahl der besten physikalischen Modelle und Randbedingungen, die für den Simulationsaufbau hilfreich sind. Es wurde eine numerische Simulation durchgeführt und mit KSS (Kinetic Spray Solutions) verglichen, um die Existenz von Schockdiamanten für eine bestimmte Geometrie und die Entstehung von Bugschocks nahe der Oberfläche nachzuweisen. Der in dieser Arbeit verwendete Simulationsaufbau erzeugte im Vergleich zur numerischen Lösung einen Fehler von 0,8% und zeigte im Vergleich zu KSS verbesserte Strömungseigenschaften. Darüber hinaus wurde eine Partikelsimulation mit Hilfe der Software ESSS Rocky durchgeführt, um die Eigenschaften eines Partikels im Substratbereich und im divergierenden Abschnitt der Düse in Gegenwart von Flüssigkeit zu untersuchen. Die Simulationsergebnisse zeigen, dass das Teilchen in der Nähe des Substrats eine maximale Geschwindigkeit von  $536 \text{ m/s}$  erreicht und damit die kritische Geschwindigkeit des Kupferteilchens von  $328 \text{ m/s}$  überschreitet. Darüber hinaus wurden Empfehlungen für künftige Zwei-Wege-Simulationen gegeben, um den Verstopfungseffekt im Inneren der Düse zu untersuchen.



## **Acknowledgment**

One of the most rewarding experiences I had while working on this project was the ability to engage and communicate with a broad group of multi-talented people.

Firstly, I would like to express my sincere gratitude to Braun Thomas, M.Sc and Dr.-Ing. Christian Schmiedel whose constant support and encouragement from the day one motivated to focus on my work. This work would not be possible without their continuous guidance and sharing of their immense knowledge which shaped the direction of this work. I would also be thankful to Dr. Jan-Philipp Fürstenau and Sami Yabroudi for sharing their knowledge of simulation that helped me to identify my mistakes which paved a way for this report.

I am extremely thankful to Prof. Dr.-Ing. Erwin Buerk who graciously accepted to be my co-supervisor for this work. His immense knowledge in fluid mechanics and thermodynamics helped me in every situation to overcome the mistakes from the work. His constant support throughout the thesis work helped me to possess confident that could reflect in my work.

I am greatly indebted to my friends Yuvan, Noel, Krishna and Venkat who never failed to support and inspire me to fulfil my dreams. Without their constant encouragement this work would not be possible.

My unconditional love and support goes to my family. My family is the backbone of all of my work and their unconditional support and selfless deeds inspire me to pursue my dreams. My journey would not have been possible without them, and I dedicate this achievement to them.



## **Affidavit**

I hereby declare that this Master thesis work titles "CFD Simulation of Cold Spray Nozzle Optimization and Reduction of Clogging Effect" is the result of my own independent work. This work has been carried out without any outside help whatsoever. No other sources or materials other than cited in reference section was used.

I understand that violations of this policy may result in a grade of "Insufficient/Fail" (5.0) on my submitted work, and in more extreme situations, further disciplinary action by Hochschule Furtwangen, including possible expulsion from the university.

In addition, I confirm that this thesis has not yet been presented as part of another examination process or elsewhere else, in either identical or similar form.

---

Place, Date

---

Signature



# Contents

<b>Abstract</b>	<b>i</b>
<b>Zusammenfassung</b>	<b>ii</b>
<b>Acknowledgment</b>	<b>iii</b>
<b>Affidavit</b>	<b>iv</b>
<b>List of Figures</b>	<b>ix</b>
<b>List of Tables</b>	<b>x</b>
<b>Nomenclature</b>	<b>xiii</b>
<b>Acronyms</b>	<b>xiv</b>
<b>1 Introduction</b>	<b>1</b>
1.1 Motivation . . . . .	1
1.2 Problem statement . . . . .	2
1.3 Thesis structure . . . . .	3
<b>2 Theoretical background</b>	<b>4</b>
2.1 Cold spray fundamentals . . . . .	4
2.1.1 Advantages and limitations . . . . .	5
2.1.2 Bonding mechanism . . . . .	6
2.2 de Laval nozzle . . . . .	7
2.2.1 Equations involved . . . . .	7
2.2.1.1 Reynolds number . . . . .	8
2.2.1.2 Speed of sound . . . . .	8
2.2.1.3 Mach number . . . . .	9
2.2.1.4 Choked flow condition . . . . .	9
2.2.1.5 Thrust equations . . . . .	9
2.2.2 Pressure shock waves . . . . .	10
2.3 Governing equations . . . . .	12
2.3.1 The continuity equation . . . . .	15
2.3.2 The momentum equation . . . . .	15
2.3.3 The energy equation . . . . .	18
2.4 Ansys Fluent . . . . .	20
2.4.1 Solvers . . . . .	20

2.4.2	Meshing attributes . . . . .	22
2.4.2.1	Size functions . . . . .	22
2.4.2.2	Types of meshes . . . . .	23
2.4.2.3	Mesh metrics . . . . .	24
2.4.3	Turbulence modeling . . . . .	25
2.4.3.1	$K - \varepsilon$ turbulence model . . . . .	27
2.4.3.2	$K - \omega$ SST turbulence Model . . . . .	28
2.4.3.3	Choosing the appropriate model . . . . .	30
2.4.4	Cell zone and boundary condition . . . . .	30
2.4.4.1	Choosing between real gas Vs ideal gas . . . . .	31
2.4.4.2	Boundary conditions . . . . .	32
2.4.5	Inflation layer . . . . .	33
2.4.6	Gradients . . . . .	35
2.4.6.1	Green–Gauss method . . . . .	36
2.4.6.2	Least–squares . . . . .	38
2.4.6.3	Choosing the appropriate gradient method . . . . .	40
2.4.7	Residuals . . . . .	40
2.5	ESSS Rocky DEM . . . . .	43
2.5.1	Governing equations . . . . .	44
2.5.1.1	Particle phase modeling . . . . .	44
2.5.1.2	Fluid modeling . . . . .	45
2.5.2	One–way coupling . . . . .	45
2.5.3	Simulation parameters . . . . .	46
2.5.3.1	Physics parameter . . . . .	46
2.5.3.2	Geometry parameter . . . . .	46
2.5.3.3	Particle parameter . . . . .	46
2.5.3.4	Particle input . . . . .	47
2.5.3.5	Solver parameter . . . . .	47
<b>3</b>	<b>Methodology</b>	<b>48</b>
3.1	Ansys Fluent . . . . .	48
3.1.1	Numerical approach . . . . .	48
3.1.2	Simulation approach . . . . .	50
3.1.2.1	Geometry Creation . . . . .	50
3.1.2.2	Meshing attributes . . . . .	52
3.1.2.3	Simulation setup . . . . .	54
3.2	ESSS Rocky . . . . .	59
3.2.1	Numerical approach . . . . .	59
3.2.2	Simulation approach . . . . .	60

3.2.2.1	Geometry creation . . . . .	60
3.2.2.2	Simulation setup . . . . .	60
<b>4 Results and discussion</b>		<b>67</b>
4.1 Ansys Fluent . . . . .		67
4.1.1 Final solution . . . . .		67
4.1.1.1 Contour result . . . . .		67
4.1.1.2 Numerical Vs simulation results . . . . .		72
4.1.1.3 Plotting solution graphs . . . . .		72
4.1.1.4 Ansys Fluent Vs KSS (Kinetic Spray Solutions) . . . . .		73
4.1.2 List of model comparisons . . . . .		75
4.1.3 Final discussion . . . . .		80
4.2 ESSS Rocky . . . . .		81
4.2.1 180-degree far-field simulation . . . . .		82
4.2.2 360-degree without far-field . . . . .		86
4.2.3 Final discussion . . . . .		89
4.2.4 Comparison between the simulation results . . . . .		90
4.3 Scientific answers . . . . .		92
<b>5 Conclusion</b>		<b>95</b>
5.1 Recommendations for future contribution . . . . .		95
<b>References</b>		<b>98</b>

# List of Figures

2.1	Schematic of cold spray [6] . . . . .	4
2.2	Cold spray working parameters [22] . . . . .	5
2.3	A detailed view of particle bonding on to the substrate [3] . . . . .	6
2.4	Propagation of a small pressure wave along a duct [8] . . . . .	8
2.5	Effect of backpressure in CD nozzle [8] . . . . .	11
2.6	Road map of CFD [2] . . . . .	13
2.7	Finite control volume fixed in space and moving with the fluid such that the same fluid particles are always in the same control volume [2] . . . . .	13
2.8	Illustration of substantial derivative [2] . . . . .	14
2.9	Model for momentum equation [2] . . . . .	16
2.10	Skewness of a cell [14] . . . . .	25
2.11	Turbulent velocity profile [21] . . . . .	26
2.12	Illustration of $K - \varepsilon$ & $K - \omega$ models . . . . .	28
2.13	Representation of blending function . . . . .	29
2.14	Representation of pressure inlet dialogue box . . . . .	32
2.15	Representation of boundary layer thickness [27] . . . . .	34
2.16	Representation of 1-D gradient calculation . . . . .	36
2.17	Representation of gradient face value . . . . .	36
2.18	Representation of a 3-D cell . . . . .	37
2.19	Representation of cell centroid distance . . . . .	39
3.1	Nozzle dimension . . . . .	51
3.2	Different views of nozzle . . . . .	51
3.3	Front & far-field dimensions . . . . .	51
3.4	360-degree & 90-degree models . . . . .	52
3.5	Meshing tabs . . . . .	53
3.6	Skewness & total number of cells . . . . .	54
3.7	Different views of mesh . . . . .	55
3.8	Representation of solver & model tabs . . . . .	55
3.9	Material dialogue box . . . . .	56
3.10	Inlet & outlet boundary conditions . . . . .	57
3.11	Operating condition . . . . .	57
3.12	Solution monitors . . . . .	58
3.13	Number of iterations . . . . .	59
3.14	Dimension & different views of nozzle with far-field . . . . .	61
3.15	180-degree with far-field (left) & 360-degree (right) . . . . .	61
3.16	Physics setup for 180-degree (top two images); 360-degree (bottom two images) . . . . .	62
3.17	Inlet coordinates . . . . .	62

3.18	Representation of copper material properties . . . . .	63
3.19	Particles dialogue box . . . . .	63
3.20	Input dialogue box . . . . .	64
3.21	One-way coupling dialogue box . . . . .	65
3.22	Solver dialogue box . . . . .	65
4.1	Representation of residuals and convergence . . . . .	67
4.2	Solution contours . . . . .	68
4.3	Representation of shock wave structure . . . . .	68
4.4	Flow separation . . . . .	69
4.5	Pressure contour representing the over-expanded flow . . . . .	70
4.6	Depicts the particle pathline to illustrate the shock-diamond properties . . . . .	70
4.7	Representation of bow-shock . . . . .	71
4.8	Representation of vectors . . . . .	72
4.9	Representation of graph line that was created to obtain respective plots . . . . .	73
4.10	Representation of pressure(a); temperature(b); velocity(c) plot . . . . .	73
4.11	Pressure plot . . . . .	74
4.12	Temperature plot . . . . .	74
4.13	Velocity plot . . . . .	75
4.14	Density Vs Pressure based . . . . .	76
4.15	Steady-state Vs Transient plot . . . . .	77
4.16	Turbulence models Vs $K - \omega$ SST . . . . .	78
4.17	Real Vs Ideal gas . . . . .	79
4.18	Implicit Vs Explicit . . . . .	80
4.19	Mesh metrics . . . . .	82
4.20	Steady-state simulation contours . . . . .	83
4.21	Type-1 of 180-degree far-field geometry . . . . .	84
4.22	Type-2 of 180-degree far-field geometry . . . . .	84
4.23	Type-3 of 180-degree far-field geometry . . . . .	85
4.24	Mesh Metrics nozzle-only . . . . .	86
4.25	Steady-state simulation contours of 360-nozzle . . . . .	87
4.26	Type-1 of 360-degree nozzle without far-field . . . . .	88
4.27	Type-2 of 360-degree nozzle without far-field . . . . .	89
4.28	Window of deposition by KSS . . . . .	91

## List of Tables

1	Numerical values for throat and exit condition . . . . .	50
2	Numerical & simulation results with percentage error . . . . .	72
3	Comparison between KSS and Rocky generated solutions . . . . .	90
4	Window of deposition comparison . . . . .	91

## Nomenclature

$S_k$ & $S_\omega$	User-defined source terms
$(\nabla T)_P$	Temperature gradient
$\alpha^*$	Turbulent viscosity damping by low-Reynolds number correction
$\omega_p$	Angular velocity vector
$d_{PN}$	Distance between two nodes on the face cell
$G$	Matrix vector
$\Delta t$	Time step
$\Delta x$	Length interval
$\delta_{99}$	Boundary layer thickness achieving 99% of free-stream velocity
$\dot{q}$	Heat flux ( $W/m^2$ )
$\dot{q}_c$	Heat transfer during contact with other particles or walls
$\dot{q}_{f \rightarrow p}$	Convective heat transfer between particle and fluid phase
$\varepsilon$	rate of dissipation
$\gamma$	specific heat ratio
$\hat{n}$	Normal vector
$J_p$	Moment of inertia tensor
$\mathbf{F}_c$	contact force that accounts for particle-particle and particle-wall interactions
$\mathbf{F}_{f \rightarrow p}$	Additional Force due to interactions with fluid phase
$\mathbf{M}_c$	Net torque
$\mathbf{M}_{f \rightarrow p}$	Additional torque due to fluid phase
$\mu$	Dynamic viscosity ( $Kg/m.s$ )
$\mu_t$	The turbulent (or eddy) viscosity
$\rho$	Density of fluid ( $Kg/m^3$ )
$\tilde{G}_k$	Generation of turbulence kinetic energy due to mean velocity gradients

$A$	Area ( $mm^2$ )
$A$	Thermal conductivity areas & distance
$A$	Total energy
$a$	Constants
$A_f$	Area of the face of particular cell
$B$	Heat source term
$c$	Speed of sound
$C_{1\epsilon}, C_{2\epsilon}, C_{3\epsilon}$	Constants
$c_p$	Specific heat
$d$	Distance between two cell centroid
$D_\omega$	Cross-diffusion term
$e$	internal energy
$F_1, F_2$	Blending functions
$G$	Growth ratio
$g$	Gravitational acceleration vector
$G_\omega$	Generation of $\omega$
$G_k$	Turbulent kinetic energy due to mean velocity gradient
$k$	Turbulent kinetic energy
$L$	Characteristic length ( $m$ )
$m$	mass of a substance ( $Kg$ )
$m_p$	Particle mass
$Ma$	Mach number
$N$	Number of layers
$n$	Number of moles of the gas
$P_t$	Total pressure (bar)

$P_0$	Stagnation pressure (bar)
$P_b$	Back pressure (or) Atmospheric pressure (bar)
$R$	Gas constant ( $J/Kg.K$ )
$r$	Residual vector
$Re$	Reynolds number
$S$	Strain rate magnitude
$S_\varepsilon$ & $S_k$	User-defined source terms
$T$	Absolute temperature ( $K$ )
$T_t$	Total temperature ( $K$ )
$T_f$	Face temperature
$T_N$	Neighboring node temperature
$u$	Velocity of fluid ( $m/s$ )
$V$	Volume
$V^2/2$	Kinetic energy
$w$	Weighted function
$y$	distance to the next surface
$y^+$	Non-dimensional total distance from the wall
$Y_k$ & $Y_\omega$	Dissipation of $k$ & $\omega$ due to turbulence
$y_H$	First layer height
$Y_M$	fluctuating dilatation
$y_p$	Centroid distance of $y_H$ from surface
$\Gamma_k$ & $\Gamma_\omega$	Effective diffusivity of $k$ & $\omega$
$f$	Force ( $N$ )
$V$	Velocity component of the body ( $m/s$ )
$\sigma_\omega, \sigma_K$	Turbulent Prandtl numbers for $k$ and $\omega$

## Acronyms

- AM* Additive Manufacturing. 1
- ASI* Adiabatic Shear Instability. 5, 6
- BL* Boundary Layer. 8
- CAD* Computer-Aided Design. 3
- CD* Convergent-Divergent. 4, 5, 9
- CFD* Computational Fluid Dynamics. 1, 12, 22, 23, 33, 35, 36, 38, 40–43, 45–47, 50, 65, 72, 73, 80, 82, 85, 89, 95
- CFL* Courant-Friedrichs-Lowy. 21, 22
- CGDS* Cold Gas-Dynamic Spray. 4
- CS* Cold Spray. 1, 3–7, 12, 32, 33, 40, 45–47, 49, 56, 57, 60, 62–64, 67, 71–73, 75, 77, 80, 81, 85, 93
- DBS* Density-Based Solver. 21
- DEM* Discrete Element Method. 43–46
- DPM* Discrete Phase Model. 60
- KSS* Kinetic Spray Solutions. 1, 50, 73–75, 90–92, 95
- LES* Large Eddy Simulation. 78
- PBS* Pressure-Based Solver. 20
- RANS* Reynolds-averaged Navier-Stokes equations. 27
- RNG* Re-Normalisation Group. 26
- SST* Shear Stress Transport. 29
- TBZ* Thermal Boost-up Zone. 6
- TS* Thermal Spray. 4

# **1 Introduction**

In the world of engineering, material coating is one of the important processing techniques used in many industries. Almost every product that leaves the factory has a coating applied to it to protect it from damage and to improve qualities such as heat conductivity and electrical conductivity. These coating processes may differ in coating temperatures, cost, method of coating, and thickness of the coating. This report postulates a new method of coating technology that was developed in recent years known as Cold Spray (CS) technology. The cold spray process is a matured and new invention in the field of Additive Manufacturing (AM). For most metals and metal composites, the thickness of a cold spray coating is practically limitless; as a result, the cold spray has been effectively used in additive manufacturing technologies to create individual components and repair damage. This advancement sheds fresh light on traditional additive manufacturing technologies and considerably expands the cold spray application domains[7]. In the family of additive manufacturing, the cold spray has a dominant potential to fabricate components with rotational structures, e.g., cylinder walls and flanges. Computational Fluid Dynamics (*CFD*) is a branch of fluid mechanics used to study and understand the behavior of fluids (gases and liquids) using numerical solution methods. *CFD* aids in the analysis of complex fluid-fluid, fluid-solid, and fluid-gas interactions. This works based on the Navier-Stokes equation which is a non-linear equation that explains the nature of fluids in the universe. The *CFD* has been rendering our day-to-day life since 1970 and helps engineering to move faster than the speed of sound, build better dams and reservoirs, and to help prevent natural calamities.

## **1.1 Motivation**

Cold spray technology is an emerging invention that finds its place in important sectors such as aerospace, automotive, transportation, die casting, petrochemical plants, minerals and metal processing, electronics, marine, ceramics, and glass manufacturing. Cold spray is a solid-state process that involves supersonic-velocity collision with the substrate at temperatures well below the sprayed material's melting point [7]. This gives an advantage of depositing temperature-sensitive and oxygen-sensitive material over the substrate. The nozzle is the most crucial aspect of cold spray since it is where all of the physics happens. Because cold spray uses supersonic flows, the design of the nozzle determines particle flow as well as particle adhesion to the substrate. The ability of materials to bond to the substrate is determined by whether or not the particles reach a critical velocity. The nozzle's converging and diverging sections give enough room for pressure, temperature, and velocity to fluctuate, allowing the particles to accelerate to their desired exceeding critical velocity. Since its discovery, CS has undergone much development; current CS technology is utilized in an expanding range of industries for many applica-

tions, mainly in surface restorations, as well as the wear-resistant and corrosion-resistant repair of metals and alloys [7]. This development gives a promising, yet efficient way to produce protective coatings, performance-enhancing layers, ultra-thick and thin coatings, and net near shapes. Despite the fact that much research has been done in the past to improve the cold spray qualities, it remains one of the important invention in additive manufacturing. However, various enhancements are still needed to realize the process's full potential, as there are numerous design and physical characteristics that degrade the process's quality.

## 1.2 Problem statement

Since the time of its invention, a profound amount of studies and research has been conducted on Cold spray for constant improvement of the technology. In the earlier works, McCune et al. [25] and Dykhuizen and Smith [11] used a one-dimensional isentropic flow model and deduced that the spray particle velocity is a function of gas properties, particle material density, and size. As far as these parameters are considered to be important for the particles to gain critical velocity, Alkhimov et al. [1] showed that a nozzle with a particular dimension for a given type of particle produces the maximum possible velocity. But some complex parameters such as shock formation at the exit of nozzle geometry, and bow shock near the substrate could not be analyzed with the one-dimensional model. To give it more context, Tien-Chien Jen et al. [19] observed shock diamonds using a numerical simulation and determined that bow shocks near the substrate prevent smaller particles from entering, resulting in the poor coating. It was found that the gas type, operating pressure, and temperature have a significant effect on particle velocity. The nozzle geometry, expansion ratio, and length of the nozzle showed a significant effect on particle velocity [19]. In the earlier works, Tien-Chien Jen et al. [19] make use of the RNG  $K - \epsilon$  model which was proposed by Yakhot and Orszag [30] to model the turbulence flow nature. With the necessity to reduce the computational cost and to increase efficiency, different types of turbulence models need to be compared. In the interest of improving the deposition efficiency, Masahiro Fukumoto et al. [15] modeled an optimization of nozzle design with the help of numerical simulation. The simulation process consists of air as the carrier gas, operating at 1-3 MPa which is heated up to 573 K, and concluded that a special type of nozzle is needed to reduce the bow shock produced near the substrate, as a result, the velocity of the particles is reduced. To provide more context, Chang-Jiu et al.[23] elevated the simulation by studying the deposition pattern using the titanium particles which were accelerated with nitrogen and helium at 1-2 MPa, 100-300 °C in the chamber. These simulation models are considered to be relatively running at low pressure and temperature, which produces reduced critical velocity of the particles. The goal of this research work is summarized as presenting an efficient and accurate simulation model and providing a comparison of available turbulence models using ANSYS Fluent, developing a particle simulation using ESSS Rocky, and coupling with the flow simulation, that provides a valid basis for further modeling of the clogging effect. Addi-

tionally, results are compared with the existent model to conclude an efficient discussion of the problem. To provide a strong basis for flow and particle simulation the below steps are followed:

- Creating and implementing a *CAD* geometry with Ansys Fluent to proceed with the fluid flow simulation.
- Optimizing the *CAD* geometry to provide comparisons between the turbulence model.
- Generation of different sizes of particles using ESSS Rocky and coupling with the Ansys Fluent.

With the focus on fulfilling the goal of the thesis work, visioned scientific questions have to be formed to acknowledge the research work and to believe in the enhancement of the technology. A detailed discussion about the purpose of these questions and how they are interlinked to provide basis for further modeling is explained in chapter 4.

- How does the shock wave produced in the nozzle affect the particle behavior?
- Does the particle ever reach critical velocity?
- What is clogging effect and where exactly the clogging will appear in the nozzle and what are the causes and effects?

### 1.3 Thesis structure

The thesis is structured has:

Chapter 2 discusses the theoretical background of cold spray technology history, general process, advantages and limitations, and bonding mechanism of CS. It also discusses the equations involved in the simulation process. In addition to this, comprehensive knowledge about the ANSYS Fluent and ESSS Rocky software is discussed.

Chapter 3 discuss the methodology involved in the creation of geometry, meshing attributes, boundary condition, and particle creation in the simulation.

Chapter 4 discuss the results obtained from the simulation, furthermore with a comparison of all the available turbulent model results with the existing solution.



## 2 Theoretical background

Theoretical background about a subject always proffers a predominant knowledge and a vision of insight, which can be utilized to alter future research concepts. Profound concepts and details about the CS technology, simulation processes, and the underlying equations are discussed in this chapter.

### 2.1 Cold spray fundamentals

The invention of Cold Gas-Dynamic Spray (*CGDS*) dates back to the 20th century in the mid-1980s when it was invented and patented by Dr. Anatolii Papyrin and his colleagues at the Institute of Theoretical and Applied Mechanics at Novosibirsk, Russia. While the researchers were conducting experiments in the wind tunnel, they observed that under special conditions, particles were accelerated and deposited onto the substrate. [7] The cold spray is a sub-kind of thermal spray (*TS*) technology in which the particles in *CS* are accelerated at supersonic velocity to impact the substrate to adhere to the surface. The name *CS* infers that the whole process is maintained under a limited temperature condition for better adhesion of particles to the substrate. Because of this great advantage, *CS* can be used to spray much finer particles in the range of 1-50  $\mu\text{m}$ , including nanoparticles.

The *CS* process setup consists of a high-pressure gas chamber, gas heater, powder feeder, and a converging-diverging (*CD*) de Laval nozzle. The *CD* nozzle is designed to accelerate the particles at supersonic velocity by maintaining a Mach value greater than 1 at the exit of the nozzle. Nitrogen or helium are used as carrier gas because of their inert nature and do not react with the particles while accelerated through the nozzle. Based on their application and range of coating, powder feeders can be arranged as a radial injection or axial injection. Figure 2.1 shows the schematic of the cold spray.

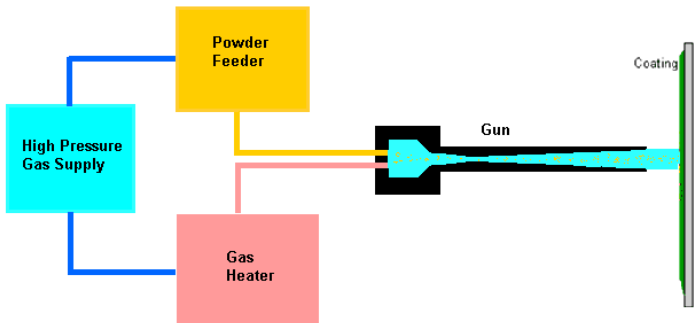


Figure 2.1: Schematic of cold spray [6]

Firstly, the high-pressure gas supply stores the nitrogen or helium reaching up to 50 bars. This gas can be passed in two ways, the first way permits the gas to pass through the powder feeder,

where the gas is mixed with the particles and accelerated through the *CD* nozzle. The second path, which consists of an electric heater helps to preheat the gas to temperatures of about 100-1100 °C [24]. As the temperature rises, the gas velocity rises as well, increasing particle velocity. The carrier gas and particle travel at supersonic speeds through the *CD* nozzle before impacting the substrate. Due to the supersonic velocity of the particles, they tend to impact the substrate to bond consequently by the process known as Adiabatic Shear Instability (*ASI*). In spite of the fact that the inlet gas is preheated to high temperatures, the particles remain unaffected and the temperature is further reduced when the gas and particle pass through the diverging section of the nozzle [7].

### 2.1.1 Advantages and limitations

The major difference between *CS* and other thermal spray processes is that the *CS* can operate at relatively low temperature and high particle velocity without compromising the properties of particles as well as the substrate. Thermal spray, as the name implies, causes particles to melt inside the nozzle, causing them to adhere to the nozzle's walls, lowering efficiency to a certain point. Furthermore, because the feed-stock powder is neither heated nor melted during the coating process, it can be reused in subsequent cycles [10]. On account of operating the thermal spray under high temperature, particles tend to react with the surrounding gas giving rise to chemical reactions inside the nozzle. These chemical reactions tend to break the particles apart even before they come out of the nozzle. Because of the blistering heat of the gas, some particles are prone to phase change. Another benefit is the ability to coat substrates with a thickness of less than 1 mm without causing damage to the substrate. Furthermore, because coatings are created with compressive pressures, the technique can produce well-bonded thick coatings or layered coatings [10].

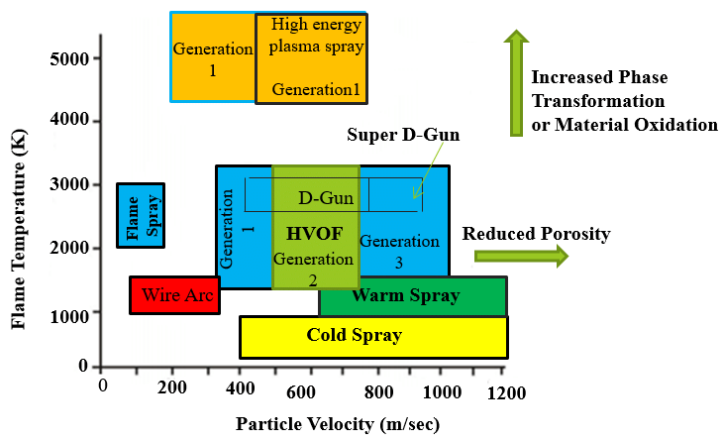


Figure 2.2: Cold spray working parameters [22]

The above picture is an illustration of the working conditions of *CS* and thermal spray processes. The *CS* tends to work under the low-temperature condition with a high velocity of particles

which leads to reduced porosity of the particles at the substrate. There is a high chance of phase transformation of material oxidation with the thermal process.

Despite being the most preferable way for coating with all the advantages, the *CS* does have limitations. The main disadvantage is the blockage of the nozzle at the throat during prolonged spraying processes. This can be reduced by providing a cooling system outside the nozzle but this cannot be eradicated because the nozzle is designed in a way to maintain sonic condition at the throat. While *CS* can work with a variety of different feed-stocks and substrates, it is limited to ductile metal powders or hard metals mixed with ductile metals; it cannot deposit hard single-species particles like ceramics [17]. This is because the particles must undergo plastic deformation when impacting the substrate which helps to adhere to the surface. Furthermore, in comparison to thermal spray methods, processing gas consumption is significant, often in the range of  $1\text{--}2 \text{ m}^3/\text{min}$  [16].

### 2.1.2 Bonding mechanism

Many studies have been conducted to better understand the bonding mechanism in *CS*, yet it appears to be the most misunderstood notion. Many researchers came up with their ideology about the concept until the latest study of adiabatic shear instability (*ASI*) made by Assadi et al. [3]. During impact, the particle-particle or particle–substrate interfacial zones undergo significant localized shear deformation, disrupting the thin oxide surface layers on the particles and allowing for intense particle–substrate contact. This process, along with the strong compressive stresses created when particles collide with the substrate, makes bonding possible.

Another study made by Bae et. Al [4] reveals the existence of a thermal boost-up zone (*TBZ*). This zone occurs at a small distance before the particles tend to impact. This region is also called a bow-shock zone, where the rise in temperature and pressure occurs rapidly resulting in reducing the efficiency. However, another study made by the same authors (Bae et. Al [4]) presumed that *TBZ* is not needed for successful bonding rather *ASI* plays a major role in the bonding mechanism for *CS*.

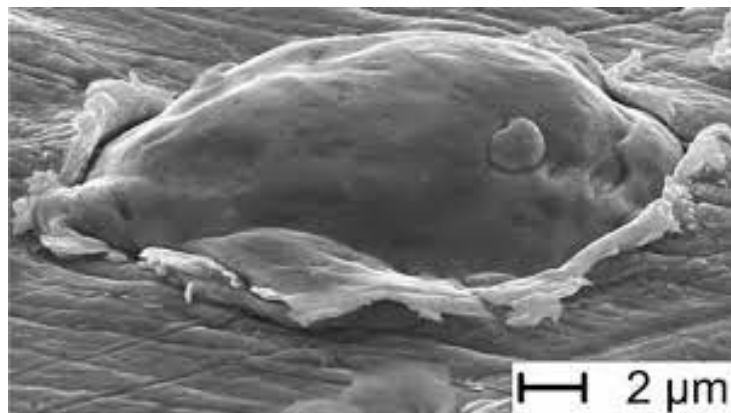


Figure 2.3: A detailed view of particle bonding on to the substrate [3]

The above picture represents the copper particle impacted on the substrate. Assadi et. Al [3] studies demonstrated that 80% of impacting particles adhere to the surface. The particles which are impacted onto the surface forms a ring of a jet-type morphology around the impact zone. Some particles tend to leave a crater on the substrate provided with non-bonding of the particle.

## 2.2 de Laval nozzle

The de Laval nozzle contributes a major aspect of the *CS* process. As the name implies the nozzle consists of three important geometry namely, the convergent section where the flow is subsonic, the throat section where the flow is relatively in sonic condition, and the divergent section where the flow is supersonic. The de Laval nozzle is also known as the convergent-divergent nozzle and was coined by Karl Gustaf Patrik de Laval in the year 1890. Laval developed a nozzle that boosts the speed of the steam jet to supersonic levels by utilizing the kinetic energy of the steam rather than its pressure. This breakthrough opened the door to a slew of new possibilities, most notably in the aerospace and aviation industries.

The behavior of fluid can be extensively classified as compressible and incompressible flows. A compressible fluid experiences a density change while the incompressible fluid does not experience such a change. Flows with a low Mach number, less than 0.3 are treated as incompressible, whereas the rest are considered compressible. When compared to incompressible flows, the compressible flows equation requires the solution of extra equations for density and temperature changes to compensate for the problem's complexity.

Nozzle geometry can be widely classified into two main shapes, conical and parabolic. A conical nozzle features a downward tapering linear input area that decreases in cross-sectional area along with the profile until the throat diameter is achieved, and then an upward tapering linear outlet area that increases in cross-sectional area along with the profile until the throat diameter is reached. A parabolic nozzle has a converging circular segment and a diverging parabolic part [5]. The nozzle that is used in the *CS* application is a combination of conical and parabolic geometry.

### 2.2.1 Equations involved

A considerable portion of the thermal energy of the gases in the chamber is transformed into kinetic energy in a converging-diverging nozzle. To maintain balance, the pressure drops at the throat (area decreases) and then gradually increases (area increases), causing the gas to return to its former state. This process is reversible, and reversible processes have constant entropy, according to the second rule of thermodynamics. The isentropic process is defined as a constant entropy across the nozzle. This requirement is built into every nozzle for important applications, and a set of formulae must be followed.

### 2.2.1.1 Reynolds number

The Reynolds number (Re) helps to predict different flow patterns in inflow regions. The low Reynolds number indicates that the flow is laminar and the high Reynolds number indicates the flow is turbulent. It is the ratio of inertial forces to viscous forces within a fluid which is subjected to relative internal movement due to different fluid velocities. The fluid particles tend to change their fluid behavior to turbulent near the wall region. This region is known as the boundary layer (*BL*). The boundary layer is an imaginary layer of the field near the wall where the fluid velocity becomes zero due to the friction and shear forces acting on the fluid particle from the boundary and the neighboring particles. Detailed information about the boundary layer is discussed later in this report. Reynolds number is represented as:

$$Re = \frac{\rho u L}{\mu} \quad (1)$$

### 2.2.1.2 Speed of sound

Fluid velocities are often described in terms of speed of sound and Mach number. Once the type of fluid is worked out, the fluid velocities can be measured using the Mach number. The speed at which an infinitesimally small pressure wave travels through a medium is known as the speed of sound (or sonic speed). A tiny disturbance that causes a slight rise in local pressure could be the cause of the pressure wave [8]. This can be visualized by imagining a control volume filled with fluid is provided with a piston that moves to the right. The piston tends to move by creating a sonic wave in the direction of movement. This wavefront moves in the direction of the piston with a velocity equal to the speed of sound and tends to create two regions of interest between the control volume. The thermodynamic characteristics of the fluid to the left of the wavefront change incrementally, while the thermodynamic properties of the fluid to the right of the wavefront remain the same [8].

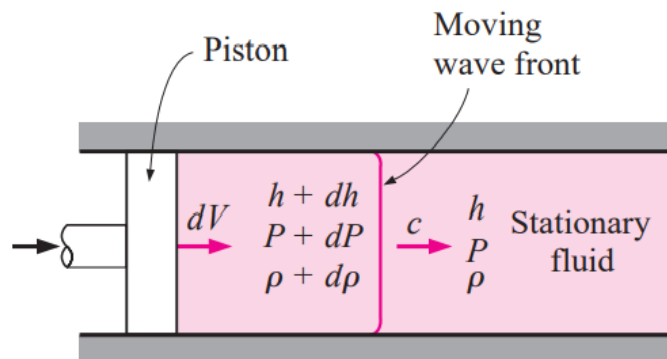


Figure 2.4: Propagation of a small pressure wave along a duct [8]

Figure 2.4 represents the changes in enthalpy, pressure, and density to the left side of the wave-

front to that of the constant values to the right of the wavefront. The speed of sound is represented by the symbol  $c$  and it is formulated as:

$$c = \sqrt{\gamma RT} \quad (2)$$

### 2.2.1.3 Mach number

Mach number is a measure of the compressibility properties of fluid flow: regardless of other variables, the fluid behaves similarly under the effect of compressibility at a certain Mach number [18]. The Mach number is used to distinguish between different types of fluid flow. When the Mach number of fluid is less than one, it is considered subsonic. The velocity of a fluid in sonic circumstances is equal to the speed of sound, which corresponds to a Mach number of one. In supersonic conditions, the Mach number tends to increase to a value of more than 1. The existence of shock waves across the flow areas, which tend to vary discontinuously, characterizes this supersonic flow. Supersonic flow has found its dominant place in numerous applications including outer space exploration and manufacturing sectors.

Mach number is a dimensionless quantity represented by the symbol  $Ma$  and it is formulated as:

$$Ma = \frac{u}{c} \quad (3)$$

### 2.2.1.4 Choked flow condition

Choked flow condition is an important aspect of a supersonic flow. As the name implies, the flow is choked at the throat region of the convergent-divergent nozzle by reducing the area of the throat to a point by which reducing the backpressure at the exit of the nozzle aids in creating a sonic condition in the throat region. This effect is known as the venturi effect and it was coined by Giovanni Battista Venturi. The maximum velocity and minimum pressure are attained at the throat of the *CD* nozzle. For a nozzle to acquire a choked flow, a certain condition must be satisfied.

$$\frac{P_b}{P_0} \leq \frac{P^*}{P_0} \quad (4)$$

### 2.2.1.5 Thrust equations

Simulating a process consists of numerical analysis, simulation analysis, and experimental analysis. The results of these three quantities must be compared, and an error analysis must be conducted, for a simulation process to be successful. Numerical analysis is the process of solving a set of equations from the available input values to obtain a unique result. For a successful

operation, nozzle employs a set of these equations. The mass flow rate, exit Mach number, exit velocity, pressure, and temperature are all included in these equations. These equations are used to calculate the nozzle's exit condition, which is then compared to the simulation findings. The following is a list of equations:

- ***Mass flow rate***

$$\dot{m} = \frac{A^* p_t}{\sqrt{T_t}} \sqrt{\frac{\gamma}{R}} \left( \frac{\gamma+1}{2} \right)^{-\frac{\gamma+1}{2(\gamma-1)}} \quad (5)$$

- ***Exit Mach***

$$\frac{A_e}{A^*} = \left( \frac{\gamma+1}{2} \right)^{-\frac{\gamma+1}{2(\gamma-1)}} \frac{\left( 1 + \frac{\gamma-1}{2} M_e^2 \right)^{\frac{\gamma+1}{2(\gamma-1)}}}{M_e} \quad (6)$$

- ***Exit Temperature***

$$\frac{T_e}{T_t} = \left( 1 + \frac{\gamma-1}{2} M_e^2 \right)^{-1} \quad (7)$$

- ***Exit Pressure***

$$\frac{p_e}{p_t} = \left( 1 + \frac{\gamma-1}{2} M_e^2 \right)^{\frac{-\gamma}{\gamma-1}} \quad (8)$$

- ***Exit Velocity***

$$V_e = M_e \sqrt{\gamma R T_e} \quad (9)$$

### 2.2.2 Pressure shock waves

It's no certainty that forcing a fluid through a converging-diverging nozzle will accelerate it to supersonic velocity. In the diverging section, if the backpressure isn't in the right range, the fluid may decelerate rather than accelerate. The overall pressure ratio  $P_b/P_0$  determines the state of the nozzle flow. As a result, the flow through a converging-diverging nozzle is governed by the backpressure  $P_b$  for particular intake parameters [8]. By reducing the backpressure of the nozzle, a high-pressure region of shocks is created inside and outside the nozzle and can be visualized in the pressure diagram below.

- $P_e$  - Exit pressure
- $P_b$  - Backpressure (or) Atmospheric pressure
- $P_0$  - Chamber pressure
- $P^*$  - Throat pressure

The pressure diagram 2.5 depicted here represents the various stages of pressure changes inside the nozzle due to the changes in the backpressure  $P_b$ .

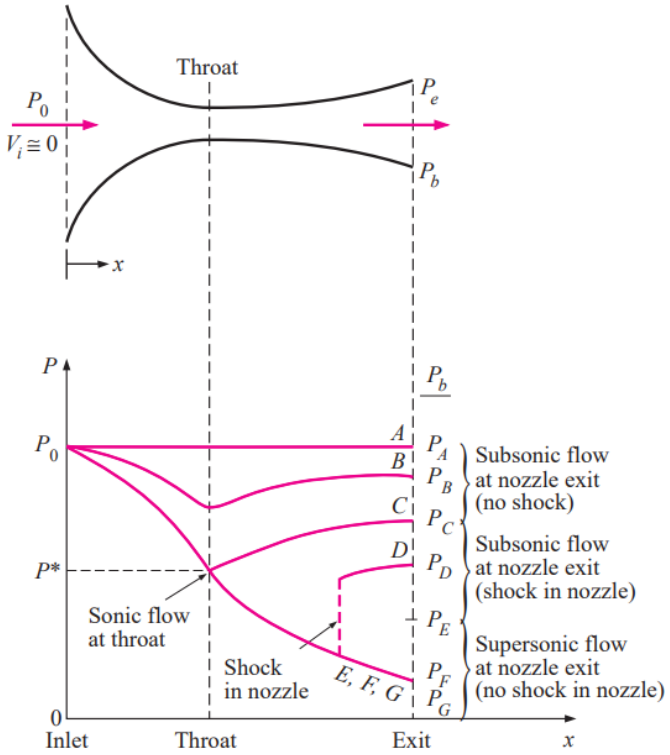


Figure 2.5: Effect of backpressure in CD nozzle [8]

- **Point A:** When  $P_b = P_0$ , fluid that enters the nozzle from the converging section does not flow because of no pressure difference between the nozzle inlet and exit. This condition is known as the "No Flow" condition.
- **Point B:** The fluid tends to flow from high pressure to a low-pressure zone when the back pressure is reduced to a certain limit,  $P_0 > P_b$ , due to the pressure differential inside the nozzle. However, because the backpressure has been reduced to a minimum, the flow near the throat is subsonic ( $Ma = 1$ ), and the acquired velocity is lost in the nozzle's diverging region.
- **Point C:** To establish a sonic condition in the throat area, the backpressure is further reduced. Although the pressure at the throat has increased to  $P^*$ , the diverging part of the nozzle continues to operate at subsonic speeds. Changes in the backpressure  $P_b$  do not affect the subsonic condition in the converging region of the nozzle at this point.
- **Point D:** This is where the normal shock begins to occur inside the nozzle. The nozzle tries to get pressure at the exit equal to  $P_b$  by lowering the backpressure even more. As a result, a normal shock forms inside the nozzle, and the flow becomes subsonic after the normal shock. The position of the normal shock inside the nozzle is determined by the pressure ratio  $P_b/P_0$ .
- **Point P<sub>E</sub>:** When  $P_b = P_e$ , a normal shock arises at the nozzle's exit. Throughout the

diverging region of the nozzle, the flow is supersonic. The final  $P_b$  solution will induce changes inside the nozzle, and as the pressure changes progress, differences outside the nozzle will appear.

- **Point  $P_F$ :** This flow is known as overexpanded flow, and it is a widely utilized flow of study in rocket nozzle applications. The pressure is reduced even more, forming a shock between the point of normal shock and  $P_F$ . The pressure is increased by a weaker oblique shock since the standard shock is too severe (non-isentropic). The flow is called overexpanded because the nozzle expanded the flow too much, resulting in a  $P_e$  that is excessively low in comparison to  $P_b$  ( $P_e \neq P_b$ ). The magnificent diamond shocks that can be observed in every rocket nozzle are the result of these oblique shocks. Overexpanded flow is very important in applications like CS where the particles tend to flow in an orderly fashion along the axis rather than in disorder orientation.
- **Point  $P_G$ :** This is known as under expanded flow, and it occurs near the nozzle's exit as a result of the backpressure being reduced to a final state. Because the nozzle is unable to expand the gas sufficiently, the exit pressure ( $P_e \neq P_b$ ) exceeds the back pressure. When expansion fans are employed to lower the pressure, diamond shocks appear.

## 2.3 Governing equations

*CFD* is based on the fundamental governing equations of fluid dynamics - continuity, momentum, and energy equations - in some form or another. They are mathematical expressions of three fundamental physical concepts that underpin all fluid dynamics:

1. Mass is conserved
2. Newton's second law,  $F = ma$
3. Energy is conserved

These equations are available in different forms, and usage of a particular form for a certain application may lead to accurate results, whereas the converse of this equation leads to instability in the solution.

The route map for solving the equations is shown in Figure 2.6. The fluid dynamics are all based on three basic physical principles, which are shown in the top left corner. These physical laws are applied to the model flow, resulting in mathematical statements including continuity, momentum, and energy equations. Below the model flow, on the left side of the map, a different set of equations in conservative and non-conservative forms is generated. These equations are combined to solve the problem with suitable boundary conditions. The boundary condition box is drawn separately from the road map because the boundary condition does not have any influence over the equations [2].

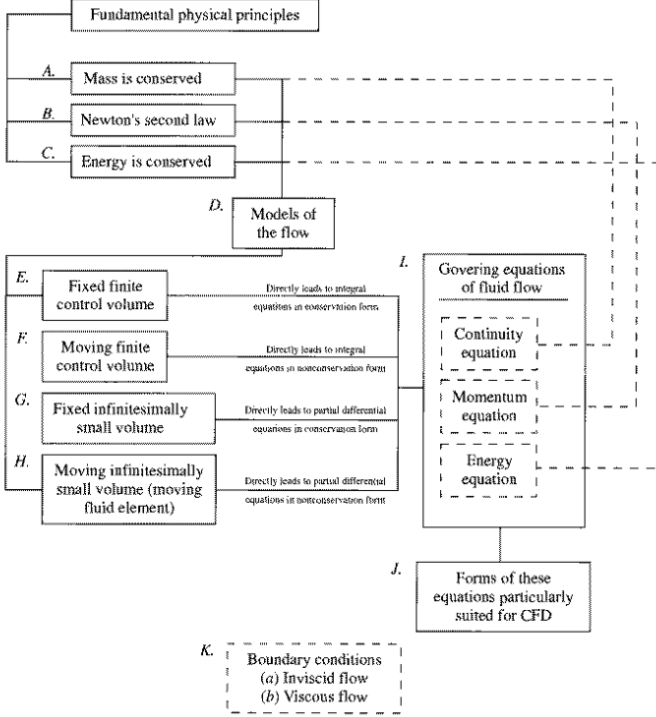


Figure 2.6: Road map of CFD [2]

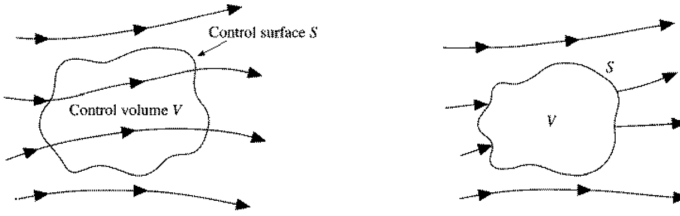


Figure 2.7: Finite control volume fixed in space and moving with the fluid such that the same fluid particles are always in the same control volume [2]

Before trying to solve these equations few fluid models need to be understood in advance. While solving for a fluid, it is obvious that the equations are solved by considering a small fluid element of volume. This is to reduce the overall error that arises during the iterations. Consider a small fluid volume in a flow field with a volume  $V$  confined with a surface  $S$  as shown in figure 2.7. The control volume  $V$  is fixed in space and fluid is passing through it on the left side of the picture, whereas the control volume is moving with the fluid on the right side of the figure and the same fluid particles are always inside it on the right side of the figure.

By applying fundamental physical principles to the control volume, a set of the integral forms of equations arrive and this integral form can be manipulated to partial differential equations. The equation that is obtained from the fixed control volume is called the ***conservative form*** of the governing equations. The equation obtained from moving control volume is called the ***non-conservative form*** of the governing equations.

A substantial derivative is an important physical meaning of the equations. This substantial

derivative gives the rate of change of fluid properties at every point of the flow field. Consider an infinitesimally small fluid element moving with the flow as shown in figure 2.8.

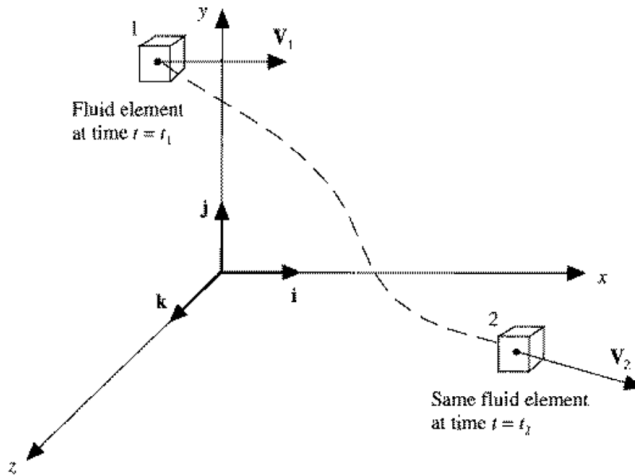


Figure 2.8: Illustration of substantial derivative [2]

The fluid element inside the control volume is fixed, and the control volume moves from points 1 to 2. The state of the equation that explains the fluid properties is given as:

$$\frac{DT}{Dt} = \frac{\partial T}{\partial t} + (\mathbf{V} \cdot \nabla) \equiv \frac{\partial T}{\partial t} + u \frac{\partial T}{\partial x} + v \frac{\partial T}{\partial y} + w \frac{\partial T}{\partial z} \quad (10)$$

The substantial derivative,  $\frac{DT}{Dt}$ , on the left-hand side represents the temporal rate of change following a moving fluid element. The physical representation of the time rate of change of a certain attribute at a fixed position is the local derivative  $\frac{\partial T}{\partial t}$ . The physical representation of the temporal rate of change owing to the transfer of a fluid element from one site to another where the flow characteristics are spatially varied is the convective derivative ( $\mathbf{V} \cdot \nabla$ ). Other flow properties such as temperature T, pressure P, density  $\rho$ , and velocity V can be calculated using this substantial derivative.

The equation 10, states physically that the temperature of the fluid element changes as it sweeps past a point in the flow because the temperature of the flow-field itself may be fluctuating with time (the local derivative) at that point and because the fluid element is simply on its way to another point in the flow field where the temperature is different (the convective derivative).

In fluid dynamics, the divergence of a vector field is an important feature of the equation that appears more frequently. Divergence of a fluid vector field can be considered as a source and sink term, in which fluid rise up from a point is known as source and descend to a point is known as sink term. The Source field gives a positive divergence and the sink field gives a negative divergence. This can be visualized by considering a control volume moving with the fluid. This control volume is made of the same particles and its mass is fixed, but the volume  $V$  and control surface  $S$  change with time. In addition, a small infinitesimal element of surface  $ds$  with local

velocity  $v$  and change in control volume  $\partial V$  is considered. The total divergence of velocity is represented as:

$$\nabla \cdot \mathbf{V} = \frac{1}{\delta V} \frac{D(\delta V)}{Dt} \quad (11)$$

The divergence of velocity represents the physical time rate of change of the volume of a moving fluid element, per unit volume.

### 2.3.1 The continuity equation

The physical principle of continuity equation is termed as mass is conserved. The term mass is conserved represents the total mass of a control volume or an infinitesimally small element is constant when the control volume moves from one point to another, and the net mass flow out of the control volume is always equal to the time rate of decrease of mass inside the control volume [2]. The three fundamental physical principles result in a variety of equations, each of which is identical to the others and can be utilized for a variety of applications and boundary conditions. Conservative and non-conservative are the two basic types.

As discussed, the conservative equation is the model of the finite control volume that is fixed in space, while considering a small infinitesimal volume  $dv$  and the elemental surface area  $ds$ . The non-conservative equation is the model of the infinitesimal small fluid element moving with the flow. The equations are given as:

- *Conservative form of the equation:*

$$\frac{\partial \rho}{\partial t} + \nabla \cdot (\rho \mathbf{V}) = 0 \quad (12)$$

- *Non-conservative form of the equation:*

$$\frac{D\rho}{Dt} + \rho \nabla \cdot \mathbf{V} = 0 \quad (13)$$

The integral version of the equation is also available, although the partial differential form is more commonly employed in numerical analysis. When there are discontinuities inside the fixed control volume, the integral form of the equation is useful. The differential form, on the other hand, assumes that the flow properties are differentiable. The divergence theorem on the integral form is used to obtain the differential form, and it is clear that the integral form of the equation is believed to be more basic than the differential form.

### 2.3.2 The momentum equation

The momentum equation is derived using newton's second law of motion. The momentum equation, unlike the continuity equation, is obtained from the non-conservative form and can

be adjusted to obtain the conservative form and Navier-Stokes equations. The equation can be calculated by examining the cube's control volume, which includes normal stresses, shear stresses, and velocity components in the  $x$ ,  $y$ , and  $z$  directions. The control volume moves from one point to another while maintaining the same amount of fluid particles in the control volume at all times. The second law of newton is as follows:

$$F_x = ma_x \quad (14)$$

Where  $F_x$  and  $a_x$  are the scalar  $x$  components of force and acceleration respectively. The forces acting on the control volume are widely divided into two components namely:

- **Body forces**, affect directly the fluid element's volumetric bulk gravitational, electric, and magnetic forces are examples of "at a distance" forces.
- **Surface forces**, which act immediately on the fluid element's surface are caused by only two factors: (a) the pressure distribution imposed on the surface by the outside fluid surrounding the fluid element, and (b) the shear and normal stress distributions imposed on the surface by the outside fluid "tugging" or "pushing" on the surface through friction [2].

The shear stress, denoted by  $\tau_{xy}$  is the time rate of change of shear deformation of the fluid element, whereas the normal stress  $\tau_{xx}$  is the time rate of change of volume of the fluid element. The control volume is moving in the  $x$ -direction and shear stresses are sketched in the picture below.

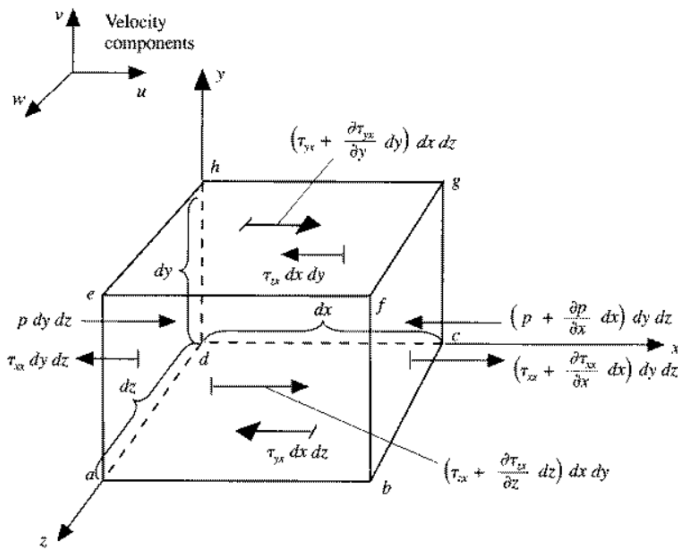


Figure 2.9: Model for momentum equation [2]

On the face "abcd", the force acting in the  $x$ -directions is shear force. On the face "efgh", the shear force is given as. By noticing the diagram, the bottom face direction is on the left side

(negative  $x$ -direction), whereas the top face direction is on the right side (positive  $x$ -direction). While concentrating on the top face "efgh", the velocity component  $u$ ,  $v$ , and  $w$  tends to increase in the  $x$ -direction, this causes a "tugging" action that tries to pull the fluid element in the positive  $x$ -direction. In the bottom face, the fluid element below the face tends to move in the negative  $x$ -direction causing the fluid to drag on the fluid element. All of the other viscous stresses' directions can be rationalized in the same way [2]. The total force in the  $x$ -direction  $F_x$  is given as:

$$F_x = \left[ -\frac{\partial p}{\partial x} + \frac{\partial \tau_{xx}}{\partial x} + \frac{\partial \tau_{yx}}{\partial y} + \frac{\partial \tau_{zx}}{\partial z} \right] dx dy dz + \rho f_x dx dy dz \quad (15)$$

Considering the right-hand side of newton's law, the mass and acceleration in the  $x$ -directions are represented as:

$$m = \rho dx dy dz \quad (16)$$

$$a_x = \frac{Du}{Dt} \quad (17)$$

By combining the above equations, various components of momentum equations are obtained. These equations represent the  $x$ ,  $y$ , and  $z$  components of the velocities and can be represented in conservative and non-conservative forms. These scalar equations are also known as Navier – Stokes equations named after Claude – Louis Navier and George Gabriel Stokes.

- ***Non-conservative form***

- ***x-component:***

$$\rho \frac{Du}{Dt} = -\frac{\partial p}{\partial x} + \frac{\partial \tau_{xx}}{\partial x} + \frac{\partial \tau_{yx}}{\partial y} + \frac{\partial \tau_{zx}}{\partial z} + \rho f_x \quad (18)$$

- ***y-component:***

$$\rho \frac{Dv}{Dt} = -\frac{\partial p}{\partial y} + \frac{\partial \tau_{xy}}{\partial x} + \frac{\partial \tau_{yy}}{\partial y} + \frac{\partial \tau_{zy}}{\partial z} + \rho f_y \quad (19)$$

- ***z-component:***

$$\rho \frac{Dw}{Dt} = -\frac{\partial p}{\partial z} + \frac{\partial \tau_{xz}}{\partial x} + \frac{\partial \tau_{yz}}{\partial y} + \frac{\partial \tau_{zz}}{\partial z} + \rho f_z \quad (20)$$

- ***Conservative form***

- ***x-component:***

$$\frac{\partial(\rho u)}{\partial t} + \nabla \cdot (\rho u \mathbf{V}) = -\frac{\partial p}{\partial x} + \frac{\partial \tau_{xx}}{\partial x} + \frac{\partial \tau_{yx}}{\partial y} + \frac{\partial \tau_{zx}}{\partial z} + \rho f_x \quad (21)$$

- ***y-component:***

$$\frac{\partial(\rho v)}{\partial t} + \nabla \cdot (\rho v \mathbf{V}) = -\frac{\partial p}{\partial y} + \frac{\partial \tau_{xy}}{\partial x} + \frac{\partial \tau_{yy}}{\partial y} + \frac{\partial \tau_{zy}}{\partial z} + \rho f_y \quad (22)$$

– *z-component:*

$$\frac{\partial(\rho w)}{\partial t} + \nabla \cdot (\rho w \mathbf{V}) = -\frac{\partial p}{\partial z} + \frac{\partial \tau_{xz}}{\partial x} + \frac{\partial \tau_{yz}}{\partial y} + \frac{\partial \tau_{zz}}{\partial z} + \rho f_z \quad (23)$$

### 2.3.3 The energy equation

The energy equation is the third physical principle depicted in Figure 2.8 of the road map. This equation is derived from the first rule of thermodynamics, which states that heat is a type of energy and that thermodynamic processes must follow the principle of energy conservation. The law is written as follows:

***Rate of change of energy inside fluid element = Net flux of heat into the element + Rate of work done on element due to body and surface forces [2]***

The work done, heat flux, and change in energy mentioned in the equation above are separated into different aspects of forces and energy acting on the fluid element.

- ***Work done on the element:***

The work done on the element is divided into body forces and surface forces that are acting in the control volume. Work done on the moving body is the product of force and component of velocity in that direction. This is represented as:

$$\rho \mathbf{f} \cdot \mathbf{V} (dxdydz) \quad (24)$$

The surface forces include pressure, and normal and shear stresses are considered in the *x*-direction. The forces in the positive *x*-direction perform positive work and the forces in the negative *x*-direction perform negative work. Considering all the surface forces, the net rate of work done on the element by these forces is given by:

$$\left[ -\frac{\partial(up)}{\partial x} + \frac{\partial(u\tau_{xx})}{\partial x} + \frac{\partial(u\tau_{yx})}{\partial y} + \frac{\partial(u\tau_{zx})}{\partial z} \right] dxdydz \quad (25)$$

While combining the body forces and surface forces obtained in the above equation in *x*, *y*, and *z*-direction, the total net work done on the element is represented as:

$$\begin{aligned}
C = - & \left[ \left( \frac{\partial(up)}{\partial x} + \frac{\partial(vp)}{\partial y} + \frac{\partial(wp)}{\partial z} \right) + \frac{\partial(u\tau_{xx})}{\partial x} + \frac{\partial(u\tau_{yx})}{\partial y} \right. \\
& + \frac{\partial(u\tau_{zx})}{\partial z} + \frac{\partial(v\tau_{xy})}{\partial x} + \frac{\partial(v\tau_{yy})}{\partial y} \\
& + \frac{\partial(u\tau_{zy})}{\partial z} + \frac{\partial(w\tau_{xz})}{\partial x} \\
& \left. + \frac{\partial(w\tau_{yz})}{\partial y} + \frac{\partial(w\tau_{zz})}{\partial z} \right] \\
& dxdydz + \rho \mathbf{f} \cdot \mathbf{V} dxdydz
\end{aligned} \tag{26}$$

- ***Heat flux into the element:***

The heat flux added into the element is due to volumetric heating such as absorption or emission of radiation and thermal conduction.  $\dot{q}$  is the rate of volumetric addition of heat per unit mass, while the mass of a moving fluid element is given as  $\rho dxdydz$ .

- ***Volumetric heating of element***

$$\rho \dot{q} dxdydz \tag{27}$$

The heat flux in a given direction is defined as the heat transfer in that direction expressed in dimensions of energy per unit time per unit area perpendicular to the direction [2]. The heating of fluid elements by thermal conduction is represented as:

$$B = \left[ \rho \dot{q} - \left( \frac{\partial \dot{q}_x}{\partial x} + \frac{\partial \dot{q}_y}{\partial y} + \frac{\partial \dot{q}_z}{\partial z} \right) \right] dxdydz \tag{28}$$

By combining the above equation with the Fourier's law of heat conduction to the local temperature gradient, the net heat flux is given as:

$$B = \left[ \rho \dot{q} + \frac{\partial}{\partial x} \left( k \frac{\partial T}{\partial x} \right) + \frac{\partial}{\partial y} \left( k \frac{\partial T}{\partial y} \right) + \frac{\partial}{\partial z} \left( k \frac{\partial T}{\partial z} \right) \right] dxdydz \tag{29}$$

- ***The internal energy of the element:***

Internal energy and kinetic energy are two ways to express the rate of change of energy inside a fluid element. The atoms and molecules that make up the fluid particle provide internal energy, and if the system is formed of gas, the atoms and molecules moving within the system provide translational kinetic energy. Molecules, on the other hand, tend to rotate and vibrate, imparting energy to the molecule through rotation and vibration. The electron that orbits the nucleus gives the particle more electronic energy. Finally, a particle's total internal energy is calculated by adding rotational, translational, vibrational, and electronic energy [2].

The kinetic energy is produced due to the consideration of moving fluid elements and the translational motion of fluid elements. The total internal energy and kinetic energy are given in substantial derivative due to the moving fluid element, and it is represented as:

$$A = \rho \frac{D}{Dt} \left( e + \frac{V^2}{2} \right) dx dy dz \quad (30)$$

By considering all the above equations, the energy equation can be implemented in conservative and non-conservative forms by manipulating the equations.

## 2.4 Ansys Fluent

Ansys Fluent is a cutting-edge computer program for modeling fluid flow and heat transport in complex shapes. This application is developed in the C programming language, which gives the user a lot of flexibility in terms of generating results and controlling the solver. Fluent software has unbelievable meshing capabilities, allowing you to change every cell in the meshing for exact results. For each application, Ansys Fluent has a variety of options, and the most important features are highlighted in this study.

### 2.4.1 Solvers

Ansys Fluent is equipped with two main solvers to solve the equations that are discussed above namely:

- Pressure-Based Solver (PBS)
- Density-Based Solver (DBS)

Both solvers can handle a wide range of flows, however in some cases, one may outperform the other (i.e., produce a solution faster or resolve specific flow aspects better). The pressure-based and density-based approaches answer the continuity, momentum, energy, and species equations in distinct ways.

#### • *Pressure – Based Solver (PBS)*

The pressure-based solver can handle a wide range of flows, from low compressible to high-speed compressible. The pressure-based solver takes its name from how mass conservation is enforced in the numerical solution. Pressure velocity coupling is the name of the numerical techniques that are utilized, and they function by stating the continuity equation in terms of a pressure correction. To guarantee that the continuity equation is satisfied, the pressure correction equation is computed and utilized to adjust the velocity field obtained from solving the momentum equations. There are two versions of the *PBS*, the segregated and the coupled version. All of the equations are solved one at a

time in the segregated version, starting with the momentum equations and ending with the pressure correction equation. In the coupled version, however, all of these equations are solved simultaneously and in a coupled way. After solving the momentum and continuity equations, the rest of the equations are solved sequentially, including energy and any other scalar equations (e.g., turbulence, transport equations) that may be included in the problem.

- ***Segregated Vs Coupled solver***

The momentum equation and the continuity equation are solved independently one after the other, as indicated by the name segregated solver, and then the energy and turbulence equations are solved. The coupled solver, on the other hand, solves the momentum and continuity equations simultaneously before moving on to the transport equations. The segregated solver requires less memory, whereas the coupled solver requires 1.5–2 times more memory. Because distinct solution controls can be applied for each equation, segregated offers greater flexibility in the solution technique. The pressure-based coupled solution is appropriate for most flows since it outperforms the segregated solver in terms of convergence time.

- ***Density-Based Solver (DBS)***

As a coupled equation, the *DBS* solves the continuity, momentum, energy, and species equations. After that, any other equations, such as turbulence model equations or other scalars, are solved in order. It can be used when density, energy, momentum, and/or species have a high linkage or interdependence. *DBS* comes in two forms: coupled implicit and coupled explicit solvers.

- ***Implicit Vs Explicit solver*** The implicit option is often favored over the explicit option since the explicit option has a very strict time scale size limit due to *CFL* constraints, but the implicit option does not. When the flow's characteristics time scale is in the same order as the acoustic time scale, the explicit technique is utilized. In a time step, the Courant number is the ratio of length or fraction of the cell that the flow goes over. The *CFL* (Courant – Friedrichs – Lewy) number is an important part of the density-based solver's time-stepping scheme control. The *CFL* is written as follows:

$$\text{Co} = \frac{U\Delta t}{\Delta x} \quad (31)$$

The physical interpretation of equation 31 is that when the courant number in a time step is 0.3, the flow moves 30% of the distance across the cell. It represents the convergent stability conditions for a simulation depending on the physics and solver selected. The density-based implicit and explicit stability limits differ greatly. In

Ansys Fluent, the default value for explicit form *CFL* is 1.0, which can be increased to 2.0. If the solution tends to diverge, i.e., if residuals are rapidly growing, it is a good sign to reduce the *CFL* number to 1.0 to 0.5 to get started. The *CFL*, on the other hand, is unconditionally stable in the implicit formulation. The default *CFL* is 5.0, although it can be increased if there are concerns with high Mach numbers.

- **Choosing the appropriate Solver and CFL condition**

- Because the density-based approach was initially created for high-speed compressible flows, using a high compressible flow density-based solver is an advisable choice for challenges like cold spray applications. Incompressible and weakly compressible flows, on the other hand, are generally solved using a pressure-based solver.
- The density-based solver employs implicit and explicit conditions, calculating current information from prior cell data and solving the equation in a coupled manner.
- For density-based implicit conditions, the *CFL* number is unconditionally stable, which implies that even if the *CFL* number is increased or decreased to a specific limit, there will be no perceptible changes in the solution's convergence.
- Because it does not have a tight time scale size limit (*CFL*), the implicit condition is preferred for high-speed compressible flows with combustion and hypersonic flows with shock interactions.

### 2.4.2 Meshing attributes

Mesh is the process of breaking down geometry into thousands or millions of small shapes as a result of applying fundamental physical models (described above) and other equations to each cell to generate results. It's an important characteristic of *CFD* simulation that a slight change in meshing can lead to bad results and a significant increase in computational resources.

The meshing process can be separated into two categories: global mesh and local mesh. Global meshing, as the name implies, is applied to the entire geometry without any specific consideration for crucial points. Local meshing, on the other hand, allows the user to specify a small meshing size for the area of the geometry that is more susceptible to high stresses or high flow rates. Certain size function parameters in the fluent meshing tool are required to provide local meshing for a geometry.

#### 2.4.2.1 Size functions

The size functions can be used to manage the mesh size distribution on a surface or within a volume. The mesh distribution receives more accurate sizing information as well as more precise refinement control when the enhanced size capabilities are activated [14]. The minimum

and maximum size values, growth rate, and normal angle all influence the size functions. There are many size functions in Fluent that may be utilized for a variety of applications, but this report is required to deal with curvature and proximity size functions because they are the most common in nozzle applications.

- ***Curvature size function***

The curvature size function computes element sizes on edges and faces that do not violate the size or normal angle, which are either computed or defined automatically [14]. The lowest and maximum size values represent the smallest and largest cells that the fluent tool can generate on the geometry. Fluent calculate the minimum size by default based on the geometry, and the maximum size is user-defined based on the correctness of the projected output. The growth rate represents the increase in element edge length with each succeeding layer of elements from the edge or face. A 20% increase in element edge length is represented by a growth rate of 1.2. The maximum angle that one of an element's edges can span is called the normal angle. These curvature values aid in the creation of a better mesh for rounded objects in the geometry; without them, the mesh sizes would be huge, resulting in poor result generation.

- ***Proximity size function***

The proximity size function is used to ensure that the number of element layers formed in gaps is kept to a minimum. Gaps are defined as the volumetric region between two faces as well as the area between two objects. To produce accurate results in *CFD* simulation, edges and gaps must be considered.

#### **2.4.2.2 Types of meshes**

Ansys Fluent has tetrahedral, hexahedral, polyhedral, and pyramid cells that can be utilized for a variety of purposes. Certain concerns and conditions should be addressed while choosing a mesh type, as listed below:

- ***Setup time***

The time it takes to set up each mesh type varies depending on the application and the mesh type selected. The most popular mesh types are hexahedral or quadrilateral and tetrahedral or triangle mesh, both of which are less expensive than the others. Structured meshes, such as hexahedral elements, are more commonly utilized in 3-D models that feature flow or heat transmission inside the object. For the same degree of the polynomial, the space generated by hexahedral elements is richer than the space generated by tetrahedral elements. Tetrahedral elements, on the other hand, are ideal for modeling complex geometric domains with the least amount of mesh deformation.

- *Computational expenses*

Tetrahedral cells are formed with fewer cells in a specific region for complex geometry. Because a triangular/tetrahedral mesh allows cells to cluster in specific parts of the flow domain [14], this is the case. Structured hexahedral/quadrilateral meshes tend to force cells into areas where they aren't needed. This results in higher computational costs, but better results. When opposed to triangular/tetrahedral cells, the main advantage of hexahedral/quadrilateral cells is that they allow for a higher aspect ratio for each cell. On the surface of the geometry, triangular/tetrahedral meshes are utilized, whereas hexahedral/quadrilateral meshes are employed inside the geometry for better results and lower computing costs.

For basic geometry, tetrahedral meshes are employed, and the simulation results are an approximation of the cells provided. This is due to the utilization of cells in areas of curvature and closeness. Because of their low aspect ratio, cells fail to stretch in accordance with the geometry, making them less precise in any application. Because of the utilization of aspect ratio, which allows the cell to produce more volume in a specific region, hexa-core and hexahedral meshes are more useful in complex geometry. An inner zone of cartesian cells and an exterior region of tetrahedral elements are used to produce the hex-core region. When compared to two other meshing types, polyhedral cells have a lower volume element count and a higher convergence rate and accuracy. The polyhedral mesh is created by creating a polygon around each node in the tetrahedral mesh. This meshing type outperforms both mesh types, resulting in better and faster convergence with fewer iterations. Poly-hexcore is made up of a hexahedral mesh in the center and a polyhedral mesh on the geometry's surface.

#### 2.4.2.3 Mesh metrics

Mesh metrics are a good approach to determine whether or not a mesh is good enough to produce correct results. Mesh metrics are automatically created after meshing and can be viewed in the console area of the fluent workspace. The quality of the mesh ensures the best potential analysis findings for the problem, lowers the need for additional analysis runs and improves prediction abilities. The following are the basic mesh metrics:

- *Element quality*

Once the meshing is complete, the element quality is represented as a volume statistic. A value of 1 denotes a perfect cube (or) square, whereas a value of 0 denotes a volume of zero (or) negative volume. The statistic will include the minimum, maximum, and average values for all mesh metrics. When inspecting element quality, these three metric features should be taken into account.

- **Aspect ratio** The aspect ratio of a face or cell is the ratio of the longest edge length to the shortest edge length. The aspect ratio of triangular, tetrahedral, quadrilateral and hexahedral elements is specified differently for each element type [14].

- The aspect ratio of an equilateral face or cell (e.g., an equilateral triangle or a square, etc.) is 1.
- Because the edges of less regularly-shaped faces of cells differ in length, the aspect ratio will be greater than one.

- ***Skewness***

Skewness is the most extensively used and most critical mesh statistic for mesh quality. The skewness of a distorted object determines how close it is to its original shape. When compared to the original shape, the deformation (or) stretching is depicted in the diagram below.

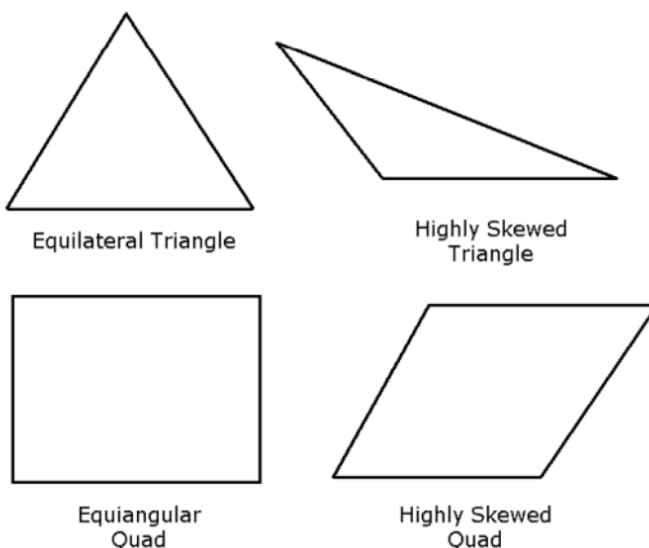


Figure 2.10: Skewness of a cell [14]

A degenerate cell has a value of 1, while an equilateral cell (ideal) has a value of 0. Degenerate cells are characterized by nodes that are almost coplanar (slivers). The skewness value of invalid cells is more than one. Faces and cells with a lot of skews should be avoided since they generate less accurate results than equilateral/equiangular faces and cells [14]. For all geometries, including 2-D and 3-D, these are the three main and most often used mesh metrics. When comparing 2-D and 3-D geometries, a little variation in the mesh metric may show.

#### 2.4.3 Turbulence modeling

The most important aspect of a simulation is selecting a good physics model that will yield the desired results. Choosing an inappropriate model for an application will cause simulation and computing costs to rise. Necessary care should be taken before considering a physics model. Turbulent flows are characterized by varying velocities in the flow field due to frictions and eddy viscosity. When compared to laminar flows, turbulent flows vectors are arbitrarily indicated, resulting in flow field divergence. In turbulent flows, inertial forces are dominant. When the

Reynolds number exceeds 5000, the flow transitions from laminar to turbulent. The maximum velocity is at the center of the flow, and the velocity profile of a laminar flow is considered to be a no-slip (friction) condition near the wall region. The average velocity profile is essentially constant or flattens away from the wall when turbulent flows are evaluated with the no-slip condition, as shown in figure 2.11. This is because turbulence introduces a lot of mixing between different layers of flow, and this momentum transfer tends to homogenize the flow across the pipe.

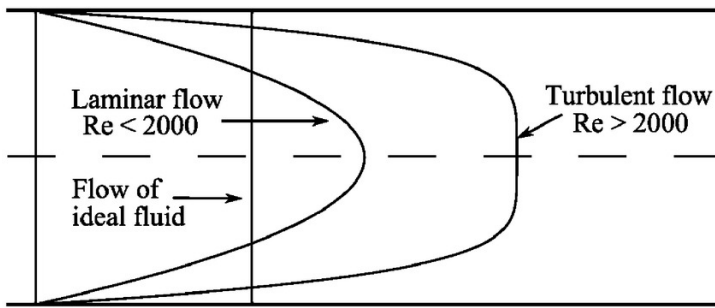


Figure 2.11: Turbulent velocity profile [21]

The velocity profile and boundary layer are explored in further detail later in this chapter. The concentration of the transported quantities tends to fluctuate as the turbulence intensity of the flow is considered when examining equations that could be used to solve turbulent flows such as momentum, energy, and species concentration. In real-world engineering computations, simulating these fluctuations is prohibitively expensive. However, to resolve the small scales, these equations are time-averaged and ensemble-averaged, resulting in updated governing equations that are less expensive [13].

Ansys Fluent has several turbulence models that may be tweaked to produce precise results for a variety of applications. The two major turbulence models,  $K - \varepsilon$  and  $K - \omega SST$ , belong to the family of eddy viscosity models and are well suited for problems dealing with flow over a surface or flow through a pipe. Certain factors must be addressed when selecting a model, including the level of accuracy necessary, the availability of computer resources, and the amount of time required for the simulation to deliver accurate results.

- *Computational effort*

When compared to the Spalart – Allmaras model (a turbulence model that employs just one transport equation and is the less expensive), the standard  $K - \varepsilon$  model uses an additional transport equation, which increases the computational expenses and time when compared to other turbulence models. The realizable  $K - \varepsilon$  and  $RNG K - \varepsilon$  models are two types of  $K - \varepsilon$  models. The  $RNG K - \varepsilon$  model consumes 10–15 percent more CPU time than the regular  $K - \varepsilon$  model. Because of the increasing number of transport equations for Reynolds stresses in the equation [13],  $K - \omega$  models demand more memory and CPU time.

Mesh is a key factor for a successful computation of turbulent flows because turbulence flows

play a prominent role in the transport of momentum and other parameters, which must be finely tuned near the walls for high accuracy. The importance of wall functions is discussed later in this chapter.

#### 2.4.3.1 $K - \varepsilon$ turbulence model

The  $K - \varepsilon$  model was proposed by Launder and Spalding in the early 1970s, and it has gained popularity in industrial flows and heat transfer applications due to its robustness, economy, and reasonable accuracy for a wide variety of turbulent flows. The following are the steps involved in solving  $K - \varepsilon$  models:

- Solve transport equation for  $K$  and  $\varepsilon$
- Substitute  $K$  and  $\varepsilon$  for  $\mu_t$  to solve for eddy viscosity
- Substitute  $\mu_t$  in Boussinesq hypothesis to solve for Reynolds stresses
- Apply Reynolds stress in the RANS equation.

The standard  $K - \varepsilon$  model is a semi-empirical model based on model transport equations  $\varepsilon$  for turbulence kinetic energy ( $K$ ) and dissipation rate. The model transport equation for ( $K$ ) is obtained from the precise equation, whereas the model transport equation for epsilon was constructed from physical reasoning and bears little resemblance to its mathematically accurate counterpart.

$$\frac{\partial}{\partial t}(\rho k) + \frac{\partial}{\partial x_i}(\rho k u_i) = \frac{\partial}{\partial x_j} \left[ \left( \mu + \frac{\mu_t}{\sigma_k} \right) \frac{\partial k}{\partial x_j} \right] + G_k + G_b - \rho \varepsilon - Y_M + S_k \quad (32)$$

$$\frac{\partial}{\partial t}(\rho \varepsilon) + \frac{\partial}{\partial x_i}(\rho \varepsilon u_i) = \frac{\partial}{\partial x_j} \left[ \left( \mu + \frac{\mu_t}{\sigma_\varepsilon} \right) \frac{\partial \varepsilon}{\partial x_j} \right] + C_{1\varepsilon} \frac{\varepsilon}{k} (G_k + C_{3\varepsilon} G_b) - C_{2\varepsilon} \rho \frac{\varepsilon^2}{k} + S_\varepsilon \quad (33)$$

The transport equations for  $K$  and  $\varepsilon$ , respectively, are represented by the equations 32 & 33. In the RNG, realizable, and standard  $K - \varepsilon$  models, the transport equation for turbulent kinetic energy  $K$  is the same. The time derivative, convection of turbulent kinetic energy, is represented on the left-hand side of the equation, whereas diffusion and source terms are represented on the right-hand side. Based on model coefficients  $C_1$ ,  $C_2$ , and  $C_3$ , the transport equation for all models changes.

Mixing length models and Van dries mixing models are used to calculate eddy viscosity. The mixing length model is the oldest, and it indicates the sizes of turbulent eddies in a flow regime. The formulation of a viscous sub-layer very close to the wall, where the flow is laminar, is missing from this model. By taking into account the viscous sub-layer, the Van Driest mixing model improves on the traditional mixing length. Because the viscosity in the viscous sub-layer

dampens and reduces the size of the eddies, instead of calculating for mixing length,  $\varepsilon$  would be solved for eddy viscosity, which is mentioned below in the equation 34.

$$\mu_t = \rho C_\mu \frac{k^2}{\varepsilon} \quad (34)$$

The Reynolds stresses are determined by applying the solution obtained from the transport equation to the eddy viscosity equation  $\mu_t$ , which is then applied to the Boussinesq hypothesis. The Boussinesq hypothesis is applied to the Reynolds Averaged Navier – Stokes equations in the final stage of solving the  $K - \varepsilon$  models (RANS).

#### 2.4.3.2 $K - \omega$ SST turbulence Model

The  $K - \omega$  model was proposed by Menter in 1992 which is an improved version of turbulence modeling when compared to the  $K - \varepsilon$  model. The  $K - \varepsilon$  model tends to offer correct findings in the free stream velocity region but performs poorly in the near-wall velocity region, necessitating the development of a new model. For a range of flows, the near-wall damping function ( $f$ ) utilized by the  $K - \varepsilon$  model was proven to be incorrect. The  $K - \omega$  model, on the other hand, is sensitive to the inlet free stream velocity, and the wall shear stress is too large to separate the flow from smooth surfaces. Because of the shortcomings of the  $K - \omega$  model, the  $K - \omega$  SST (Shear Stress Transport) model was developed in an attempt to overcome some of these issues and provide improved separation prediction for exterior aerodynamics applications.

The  $K - \omega$  SST model is a hybrid of the  $K - \varepsilon$  and  $K - \omega$  models, with the two models combined using a blending function.

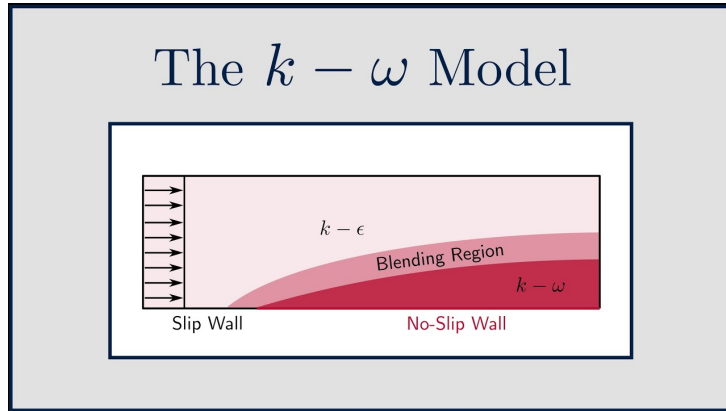


Figure 2.12: Illustration of  $K - \varepsilon$  &  $K - \omega$  models

According to figure 2.12,  $K - \omega$  acts near the wall, and  $K - \varepsilon$  acts in the free stream region, whereas both models tend to blend in the blending region. The blending function  $F_1$  is used to mix the models. When  $F_1$  is 0, the model used is  $K - \varepsilon$ , and when  $F_1$  is 1, the model used is  $K - \omega$ . As a result, the blending function near the wall would be 1 while the blending function further away from the wall would be 0. Figure 2.13 depicts this in mesh form.

## The $k - \omega$ SST model

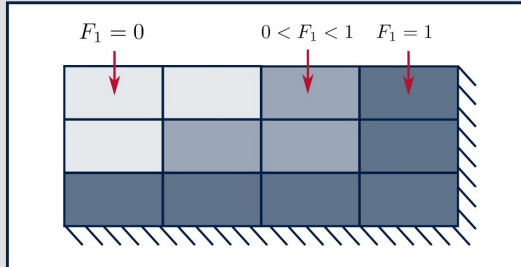


Figure 2.13: Representation of blending function

The above figure 2.13 represents a section of the mesh near the wall. The dark grey area near the wall represents the blending function, and  $F_1 = 1$  indicates that the  $K - \omega$  model is being employed near the wall. The  $K - \varepsilon$  model is represented by a value of blending function  $F_1 = 0$  far away from the wall. The blending function  $0 < F_1 < 1$  represents a blend of the  $K - \omega$  and  $K - \varepsilon$  models in the moderate grey area between the two models employed. The blending function is written as follows:

$$F_1 = \tanh(\Phi_1^4) \quad (35)$$

$$\Phi_1 = \min \left[ \max \left( \frac{\sqrt{k}}{0.09\omega y}, \frac{500\mu}{\rho y^2 \omega} \right), \frac{4\rho k}{\sigma_{\omega,2} D_{\omega}^{+} y^2} \right] \quad (36)$$

$$D_{\omega}^{+} = \max \left[ 2\rho \frac{1}{\sigma_{\omega,2}} \frac{1}{\omega} \frac{\partial k}{\partial x_j} \frac{\partial \omega}{\partial x_j}, 10^{-10} \right] \quad (37)$$

The smooth transition between the  $K - \omega$  and  $K - \varepsilon$  models is represented by tanh. The *SST* model, which is expressed as a shear stress transport equation, is a viscosity limiter model near the wall that employs the  $F_2$  blending function. Reducing the viscosity that forms near the wall may aid in speedier separation from the wall region. The following is a representation of the blending function and turbulent viscosity (*SST*):

$$F_2 = \tanh(\Phi_2^2) \quad (38)$$

$$\Phi_2 = \max \left[ 2 \frac{\sqrt{k}}{0.09\omega y}, \frac{500\mu}{\rho y^2 \omega} \right] \quad (39)$$

$$\mu_t = \frac{\rho k}{\omega} \frac{1}{\max \left[ \frac{1}{\alpha^*}, \frac{SF_2}{a_1 \omega} \right]} \quad (40)$$

The turbulent kinetic energy ( $K$ ) and turbulent dissipation energy ( $\omega$ ) of the  $K - \omega$  *SST* model

were obtained from the  $K - \varepsilon$  and  $K - \omega$  models. When turbulence models are selected in the Ansys Fluent physical model, both use the same turbulent equations, with the addition of a factor for shear stress transport. The final  $K - \omega$  SST model is represented like this:

$$\frac{\partial}{\partial t}(\rho k) + \frac{\partial}{\partial x_i}(\rho k u_i) = \frac{\partial}{\partial x_j} \left( \Gamma_k \frac{\partial k}{\partial x_j} \right) + \tilde{G}_k - Y_k + S_k \quad (41)$$

$$\frac{\partial}{\partial t}(\rho \omega) + \frac{\partial}{\partial x_i}(\rho \omega u_i) = \frac{\partial}{\partial x_j} \left( \Gamma_\omega \frac{\partial \omega}{\partial x_j} \right) + G_\omega - Y_\omega + D_\omega + S_\omega \quad (42)$$

#### 2.4.3.3 Choosing the appropriate model

In the preceding discussion, two turbulence models were presented and explained in depth. Every turbulence model has benefits and drawbacks, and each turbulence model must be chosen based on processing times and numerous equations required to provide an exact solution to the problem. There are numerous benefits and drawbacks to using  $K - \omega$  SST over other models:

- The  $K - \varepsilon$  model is less accurate and efficient in separating flows from the region for boundary layer problems. The  $K - \omega$  model, on the other hand, is less effective towards the viscous sub-layer (a layer that is formed very close to the wall where the flow is laminar).  $K - \omega$  SST combines both models and employs blending functions instead of damping functions to accurately anticipate flow and viscous sub-layer separation.
- When estimating boundary layers with adverse pressure gradients,  $K - \varepsilon$  is ineffective. When shocks are present in the flow, this prediction becomes considerably worse.
- Because all of the models discussed below use two transport equations, the computational time and costs are the same for all of them, with the exception of the correctness of the solution for each model.

#### 2.4.4 Cell zone and boundary condition

The cell zone and boundary conditions define the thermal and flow variables at the physical model's edges. As a result, they're an important part of the Ansys Fluent simulation. The cell zone option is in charge of deciding which material will be used in the simulation. Ansys Fluent has a variety of materials to choose from in its material database, and the material chosen must be defined in the cell zone configuration option. The Cold spray process uses nitrogen as a processing gas, and each gas in Ansys Fluent is divided into two categories: real gas and ideal gas. Choosing the right gas model is a difficult element of the simulation since it affects the computational time, resources, and, in certain cases, simulation outcomes. A detailed argument for choosing the appropriate gas model is mentioned in the upcoming segments.

#### 2.4.4.1 Choosing between real gas Vs ideal gas

Real gas has the properties of a real gas, hence the name. An ideal gas is a theoretical gas, but an ideal gas has the properties of a theoretical gas. Particles in real gases are thought to have volume, so when a unit volume is measured, the particle volume is also taken into account. The intermolecular forces are also taken into consideration for the real gas due to the particle volume. In an ideal gas, however, the particle volume is always minimal, and hence no particle contact occurs.

- ***Ideal gas law***

The ideal gas law is used to describe gases that have perfect elastic collisions, have no volume, and do not interact with other particles. The ideal gas law is written as follows:

$$PV = nRT \quad (43)$$

- ***Real gas law***

Under normal circumstances, many real gases behave like ideal gases. Air, nitrogen, oxygen, carbon dioxide, and noble gases, for example, all follow the ideal gas law near ambient temperature and atmospheric pressure. The behavior of real gases, on the other hand, differs from that of ideal gases in various ways [9]:

- ***High pressure*** Gas particles are brought together close enough to interact under high pressure. The particle volume is also more important because the distance between molecules is less.
- ***Low temperature*** At low temperatures, gas atoms and molecules have less kinetic energy. Particle interactions and energy expended in collisions are important because they travel slowly enough. A real gas, unlike an ideal gas, can become a liquid or solid.

Real gas law is represented as the Van der Waals equation:

$$\left[ P + \frac{an^2}{V^2} \right] (V - nb) = nRT \quad (44)$$

The correction factor that accounts for intermolecular attractions is  $a(n^2/v^2)$ , and the correction factor for the finite size of the molecules is  $nb$ .

There are no major differences between real gas simulation and ideal gas simulation based on simulation results and study findings. In chapter 4 of this report, the simulated results for various real and ideal gases are discussed. It is safer to utilize ideal gas for simulation when the entire fluid flow regime is studied and real gas to investigate a control volume in the flow regime for cold spray nozzle simulation where the pressure and temperature are in the range of 1.0 – 5.0 MPa and 100 – 800 °C, respectively.

#### 2.4.4.2 Boundary conditions

The information on the flow variables at the domain boundaries is specified using boundary conditions. Ansys Fluent provides ten types of boundary zone types for the specification of flow in inlets and exits. Boundaries indicate inlet, outlet, fluxes of mass, momentum, energy, and so on. Identifying the position of the boundaries entails defining boundary conditions based on the information available (e.g., inlets, walls, symmetry). Inlet pressure and inlet temperature are supplied for CS nozzle simulation, and they are based on the pressure inlet condition, which is used to specify the fluid pressure at flow inlets, as well as all other scalar properties of the flow. When the inlet pressure is known but the mass flow rate or velocity of the flow is unknown, the pressure inlet condition can be employed.

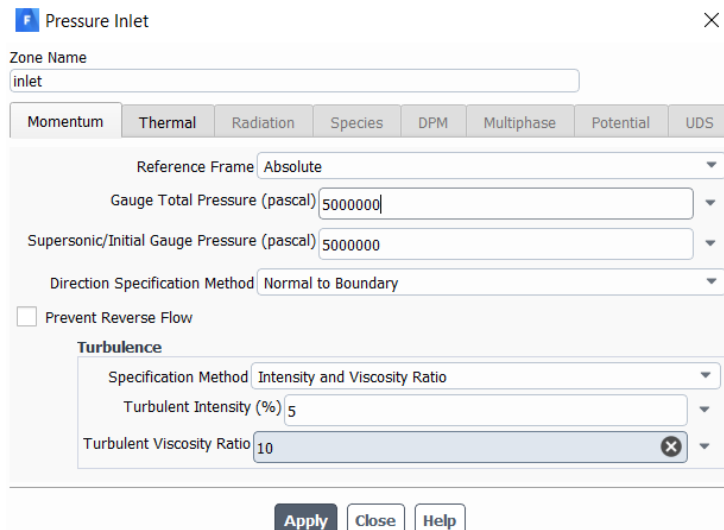


Figure 2.14: Representation of pressure inlet dialogue box

Figure 2.14 represents the pressure inlet dialogue box that can be activated from the boundary conditions task page. Temperature is set on the thermal sub-tab.

- **Reference frame:** It refers to the geometry's meshing properties. A fixed mesh is represented by the absolute frame, whereas a mobile mesh is represented by the relative frame.
- **Gauge total pressure:** It is the known inlet pressure value, while the total pressure value is the gauge pressure value for the operating pressure set in the operating conditions dialog box.
- **Supersonic/Initial gauge pressure:** When the flow becomes (locally) supersonic, the static pressure on the boundary is established. If the pressure inlet boundary condition is selected for computing initial values, it is also used to compute initial values for pressure, temperature, and velocity.
- **Turbulent intensity:** It's the ratio of the velocity fluctuation's root – mean – square to the mean flow velocity. A turbulence intensity of 1% is considered extremely low, while a

turbulent intensity of 10% is considered extremely high. The turbulent intensity of internal flows, such as the CS application, is determined by the flow history upstream. Low intensity might be employed if the flow is underdeveloped. The turbulence intensity can be as high as a few percent if the flow has fully evolved at the upstream flow. According to the formula, the turbulence intensity would be 4% at a Reynolds number of 50,000 [13].

- **Turbulent viscosity ratio:** Turbulent viscosity ratio is directly proportional to the turbulent Reynolds number. Typically, the turbulent parameter is set between 1 to 10.

#### 2.4.5 Inflation layer

If unstructured (tetrahedral, triangular, or polyhedral) meshes are used for *CFD* applications, inflation layers or prism layers on the geometry's surface should be considered. These are thin layers of cells grown parallel to the surface to aid in the resolution of velocity and temperature profiles close to the wall, allowing for more precise predictions of the heat transfer coefficient and wall shear stress. Some considerations must be made before moving on to the equation that can solve for the inflation layer.

- **The necessity of inflation layers** The gradients of flow variables are kept at the cell centroid or center of the meshes after the equations given above are solved. The gradients are far away from each cell in a mesh without any inflating layers near the wall, and the flow variables vary linearly across the cells. Because of the no-slip condition, the flow variable gradients near the wall tend to vary very steeply normal to the surface. Because the variation between the centroids can be recorded linearly by the *CFD* solution, a large number of tiny cells must be used where the flow variable fluctuation is steep.
- **Boundary-layer thickness** An imaginary layer created normal to the surface or boundary along the flow direction is known as a boundary layer thickness. The thickness depicts the variations in flow variables caused by no-slip and turbulent circumstances, with the highest point (far away from the surface) representing the flow attempting to maintain 99 percent of its free stream velocity.

The velocity profile of fluid on a flat surface is depicted in Figure 2.15. The velocity of a laminar flow is virtually zero near the surface and maximally far away from it. As a result, the velocity profile for laminar flow has a parabolic shape. The transition area is when laminar to turbulent flow transitions. The velocity profile of a turbulent flow is the time-averaged value at all locations on the curve. The crucial point to note is that the velocity profile along the wall fluctuates significantly more slowly than the velocity profile normal to the wall. Numerous thin cells should be implemented near the surfaces due to the variance of velocities in different sections of the geometry and to capture the difference in gradients. The importance of inflation layers can be summarized as follows:

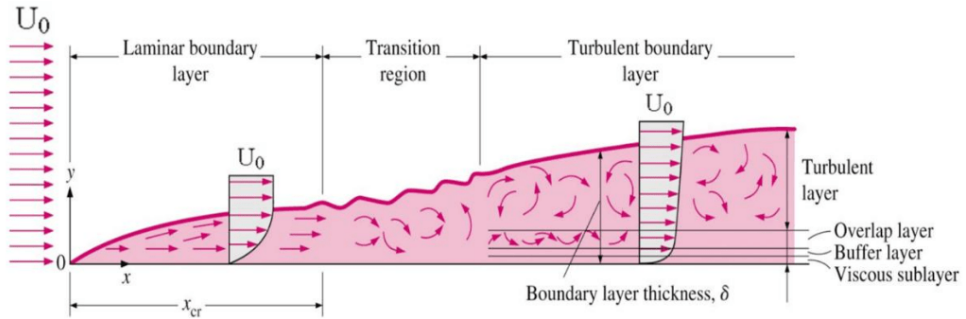


Figure 2.15: Representation of boundary layer thickness [27]

- Inflation layers provide reliable results at the surface for unstructured meshes.
- Close enough gradients at the surface should represent the severe variation in flow characteristics.
- The thickness of the boundary layer should always be lower than the thickness of the inflating layers.
- In turbulent flows, a viscous sub-layer is present very close to the surface where the flow is always laminar, and a buffer layer is present away from the sub-layer where the flow tends to change from laminar to turbulent, requiring a very thin and numerous Inflation layers to capture those variable changes.

Now that the need for an inflation layer for the mesh has been established, the user must choose various settings based on the application. The following are the various parameters:

1. **Height of the first layer  $y_H$ :** The thickness of the first cell,  $y_H$ , is the height of the centroid from the wall, and  $y_P$  is the height of the centroid from the wall. To reach a desired value of  $y^+$ , the first layer height is supplied. Because the value of  $y^+$  should develop correctly throughout the simulation process, even if the free stream flow conditions or shape of the geometry changes, it is dimensionless. The following is the equation for determining the first layer height:

$$y^+ = \frac{\rho u_\tau y_P}{\mu} \quad (45)$$

The velocity  $u_\tau$  represented here uses wall shear stress that occurs near the surface of the boundary.

2. **Number of layers  $N$  and Geometric growth  $G$ :** The number of inflation layers that must be generated must always be more than the boundary layer. Every inflation layer that forms is always larger than the one before it, and the total number of layers formed is:

$$y_T = y_H \frac{1 - G^N}{1 - G} \quad (46)$$

Now that the whole height of inflation layers has been represented, there are two independent variables ( $G$ ) and multiple layers ( $N$ ). To solve this, assume that the inflation layer ( $y_T$ ) is equal to the thickness of the boundary layer ( $\delta$ ).

$$\delta_{99} = y_H \frac{1 - G^N}{1 - G} \quad (47)$$

This assumption allows the user to verify that the inflating layers, regardless of their number or size, always match the thickness of the border layer. The growth rate represents the increase in element edge length with each succeeding layer of elements from the edge or face. A growth rate of 1.2 results in a 20% increase in element edge length with each succeeding layer of elements. The recommended growth ratio is between 1.05 and 1.3.

#### 2.4.6 Gradients

Gradients indicate the transformation of any variable from its starting to its final state. To calculate the gradients that represent those changes, OpenFOAM, Ansys Fluent, and Star CCM use three different approaches. The variable data is always saved at the cell centroid of the meshes, as previously stated. This information is utilized to determine the gradients on the faces of the cells, which can be regarded as the simulation's ultimate solution. The variable that changes in temperature, and the gradient of temperature in cartesian co-ordinates is expressed as:

$$\nabla T = \left( \frac{\partial T}{\partial x}, \frac{\partial T}{\partial y}, \frac{\partial T}{\partial z} \right) \quad (48)$$

This indicates the temperature change in all three cell locations. These gradients can be estimated in two dimensions (2-D) and three dimensions (3-D), with three-dimensional cells having several faces pointing in different directions. The following are the primary reasons why a gradient is required in *CFD* simulation:

- Discretization schemes in convection terms, linear upwind differencing
- Non-orthogonal correctors
- Source terms

The gradient of 1-D cells is shown in Figure 2.16, where  $T_p$  denotes the temperature of a cell centroid. The face value ( $T_f$ ) of that particular cell can be computed if the gradient at the cell centroid ( $\nabla T$ ) is known. The gradient's principal purpose is to extrapolate from the cell centroid and calculate the face values of each cell using that information.

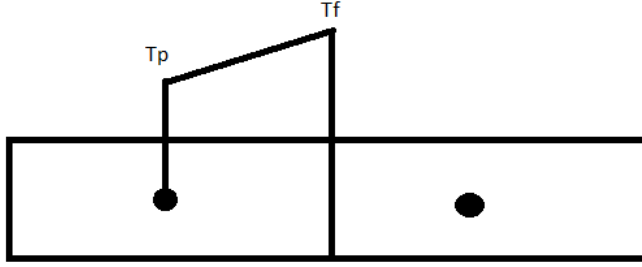


Figure 2.16: Representation of 1-D gradient calculation

Consider a 1-D cell, as shown in figure 2.17, to determine the gradients and face value. The gradient at the cell's face will be determined by the difference between  $T_p$  and  $T_n$ , as well as the actual distance between the two cells ( $d_{pn}$ ).

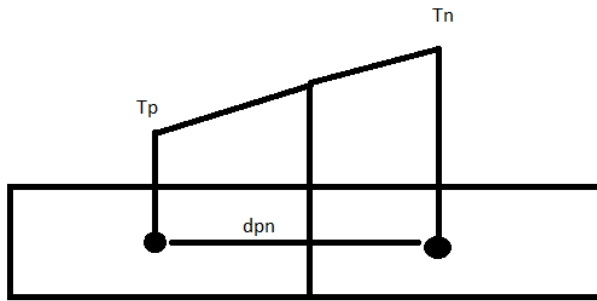


Figure 2.17: Representation of gradient face value

The final equation for calculating the gradient at the face of the cell in 1-D is given as:

$$(\nabla T)_f = \left( \frac{T_N - T_P}{d_{PN}}, 0, 0 \right) \quad (49)$$

#### 2.4.6.1 Green–Gauss method

To calculate the face values and gradients, the Green–Gauss technique employs the divergence theorem for a generic vector field. Every *CFD* code employs three major methods:

- Green–Gauss cell-based
- Green–Gauss node based
- Least–Squares

The divergence theorem of a particular field is the volume integral of that particular field is equal to the surface integral of fluxes that are accumulated out of that volume considered. This can be physically imagined by considering a box containing a substance which is the volume integral of that substance and the fluxes that are produced onto the surface by the substance

is the surface integral of that substance. Consider a polyhedral cell and substitute the surface integral with the surface integral over each face of the cells to determine gradients in 3-D cells.

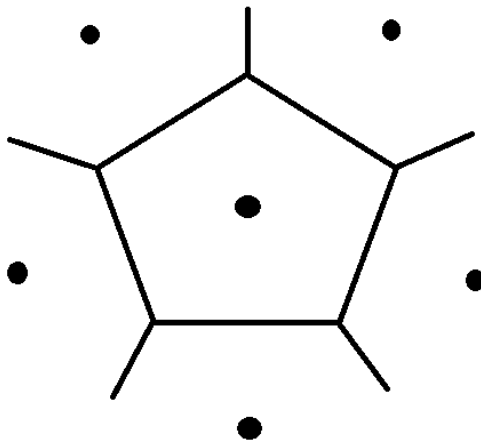


Figure 2.18: Representation of a 3-D cell

Figure 2.18 represents a part of the 3-D cell, which has multiple faces. Instead of taking the surface integral over the entire surface, a series of surface integral are taken for each side of the cell and added to give a summation equation:

$$\int_V [\nabla T] dV = \sum_N \int_S [T \hat{n}] dS \quad (50)$$

This equation tells that the volume integral of the centroid of that cell temperature is equal to the surface integral of temperature fluxes on each side of the cell.

If the second-order finite volume method is used, the variation of quantities across those faces will be linear, which means that the temperature value at the ends of the cell will be stored linearly at the center of the faces, and the variation between them will be stored linearly at the center of the faces. As a result, the integral over the surface equals the value at the face's center multiplied by the area. Selecting the temperature gradient at the cell center and multiplying it by the volume, can be utilized to rewrite the volume integral. This removes the integral from equations that are simple to calculate for the gradient.

$$(\nabla T)_p = \frac{1}{V_p} \sum_N [T_f \hat{n}_f A_f] \quad (51)$$

The most simplest approach for obtaining gradient is as follows:

1. Get the face center value ( $T_f, P_f$  etc.,)
2. Multiply by the normal vector and the area ( $\hat{n}A_f$ )
3. Add up the contribution from each face ( $\sum N$ )

4. Divide by the cell volume ( $V_p$ )

- ***Green–Gauss cell-based***

The Green–Gauss cell-based technique calculates the face value  $T_f$  on the face of the two connecting cells by interpolating between the owner and the neighboring cell. If the face is relatively close to one of the cells, linear interpolation will favor that cell. Because the values of the centroids of the two cells were implicitly utilized to border that face, this is referred to as a cell-based method. The following is a representation of the equation:

$$T_f = T_P f + T_N (1 - f) \quad (52)$$

- ***Green–Gauss node-based***

The node-based method is an alternative to the cell-based scheme, in which the temperatures of all the nodes that surround the face are summed up. To compute the temperature at the center of the face, the temperatures at the nodes are added together and averaged. The equation for a node-based architecture is:

$$T_f = \frac{1}{N_{\text{Nodes}}} \sum_{\text{Nodes}} T_{\text{Node}} \quad (53)$$

On orthogonal meshes, the Green–Gauss cell-based technique for determining  $T_f$  has a skewness error. This means that when the center points of two cells do not meet at the same position, the centroid of one cell is not equal to the centroid of the other, and this is the skewness error that the cells share. The node-based technique, on the other hand, does not have this skewness mistake since the values are calculated at the nodes of the cells. However, computing the values at the node is a time-consuming task when compared to the cell-based method. On bad and unstructured meshes, least squares and Green–Gauss node–based methods should be favored because they do not have skewness mistakes.

#### 2.4.6.2 Least–squares

When compared to the different gradient schemes that can be utilized in the *CFD* code, the least-squares gradient scheme is the most preferred. The least-square technique, unlike the Green–Gauss approach, does not require any face values to calculate the variable gradients. Rather, it solves for the gradients via error interpolation and matrix multiplication. To begin, use the equation in figure 2.17, where  $T_p$  is the temperature of a cell at the centroid and  $T_n$  is the temperature of a cell adjacent to it. The distance between these two-cell centroids is given as  $d_{pn}$ , and the gradient between them is  $(\nabla T)_p$ , which must be determined.

$$T_N = T_P + d_{PN} \cdot (\nabla T)_p \quad (54)$$

In addition, by considering the distance from the cell centroid and extrapolating using the gradient and the distance vector, equation 54 may be written for all of the cell's faces. For each face, the distance vector and the nearby temperature  $T_n$  will be different.

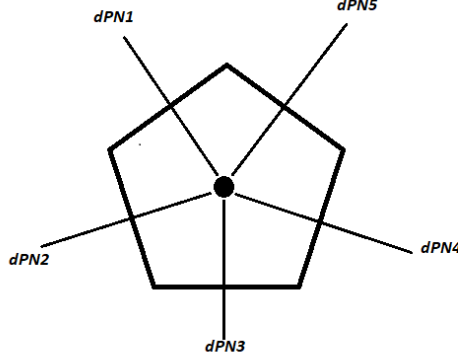


Figure 2.19: Representation of cell centroid distance

$(\nabla T)_p$  is the distance between the cell centroid and each neighboring cell in each equation constructed from each face of the cell, and  $d_{p_n}$  is the distance between the cell centroid and each neighboring cell. These equations can be recast as matrices, but there's a problem: these matrices produce a non-square matrix. The non-square matrix is difficult to calculate and even more difficult to solve precisely. But the greatest trick of the least square is that an approximate solution for  $(\nabla T)_p$  may be computed using all of the equations from the faces, and each approximation of  $(\nabla T)_p$  introduces an inaccuracy into the calculation.

The least-square approach minimizes error numbers by taking each of these errors, squaring them, and then adding them together. This method will provide an approximate solution that minimizes the error vector's sum of squared errors. The least-squares solution is as follows:

$$(\nabla T)_P = G^{-1}d^T (T_N - T_P) \quad (55)$$

The main disadvantage of least-squares is that when applied near boundary layers with a large aspect ratio, the stream wise gradients dominate the gradients. This means that near the surface, inflation layers arise to capture flow variables, and these inflation layers have very tiny distance vectors normal to the wall and very long distance vectors along the wall. Where the distance vectors are large, the temperature gradient computation tends to be dominated by equation 56. This is undesirable for boundary layer problems because temperature changes most quickly in the direction normal to the wall, whereas variations along the wall are minor. This means that if the least-squares gradient technique is utilized in its current form, the gradient will be dominated by stream-wise cells, resulting in erroneous results. Least-squares introduces a weighting formula to accommodate for this issue:

$$w = 1/|d| \quad (56)$$

By adding this function, where the distance is very small in the distance normal to the wall the weighting is going to be very large, and conversely in the stream-wise direction that weighting function becomes very small. This weighting function is multiplied by all the equations that were occurred from the faces of the cells, and the final equation is changed from equation 55:

$$(\nabla T)_P = G^{-1} d^T W^T W (T_N - T_P) \quad (57)$$

#### 2.4.6.3 Choosing the appropriate gradient method

Every gradient method available in *CFD* codes is addressed, and the best gradient method is always determined by the application as well as the computing time and costs. The following is an overview of how to choose the right gradient method for your *CS* application:

- The Green–Gauss cell-based approach calculates the face values of a cell by interpolating between two cells. This approach, however, has a skewness issue and cannot be used for unstructured meshes, which are the most common in real-life scenarios.
- The Green–Gauss node-based approach calculates the variables using the nodes of two cells and interpolates them to obtain a face value in the center of the face. Because this approach has no skewness errors, it can be utilized on unstructured meshes. This strategy, however, is a long shot and requires a lot of computer power.
- This leaves the least–squares approach, which calculates the gradient without using the face values or the divergence theorem. Instead, it uses matrices and error approximation, which utilizes fewer computer resources than previous approaches. It also employs a weighted function to adjust for thin boundary cells, resulting in extremely precise findings at the surface.

#### 2.4.7 Residuals

The residual, also known as the raw residual, is a local imbalance function that is used to extract unique and required solutions from a simulation by adding them to the equations. This local imbalance function can be thought of as an extra term that is added to all of the equations presented previously. To comprehend the physical significance of residuals, examine the following example.

A 1-D heat conduction bar is considered with a hot and cold surface on either side of the bar and the temperature flow is from a hot to a cold surface. For clarity, the temperature variable is used as an example; however, all of the available variables function in the same way. Meshing has now divided this bar into pieces, and the gradients have been recorded at the centroid of each cell. In this simple example, assuming there are no sources of heat on the bar, the analytical findings will be a linear solution. If there are no heat sources on the bar, the temperature

profile will be non-linear, causing temperature fluctuations between the centroid to be missed. By considering a cell from the bar and the heat flux from nearby cells, Fourier's law of heat conduction is employed to solve the problem numerically. The general form is as follows:

$$A_{21}T_1 + A_{22}T_2 + A_{23}T_3 + A_{24}T_4 = B_2 \quad (58)$$

The thermal conductivity areas and distances are represented by coefficient  $A$ , while the heat source term is represented by coefficient  $B$ . To answer the problem, this generic form can be written for all of the cells in the bar, making a matrix.

$$AT = B \quad (59)$$

For the temperature vector  $T$ , the matrix equation can be solved, and the result is the temperature at the centroid of each cell. The heat fluxes across each of the faces can be estimated using the temperature gradient of those cells once the temperature at the centroid has been calculated. Now, with only one overall iteration of the solver, this strategy is a direct single approach to calculating the temperature. *CFD* algorithms, in general, employ an iterative approach to find the answer, which means that solving the temperature equation may require numerous attempts. This iterative method tends to result in convergence, with the temperature profile matching the final profile. The temperature profile approaches the ultimate linear profile during the iterative procedure, however, when compared to the numerical analysis, the numerical solution contains some mistakes in the gradients. The numerical method solution gradients do not match the final linear solution because the solution is not converged and the temperature profile does not match the exact solution. As a result, the heat flux across the cell does not correspond to the final solution. Because of the gradient, the heat flux does not match the final solution before convergence, and as a result, energy is not conserved. This missing local energy imbalance is the residual, which may be added to the matrix equation to generate the following new matrix equation:

$$AT - B = r \quad (60)$$

In this case,  $r$  is a vector of residual values for all of the mesh cells. The closer  $r$  gets to zero, the more exact the solution will be. The solution temperature determined from equation 59 is substituted in equation 60, which determines the residual for each cell in the mesh, throughout the iterative solution process.

### Convergence

The phrase convergence refers to the one-of-a-kind solution that an iterative solver can find for a given problem. When the residual vector reaches 0, the solution is unique. However, the residual vector will never be exactly zero due to the solvers on machines with finite precision and a finite number of decimal places. This allowed the user to decide whether the iterative

solution was sufficiently converged. Every mesh in the cell has its residual factor, and some imbalance residuals are substantially greater at some places of the mesh than others. Instead of looking at each residual and charting the residual for each cell of the mesh, users can make a representative residual from all of the residuals by taking an average, and if the representative residual stops moving, we know the *CFD* simulation is approaching convergence. It's easier to track a representative residual than the complete vector field. Although linear algebra makes calculating a representative residual for small geometry simple, *CFD* codes with 10 million cells require sophisticated normalization to solve for residuals. Three types of representative residuals are used in every *CFD* code:

- ***L1 norm*** The summation of the magnitude of each residual vector component.
- ***L2 norm*** It is also called the euclidean norm and it is represented by taking the magnitude of all the vectors and providing a summation to those vectors.
- ***L(infinity) norm*** It takes the maximum absolute value of the residuals that can be used as the representative residual.

Scaling of residuals is enabled by default, and the default convergence criterion for energy and P-1 equations is  $1e^{-6}$ , and for all other equations, it is  $1e^{-3}$ .

#### • Choosing appropriate residuals and judging convergence

- The computational sources employed to solve the problem are used to choose a residual vector for the equation. A low residual rate of  $1e^{-6}$  can be used if the computer is a high-performance system. If the computational resources aren't particularly powerful, a safe figure of  $1e^{-4}$  can be employed. Ansys Fluent uses  $1e^{-3}$  for various equation quantities by default.
- Although there is no uniform method for determining the solution's convergence, it can be determined by measuring residual levels and monitoring key integrated parameters such as drag or heat transfer coefficient.
- In some equations, such as turbulence quantities, poor initial estimations can result in high-scale factors. In such circumstances, scaled residuals will begin low, increase as non-linear sources increase, and eventually drop. As a result, it's a good idea to evaluate convergence not just in terms of the value of the residual, but also in terms of how it behaves. The residual should continue to reduce for multiple iterations, according to the users.
- Another frequent method for determining convergence is to look at the unscaled residuals and see if they have dropped by three orders of magnitude. This indicates that the residual graph will start at 1 when the simulation begins, and after some time or 10 iterations, the residual should reduce by  $1e^{-3}$ . This, however, is contingent on the user's physics and initial assumptions [13].

## 2.5 ESSS Rocky DEM

ESSS Rocky is a particle simulator application that allows the user to simulate the behavior of particles by taking the fluid flow into account. Industries such as mining, oil and gas, waste disposal, energy, and chemical and nuclear which involve the simultaneous flow of fluids and particles. In all of these circumstances, the fluid flow must be taken into account for the particles to behave correctly. Designing and scaling up such processes, as well as optimizing them, necessitates a thorough grasp of thermo-hydrodynamics, which is governed by particle-level interactions between fluids, particles, and barriers. As a result, dealing with granular-fluid systems necessitates a modeling method.

Modeling these systems is difficult due to the intricacy of the fluid-solid flux involved. The principal source of difficulty is variances in order of size among the problem's characteristic scales. First and foremost, there is the device scale, which is dutifully followed. Second, in a *CFD* solution, the typical fluid-flow sizes are captured by solving the flow at the mesh scale, which is typically much larger than the particle but still fairly small when compared to the device scale. Finally, there is the scale of the fluid-particle interaction, which has the magnitude of the smaller particles, making solving the flow in a sub-particle resolution computationally impractical for most industrial applications.

Since it can represent the discrete nature of the particle phase while keeping computational tractability, the linked *DEM-CFD* technique is a potential alternative for simulating granular-fluid systems. Instead of calculating the fluid field at the precise particle level, this is performed by solving it at the cell level. This technique broadens the variety of equipment and processes that can be evaluated with numerical simulations by reducing the number of fluid calculations necessary [12].

The advantages of employing the *DEM-CFD* linked approach over *CFD* alone are stated below:

- Unlike continuous approaches, particle-particle interactions are taken into account by simulating the motion of each particle. As a result, there is no need to supply state-motion equations for granular systems, which are notoriously difficult to derive.
- Similarly, low particle size concentration has no limitations, and particle size distribution can be easily prescribed without raising the computational cost of the *CFD* solver.
- It is possible to work with particles that are not spherical.
- Modeling the attractive force between two particles and between particles and walls can be used to simulate adhesive-cohesive materials.
- Heat transport between particles and particle walls, as well as convective heat transfer with the fluid, can all be considered.

## 2.5.1 Governing equations

The fluid flow in the rocky-fluent coupling is calculated using Ansys Fluent's traditional continuum technique, in which the conservation equations for mass, momentum, and energy are solved using the finite volume method. Within rocky, the discrete technique is used to represent the solid phase flow. Because of the interaction between phases, interphase momentum and heat transfer parameters are used to achieve solid-liquid coupling. The governing equations for the fluid and solid phases are supplied in this part, as well as a detailed description of the coupling process.

### 2.5.1.1 Particle phase modeling

The translational and rotational motion of a particle, as well as the energy balance in the particle, are the two primary features of particle-phase modeling.

- ***Translational and rotational motion of particle***

The *DEM* tracks all particles within the computational domain in a Lagrangian way by directly solving Euler's first and second laws, which govern translational and rotational particle motion, respectively:

$$m_p \frac{d\mathbf{v}_p}{dt} = \mathbf{F}_c + \mathbf{F}_{f \rightarrow p} + m_p \mathbf{g} \quad (61)$$

$$J_p \frac{d\boldsymbol{\omega}_p}{dt} = \mathbf{M}_c + \mathbf{M}_{f \rightarrow p} \quad (62)$$

When compared to a pure *DEM* simulation, two additional terms occur due to the fluid interaction:  $\mathbf{M}_{f \rightarrow p}$  is the additional torque due to the fluid phase velocity gradient, and  $\mathbf{F}_{f \rightarrow p}$  is the additional force accounting for the interaction with the fluid phase.

- ***Energy balance in the particle***

When the thermal model is enabled, an additional equation for energy balance is solved in addition to the equations regulating particle motion. The differential equation can be used to calculate the temperature variation of a particle over time:

$$m_p c_p \frac{dT_p}{dt} = \dot{q} \quad (63)$$

where  $C_p$  is the specific heat of the particle material and  $\dot{q}$  is the total particle heat transfer rate. This heat transfer rate accounts for the heat transfer that occurs during the contact with other particles or walls,  $\dot{q}_c$ , and the convective heat transfer between particle and fluid phase,  $\dot{q}_{f \rightarrow p}$ , according to the expression

$$\dot{q} = \dot{q}_c + \dot{q}_{f \rightarrow p} \quad (64)$$

### 2.5.1.2 Fluid modeling

Rocky's fluid modeling provides two methods for performing two-way interaction between particles and fluid. This part would be limited to the single-phase coupling technique because the *CS* problem uses a single-phase liquid. Rocky has one-way and two-way coupling methods, in which the fluid does not influence the particle in the one-way method, but the fluid influences the simulation particle in the two-way method.

#### Single-phase coupling

When the multiphase model is disabled in the Fluent case, Rocky modifies the Fluent setup to treat the *DEM* particles as porous media and allocate momentum and energy source terms (that account for fluid-particle interactions) generated by Rocky during coupled simulations to the fluid phase. As the simulation advances, the solid phase concentration affects the porosity distribution of the domain.

### 2.5.2 One-way coupling

One-way coupling is when the fluid used in the simulation has no effect on the particles that are simulated utilizing Rocky. Even though the fluid does not affect the particles, a steady-state simulation setup with a large number of cells and improved convergence is required to give the initial variables for the particles to simulate. To build up a successful simulation using Rocky, a series of conditions must be met.

- ***Mesh generation***

The one-way coupling approach applies standard *CFD* mesh creation suggestions to *DEM-CFD* coupling instances. Apply denser meshes in zones with substantial quantity gradients, for example, to avoid poor-quality cells and large differences in nearby cell volumes. Because there is no information transfer from Rocky into the *CFD* solution, it is assumed that the particles have no effect on the flow field in the one-way coupling technique. As a result, the coupling scheme itself does not impose any additional recommendations or constraints in the *CFD* simulation. As a result, the user must concentrate on giving the greatest possible *CFD* simulation.

- ***Simulation setup***

For different applications, the simulation setup for the one-way coupling differs. The simulation setup would remain the same for the application of *CS*. For more precise outcomes, a finer mesh might be created. If the thermal mode is active, the heat transfer between the Fluent and Rocky should be activated as well.

- **One-way coupling limitations**

Data is passed from one solution to another in only one direction in a one-way coupling simulation. In this example, the *CFD* solution informs the *DEM* solution, i.e., the fluid flow impacts the particle trajectory but the particles have no effect on it.

Furthermore, the implementation of a one-way coupling simulation, as currently done by Rocky, necessitates Fluent exporting the *CFD* domain's steady-state solution. Rocky uses this constant information about the fluid flow during the simulation; there is no need for a companion Fluent process because the *CFD* domain's steady-state does not vary over time. As a result, one of the inherent limitations of the one-way coupling with Fluent is that the *CFD* domain's transient state is not simulated.

When Fluent exports the steady-state solution to Rocky, it checks the following conditions:

- Meshes that move or adapt are not supported.
- Polyhedral cells around shadow boundaries are not supported in meshes.

### 2.5.3 Simulation parameters

Setting simulation parameters entails configuring global settings as well as parameters particular to particles, geometries, materials, interactions, and inputs, among other things. A list of important simulation parameters and their threshold values for each parameter are discussed below.

#### 2.5.3.1 Physics parameter

Rocky gives the user the option of selecting from four different physics parameters: gravity, momentum, heat, and coarse-grain. Because of the pushing force supplied by the fluid in the *x*-direction, gravity in all directions would be zero for the *CS* application. Because Ansys Fluent uses the energy equation, the thermal model should be enabled for *CS* applications.

#### 2.5.3.2 Geometry parameter

Once the geometry has been imported from Ansys Fluent, Rocky provides three choices for generating inlets. The user can make a feed conveyor for a mining application, as well as an inlet option that lets them make a rectangular or circle inlet. A circle inlet is provided at the nozzle's converging section for *CS* application.

#### 2.5.3.3 Particle parameter

Rocky allows the user to specify unique particles with numerous shapes and sizes. Custom particle shapes and sizes can be added to the Rocky. The sizes of the particles can be obtained

from the “Size type” option which consists of sieve size which represents the dimension of a square hole just big enough for the particle to pass through. Equivalent sphere diameter, particle size will be based on the diameter of a sphere equivalent to volume as the shape being measured. Original shapes represent the custom particle shapes. For each cumulative percent provided, a range of sizes within the size parameter will be used if more than one size is specified for a particle set. Only the smallest size value, which has no range, is an exception. Particle diameters should be arranged in descending order with the cumulative.

#### **2.5.3.4 Particle input**

Rocky features two types of particle input, the first of which is a continuous injection, which delivers particles one by one in a continuous stream dependent on the simulation time. Volume Fill, on the other hand, fills a constrained volume selected by the user with particles, and the particles tend to simulate at the same moment once the simulation begins. Continuous injection should be employed for an application like *CS* because the particle does not need to be gathered at one spot. The inlet defined in geometry would be the entry point for particle input. If relevant, the particle mass flow rate and temperature should be specified, as well as the particle’s entry target normal velocity.

#### **2.5.3.5 Solver parameter**

During one-way coupling, Rocky is enabled with the option which can be displayed in the data editors. For one-way coupling thermal model should be enabled from the *CFD* coupling option from data editors because of the usage of the energy equation in *CFD* simulation. From the solver editor simulation duration, fluent output frequency multiplier and the number of processors can be decided. While calculating the simulation duration length and speed of the conveyors, the mass flow rate of the particles and steady-state should be considered. The output frequency is determined for Fluent two-way coupling and it determines the ratio of Rocky files saved to Fluent files saved. In the general tab, the “Release particles without Overlap check” option is displayed which means during the simulation when the continuous injection option is selected the particles will be injected continuously without any overlap. This can be disabled for other applications provided with the time for each particle to be overlapped. Several processors can also be chosen based on the requirements of the computational resources.



## **3 Methodology**

The Ansys Fluent and ESSS Rocky simulation methodologies are described in this chapter, with the Ansys Fluent methods classified into two categories: numerical approach and simulation approach. This chapter presents the final simulation methods, with chapter 4 describing several comparisons and graphs.

### **3.1 Ansys Fluent**

This is the final simulation technique, which uses a 90-degree geometry rather than the 360-degree geometry discussed later in this section. There are two sorts of simulation methods: numerical and simulation approaches. The numerical strategy covers how to solve the equations stated in the thrust equations (2.2.1.5), whereas the simulation approach describes the entire setup for running a simulation successfully.

#### **3.1.1 Numerical approach**

Every engineering problem should start with a numerical solution, then a simulation, and finally an experimental solution. When all three methodologies are considered, a value that is equivalent in each should be enough to get a good engineering result.

- **Reynolds number** For the cold spray nozzle, the first step would be finding the fluid behavior inside the nozzle using Reynolds number. From Reynolds equation 1, the values of the variables are represented as

1.  $\rho$  - Density of the nitrogen fluid =  $1.165 \text{ (Kg/m}^3\text{)}$
2.  $u$  - Velocity of the nitrogen fluid =  $16 \text{ (m/s)}$  (*This velocity is computed by first using the thrust equation to calculate the throat velocity, and then using the velocity in the Bernoulli's equation to get an approximated inlet value*)
3.  $L$  - Characteristic length =  $0.109795 \text{ m}$  (*represents the whole length of the nozzle*)
4.  $\mu$  - Dynamic viscosity =  $0.9 \times 10^{-5} \text{ Kg/ms}$

The final Reynolds number value is represented by substituting the above values in the equation.

$$Re = 227.397 \times 10^3$$

The turbulent character of the fluid inside the CS nozzle is represented by the Reynolds number above. The fluid's turbulent character aids in the production of shock diamonds outside the nozzle exit, as well as allowing the particle to proceed in a linear path for maximum efficiency.

- ***Choked flow condition***

The next step would be to determine whether or not the nozzle used in the CS application is choked. The nozzle can have a supersonic condition at the diverging section and a sonic condition at the throat section because of the choked flow. To achieve a choked flow situation, a nozzle must satisfy the equation:

$$\frac{P_b}{P_0} \leq \frac{P^*}{P_0} \quad (65)$$

1. Dimensionless critical pressure ratio = 0.528 (*can be calculated from steam tables*)
2.  $P_b$  - Back pressure (or) Atmospheric pressure = 1.01325 bar
3.  $P_0$  - Stagnation pressure (or) Inlet pressure = 50 bar

By substituting the above values in the equation, the final choked flow condition value for the given nozzle geometry is represented as:

$$\frac{P_b}{P_0} = 0.020 < 0.528 \frac{P^*}{P_0} \quad (66)$$

As the choked flow condition is satisfied, then the choked flow equations can be used to calculate the throat parameters of the nozzle.

- ***Thrust equations***

After fulfilling the Reynolds number and choked flow conditions, thrust equations can be utilized to determine the nozzle's throat and exit condition parameters. To solve the throat and exit conditions, use equations 2.2.1.5 to 9 with the area, gas constant, specific heat ratio, inlet pressure, and temperature variables. In chapter 4, the basic geometry of the CS nozzle is shown.

1. Area at throat,  $A^* = 5.72 \text{ mm}^2$
2. Area at exit,  $A_e = 57.92 \text{ mm}^2$
3. Specific heat ratio,  $\gamma = 1.4$
4. Gas constant,  $R = 287 \text{ J/Kg} - K$
5. Inlet pressure (or) Total pressure,  $P_t = 50 \text{ bar}$
6. Inlet temperature (or) Total temperature,  $T_t = 1023.15 \text{ K}$

Parameters	Throat	Exit
Mass flow rate	0.588 $Kg/s$	0.588 $Kg/s$
Mach number	1 (Sonic condition)	3.93
Temperature	852.625 $K$	250.22 $K$
Pressure	42.97 bar	0.361 bar
Velocity	585.30 $m/s$	1246.1 $m/s$

Table 1: Numerical values for throat and exit condition

The low pressure indicates that the velocity is at its maximum, and the exit Mach number shows that the flow is supersonic. This is the first step in any simulation process, where a numerical approach must satisfy the fundamental physics equations to give a useful result. In the following chapter, a comparison with numerical and simulation results will be made for a better understanding of the results.

### 3.1.2 Simulation approach

*CFD* simulation comes into play when analyzing and comprehending fluids in a situation, as stated before in this report, and the cold spray nozzle is no stranger to *CFD* simulation. This part goes through how to create geometry from provided data, meshing characteristics, and simulation setup, which is all required for running simulations with Ansys Fluent and ESSS Rocky. The geometry was created using Solidworks software, a solid modeling computer-aided design, and a computer-aided engineering program. The Fluent meshing application that comes with the Ansys was used for the meshing. The steps for creating a cold spray nozzle simulation are outlined below.

#### 3.1.2.1 Geometry Creation

Because of the simplicity with which Solidworks can create 3-D models, it was chosen over Ansys' in-built designer module for geometry. In the workbench, Ansys is willing to accept any other third-party application extension. *KSS* solution (Kinetic Spray Solution) provides the nozzle dimension, which is a software product company that provides a unique software solution for numerous *CFD* solutions. *KSS* has a program that can compute the nozzle's parameters without using simulation methods. The goal of this thesis is to provide a better solution than *KSS* and to compare the result to the simulation approach.

To have a better solution during the simulation, the geometry is first built in 2-D and then changed to 3-D, and ESSS Rocky will only support 3-D objects in particle simulation.

Different views of the nozzle geometry built-in Solidworks with the given dimension are shown in Figure 3.2. This geometry is specifically built only with the nozzle, and an outside field should be created at the nozzle's exit (diverging section) to collect the shock diamonds generated outside the nozzle. To expand the high-pressure gas produced by the gas chamber, a front field

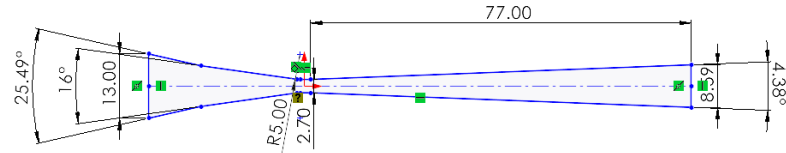


Figure 3.1: Nozzle dimension



Figure 3.2: Different views of nozzle

is created at the front of the converging section.

- **Front and far-field** The front and far fields are created at the converging and diverging sections of the nozzle respectively. The main reason for creating a far-field in the nozzle is to capture the supersonic shock diamonds that appear after the exit of the nozzle. The stand-off distance would be 100 mm, which is the maximum distance of the substrate from the diverging section.

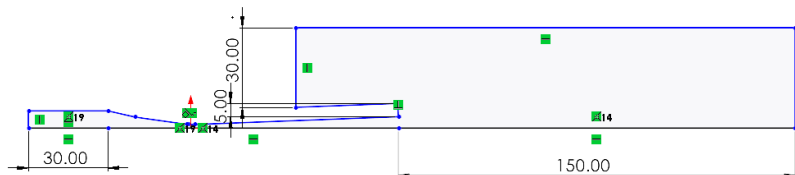


Figure 3.3: Front & far-field dimensions

The far field in figure 3.3 represents 150 mm from the nozzle's diverging portion, while the front field represents 30 mm outside the nozzle's converging section. Because of the hypothesis

presented in the section on sound speed, a 30 mm distant field has been expanded to the left of the diverging section. The thermodynamic characteristics to the left of the diverging section in the far-field change when a high-pressure shock region forms, whereas the thermodynamic properties to the right of the diverging section in the far-field are practically unchanged. An additional region has been built to meet this requirement and to improve shock formation.

- **Final geometry** The revolve function is used to turn the 2-D object into a 3-D object after establishing the outline of the geometry. The user can define the degree of rotation in Solidworks based on the application's options. Before designing the geometry and meshing, users should think about their computational resources and time. This crucial step would assist save a significant amount of computational resources and time. Even if the simulation result is unaffected by the change, it is usually recommended to use minimum extrusion of the geometry for applications that include cylindrical or circular shapes. As a result, instead of employing 360 degrees for the nozzle and surrounding fields, the simulation uses a 90-degree model geometry.

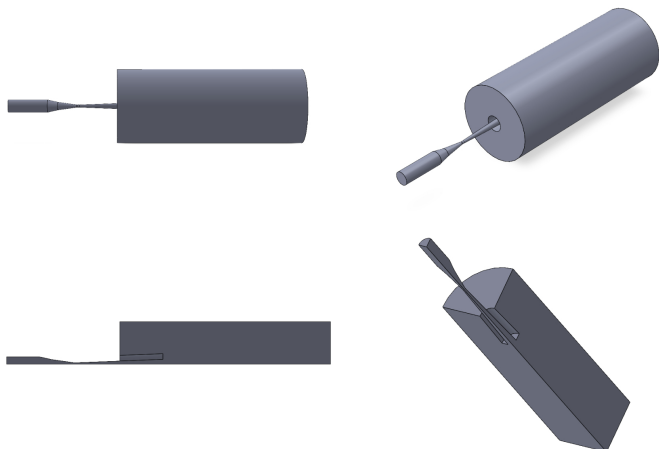


Figure 3.4: 360-degree & 90-degree models

The change in geometry from 360-degrees to 90-degrees is depicted in Figure 3.4. The geometry has two symmetry sides when converted to 90 degrees, and the results can be shown on either side of the symmetry. The key benefit of shrinking the geometry is that the number of cells can be dramatically increased for better outcomes. Due to the reduced geometry, a million or two million mesh cells might be employed in the same geometry, greatly improving the simulation output.

### 3.1.2.2 Meshing attributes

After the geometry is created, it is imported into the Ansys workbench, where the names of each side, such as inlet, outlet, wall, and symmetry, are given, and then it is imported again to the Fluent meshing tab. Ansys has two meshing approaches, with the workbench meshing

technique being the most used for 2-D objects and mechanical applications. Fluent meshing, on the other hand, is intended expressly for fluid flow applications and 3-D and offers a variety of meshing possibilities. The size options and inflation layers values are described further down.

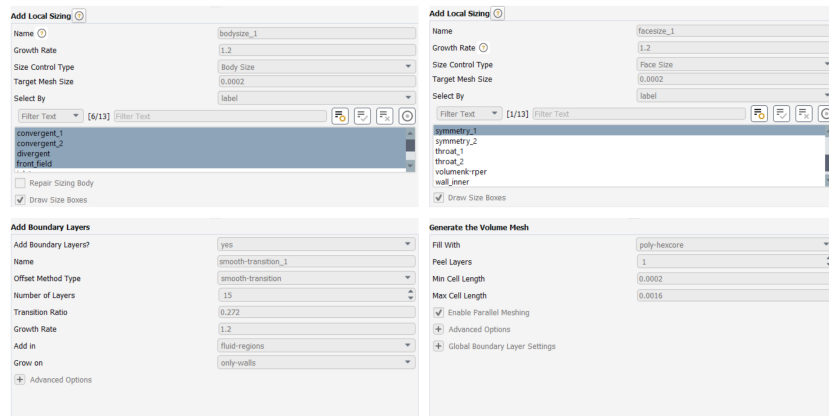


Figure 3.5: Meshing tabs

The main reason for reducing the geometry is to make finer meshes for better simulation results. Figure 3.5 represents the different values that are used for providing finer mesh at the surface of the geometry.

1. Body sizing (Front field, convergent, throat and divergent) = 0.0002
2. Face sizing (Symmetry) = 0.0002
3. Surface mesh = 0.003
4. Inflation layers = 15
5. Poly-hexcore
6. Volume mesh = 0.0016

- ***Justifications for selecting the provided values***

- The body sizing option will provide a change in mesh inside and outside the body whereas the face size will provide only at the face of the geometry. Face size is more suitable for observing the simulation results. The nozzle is the important part of the simulation; hence the nozzle is provided with body sizing and the symmetry is where the shock diamonds are observed is provided with a face sizing option.
- The surface mesh shown here is the maximum value, whereas the minimum value is calculated automatically by Fluent based on the sizing option provided. Both these options can be tweaked as per the requirements.

- Fluent applies an inflating layer to the entire geometry, which the user does not have control over. 15 inflation layers have been provided to capture the boundary layer effects, according to the calculations.
- Poly-hexcore provides a polygonal surface with a hexagonal interior body. Detailed information about the meshing has been discussed in section 2.4.2.
- The minimum and maximum cell lengths are supplied for volume meshing. The maximum cell length is represented by this value.

```

----- name skewed-cells (> 0.80) averaged-skewness maximum-skewness face count
----- solid 0 0.014105834 0.52826205 512616
----- name skewed-cells (> 0.80) averaged-skewness maximum-skewness face count
----- solid-1 0 0.014105834 0.52826205 512616
-----
----- After Surface mesh, the model consists of 1 fluid/solid regions and 0 voids.
----- Surface Meshing of Geom complete in 0.97 minutes, with a maximum skewness of 0.53.
----- fluid_domain 1744 0 0.82891789 1742155
----- name id cells (quality > 0.90) maximum quality cell count
----- Overall Summary none 0 0.82891789 1742155
[Quality Measure : Inverse Orthogonal Quality]
----- 1742155 cells were created in : 1.88 minutes
----- The mesh has a minimum Orthogonal Quality of: 0.17

```

Figure 3.6: Skewness & total number of cells

Figure 3.6 represents the final meshing attributes that should satisfy the condition which is discussed in section 2.4.2.3.

- Average skewness = 0.014105834 (*average skewness should be reduced to 0*)
- Maximum skewness = 0.5282605 (*maximum skewness should not exceed 0.9*)
- Minimum orthogonal quality = 0.17 (*minimum orthogonal should be greater than 0.1*)
- Number of cells = 1742155 (*1 million cells*)

Figure 3.7 depicts the various views of the geometry's mesh, with the first view displaying the geometry with 1 million cells, the second view displaying the inflation layers that form on the geometry's walls, and the third view displaying the poly-hexcore mesh with polyhedral cells on the surface and hexahedral cells within the geometry. In the second image, the inflation layer with a growth ratio of 1.2 and several layers of 15 can be seen as the layers increase in number when compared to the last layer from the geometry's wall.

### 3.1.2.3 Simulation setup

From the outline tree view of Ansys Fluent's simulation setup tab, the user can choose from a variety of settings. Once the geometry has been imported to the setup page, the user can utilize the console to activate the GPU in the computer for calculations by typing a simple one-line code. Below is a collection of simulation configurations that have been discussed.

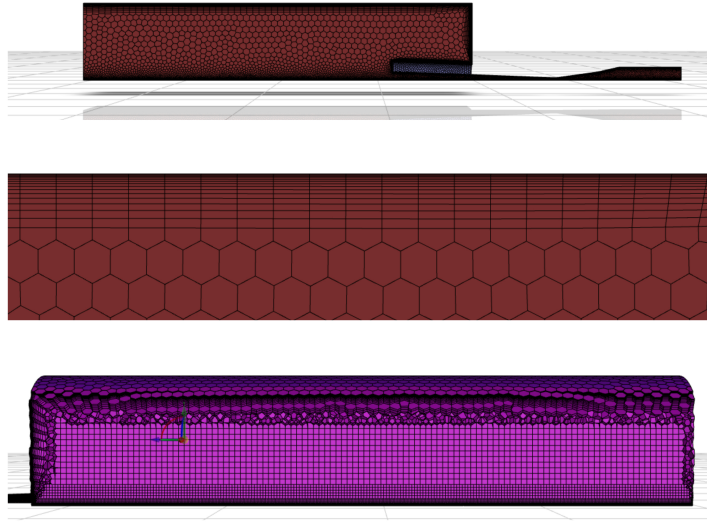


Figure 3.7: Different views of mesh

- **Solver and turbulence model**

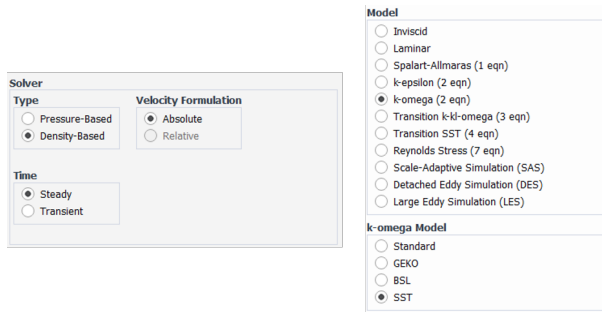


Figure 3.8: Representation of solver & model tabs

Figure 3.8 depicts the various solver and model types that can be used depending on the simulation application. Because of its robust nature for addressing high-speed compressible flows with the steady-state condition, the density-based solver type is chosen for nozzle simulation. A comparison between the different time steps and solvers is displayed in the upcoming chapter. Because the flow is concentrated inside the nozzle, the  $K - \omega$  SST model was used to capture the near-wall region and free stream velocity. The solver type and model have been discussed in depth in sections 2.4.1 and 2.4.3, respectively.

- **Material**

Cold spray can be operated using nitrogen or helium based on the application. Nitrogen is selected from the fluent material database, and ideal gas is chosen from density type. Real gas performs better with high temperature and low-pressure conditions, whereas ideal gas is best suitable for high-pressure flows. A detailed discussion has been made between ideal and real gas in section 2.4.4.1. Ansys Fluent comes with a large num-

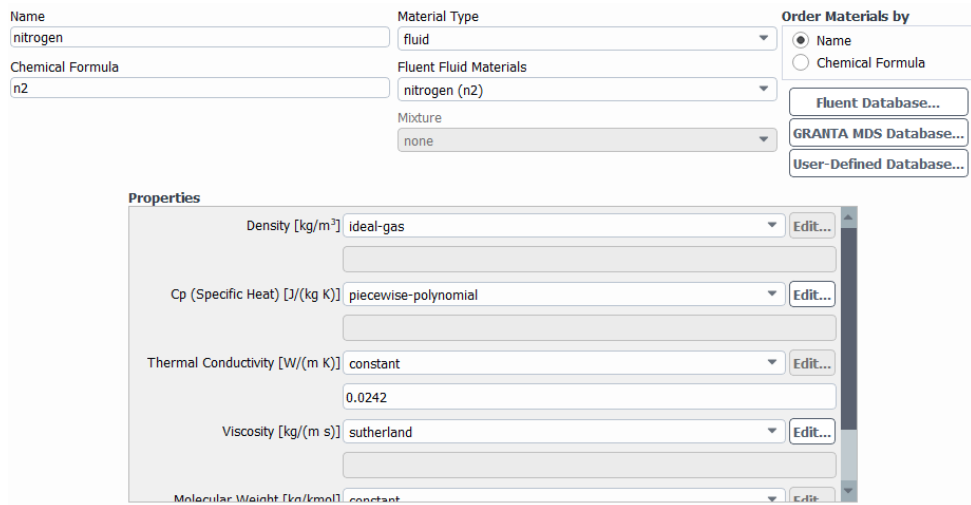


Figure 3.9: Material dialogue box

ber of constants for specific heat, thermal conductivity, and viscosity to choose from. Piecewise-linear, piecewise-polynomial, NASA-9-piecewise-polynomial, kinetic theory, and user-defined are among the constants. Piecewise, polynomial, and Sutherland are temperature-dependent constants, whereas the others do not support temperature changes and cannot be employed in heat transfer applications.

- **Specific heat ( $C_p$ ) = Piecewise polynomial**, Each piecewise polynomial dialog box has coefficients that can be selected depending on the application. It also has ranges to specify how many temperatures ranges the polynomial function is defined for.
- **Thermal conductivity = Constant** When heat transport is active, it must be defined. When modeling energy equations in the simulation, it should be defined. The influence on the energy equation is avoided by keeping the thermal conductivity constant while the energy equation is calculated for a different thermal conductivity. For a better solution, the material thermal conductivity should be kept constant when using CS.
- **Viscosity = Sutherland** Sutherland (1893) used an idealized intermolecular - force potential to derive a kinetic theory that is a function of temperature [13]. Sutherland has two constants to choose from, depending on the material and application. The constants are maintained the same for CS applications, however, the viscosity is modified to Sutherland.

#### • **Boundary conditions**

The initial condition provided for the CS nozzle simulation is Inlet pressure – 50 bar; Inlet temperature – 750 °C and Inlet gas – Nitrogen.

The inlet and outlet dialog boxes are shown in Figure 3.10. Because the flow is altered to supersonic locally, the supersonic condition will be used for the simulation, the gauge

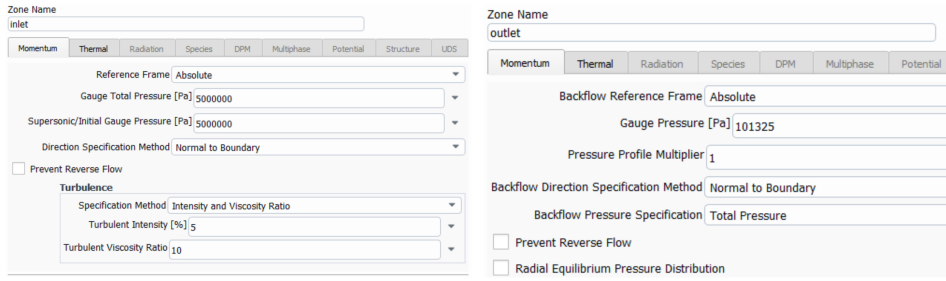


Figure 3.10: Inlet & outlet boundary conditions

total pressure and supersonic gauge pressure are both set to 50 bar. In section 2.4.4.2, the gauge pressure has been thoroughly discussed. Because the mesh provided for the CS application is not moving, the reference frame is set to absolute. Because the CS nozzle is placed in a closed chamber where the pressure and temperature are contained in the real world to protect against the supersonic sound produced while operating the machine, the outlet pressure is adjusted to 1 atm. A temperature of 1023.15 K is provided in the thermal tab of the inlet dialog box.

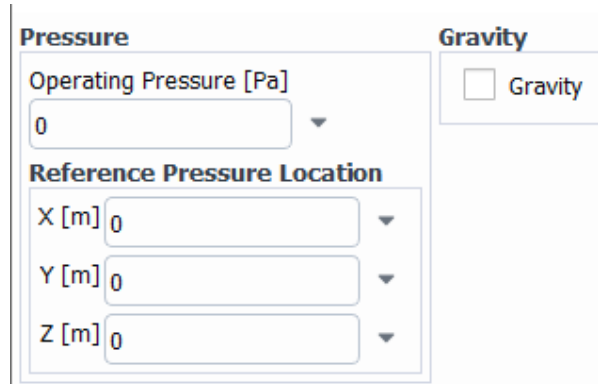


Figure 3.11: Operating condition

The density of incompressible ideal gas flows is directly determined by the operating pressure. The users must therefore be sure to set the operating pressure appropriately. Operating pressure is important for compressible flows with low Mach numbers because it helps to avoid roundoff errors. For compressible flows with a higher Mach number, operating pressure is less important. Because the pressure variations in such flows are substantially larger than those in low-Mach-number compressible flows, roundoff error is not an issue, and gauge pressure is not required. In reality, using absolute pressures in such calculations is normal practice. Because Ansys Fluent always utilizes gauge pressure, the operating pressure can be adjusted to zero, equating gauge and absolute pressures [13].

- **Monitors**

The solution monitors must be set up based on the application once the boundary condition has been established. Before starting the simulation, Ansys Fluent provides a list of

solution monitor settings to set up. Spatial discretization and residuals are the two key solution monitors to consider.

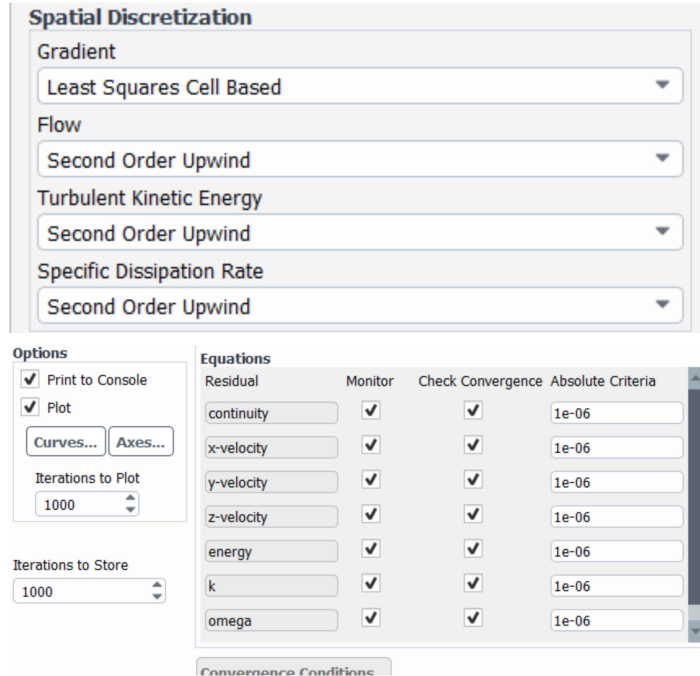


Figure 3.12: Solution monitors

The list of spatial discretization and residuals accessible in Ansys Fluent is shown in Figure 3.13. These options are provided for the simulation to satisfy for it to reach a state of convergence and produce a unique solution. When compared to the Green–Gauss technique, which employs the face value to determine the gradient, the least squares cell-based method requires less processing resources because it uses matrices and error approximation. In section 2.4.6, the many types of gradients and how to choose the right one for a particular application are discussed in detail.

Although the upwind scheme is one of the simplest and most stable discretization methods, it is more dissipative depending on the flow being simulated. Essentially, the values upstream are utilized to compute the value at the cell's center after evaluating the property on the cell's edges. Because it is an "upstream" variable, it considers the flow direction. The primary distinction between the first and second orders is the number of points used in the computation, which is one in the first and two in the second. When the flow is aligned with the mesh, first-order upwind discretization may be acceptable (e.g., laminar flow through a rectangular duct approximated with a quadrilateral or hexahedral mesh). When the flow is not aligned with the mesh (i.e., when it crosses the mesh lines obliquely), first-order convective discretization increases the numerical discretization error (numerical diffusion). Because the flow in triangular and tetrahedral meshes is never aligned with the mesh, using second-order discretization produces more accurate results. Quad/hex

meshes will also benefit from second-order discretization, especially for complex flows. Finally, while first-order discretization provides faster convergence than second-order discretization, it also produces less accurate results, especially on tri/tet meshes.

Because the geometry has meshed with 1 million cells and a residual of  $1e^{-6}$  will provide improved convergence and accurate results with the help of second-order upwind, a residual of  $1e^{-6}$  are provided for all equations. A detailed discussion has been made on residuals in section 2.4.7.

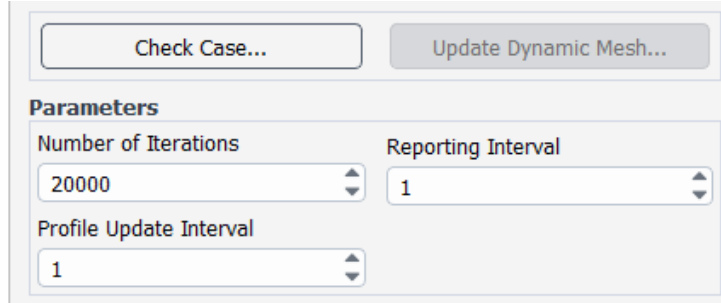


Figure 3.13: Number of iterations

The final step before beginning the simulation would be to determine how many iterations are required for the solution to converge. If the problem being addressed has never been solved before, this technique will be a trial and error method. At first, the simulation was carried out for 5000 iterations which are very less for a problem involving turbulence and supersonic condition. Then it was increased to 10,000 iterations where the solution started to change but it was never the unique solution. Finally, at 20,000 iterations the simulation has provided with convergence message in the console panel. For a simulation to attain a unique value maximum iteration has to be made so that the averaging of error done by the discretization will be accurate.

## 3.2 ESSS Rocky

The approach for setting up the particle simulation is described in this section of the methodology. As previously stated, Rocky uses one-way and two-way simulation methodologies, with the one-way simulation setup and results being reported in this research. The fluid does not impact particle behavior in a one-way simulation; instead, it provides an initial property for the particles to behave in the same way as the fluid. The numerical approach represents the method of computing the mass flow rate responsible for the particle to simulate, whereas the simulation approach represents the method of simulating the particle.

### 3.2.1 Numerical approach

ESSS Rocky, unlike Ansys Fluent, does not require any complex equations to determine the desired attributes. When setting up the simulation, three primary properties must be considered,

with the computation of mass flow rate for the particles being the most important. Schmidt, T et al., [28] conducted a study on particle acceleration and impact behavior of a *CS* nozzle with various particle sizes, using a 10% mass flow rate of the particle to the fluid.

At first, the mass flow rate of fluid is found using the equation 2.2.1.5 and then a 5% is made for the mass flow rate of fluid to find the mass flow rate of the particle.

*Mass flow rate of fluid: 0.588 Kg/s*

*Mass flow rate of particle: 0.0294 Kg/s*

### 3.2.2 Simulation approach

To calculate the velocity and temperature of a particle at the very end of the diverging section and near the substrate region, a particle simulation of the *CS* nozzle was carried out utilizing two distinct shapes of the nozzle. The ESSS Rocky particle simulator has an advantage over the Ansys *DPM* particle simulator in that it uses a complicated algorithm to solve particle behavior in fluids and offers a library of different shapes and sizes of the particle to pick from. Many different sorts of research have been done to examine particle behavior using the Ansys workbench, but only a few (or none) have been done using ESSS Rocky for *CS* applications.

#### 3.2.2.1 Geometry creation

A nozzle-only approach uses a 360-degree nozzle with no front and far-field in the interest of calculating the properties at the very end of the diverging section of the nozzle, and a 180-degree nozzle with a far-field extending to 100 mm from the diverging section in the interest of calculating the properties at the point of impact on the substrate.

- **180 – degrees with far-field** To save the simulation time and resources, a 180-degree nozzle with a far-field of 100 mm is created using Solidworks.
- **Nozzle-only (360-degrees)** To find the properties at the diverging section as well as to analyze the clogging effect of the particles, a 360-degree nozzle with no front and far-field is produced. Particle clogging occurs at the nozzle's throat due to a rise in temperature on the nozzle's surface and between the particles. The clogging effect will be discussed in depth in the following chapter. The nozzle is shown in Figure 3.2, and it is the only geometry used in the particle simulation.

#### 3.2.2.2 Simulation setup

As described in the geometry section, the technique for setting up the simulation is broadly separated into 360-degree nozzle-only and 180-degrees with far-field. One-way simulation requires first running a steady-state simulation with geometry from the Ansys workbench and then transferring the data to the Rocky tab in the Ansys workbench.

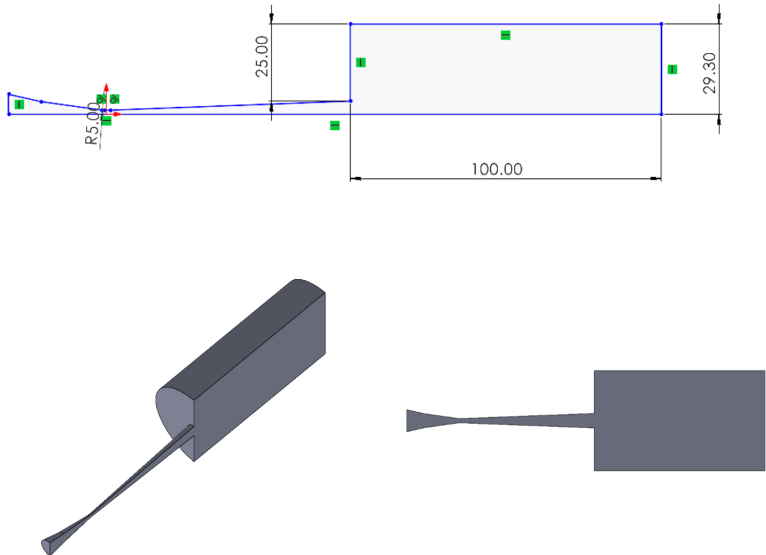


Figure 3.14: Dimension & different views of nozzle with far-field

The setup for the steady-state simulation is fairly similar to the one described in section 3.1.2.3. The case and data are stored and then imported to the Rocky tab once the simulation is completed. The geometry that has been imported can be seen by selecting the 3-D view from the windows menu.

- ***Physics setup***

Physics setup consists of gravity, momentum, and thermal tab, in which the gravity is set to "0" and the thermal model is enabled.

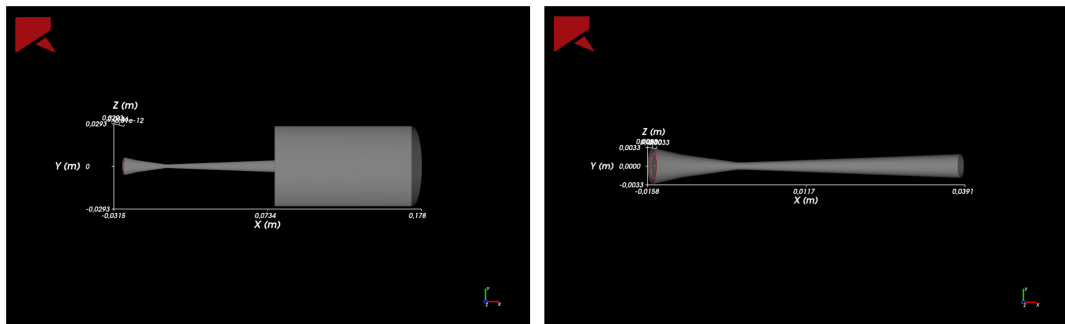


Figure 3.15: 180-degree with far-field (left) & 360-degree (right)

The physics option for 180-degrees with far-field is represented by the first two images on the top of figure 3.16 , whereas the physics option for nozzle-only is represented by the bottom two pictures. Because the particles are created to move in the direction of flow, which is in the  $x$ -direction, and there is no gravity acting on them throughout the simulation, gravity is set to "0". Rocky solves an additional equation for thermal

energy balance in addition to the equations that govern particle motion when the thermal model is activated. The temperature of ordinary single-element particles is thought to be uniform in the current version of Rocky (non-flexible). This indicates that no radial or circumferential temperature changes are permitted inside any of these particles, which makes sense given their small size and/or highly conductive construction. The Morris et al [26], Area correction is applicable for static systems. When enabled by the user in the Thermal tab of the physics panel this correction model replaces the lowered young's modulus of particles or borders with real values specified by the user for the appropriate materials when computing the contact radius.

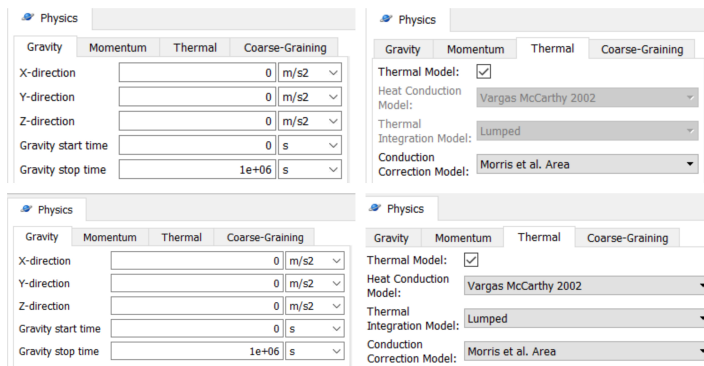


Figure 3.16: Physics setup for 180-degree (top two images); 360-degree (bottom two images)

- ***Creating inlet***

Rocky has rectangular, circular, conveyer, and user-defined inlet choices that can be employed depending on the application, which can be built from the geometry tab. Circular inlets are utilized for *CS* applications, and the coordinates for the inlets are shown below.

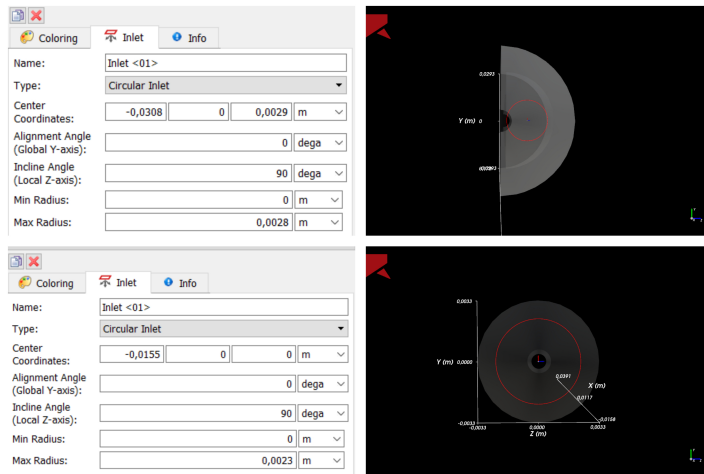


Figure 3.17: Inlet coordinates

The inlet created should be small enough so that it confines into the geometry. Inlet coordinates can be adjusted based on the geometry of inlet dimensions which is displayed

in figure 3.17.

- **Materials**

Copper is used as the primary material for *CS* application, because of its major necessity in the electrical industry, and the *CS* nozzle represented in this thesis report is used for the same purpose.

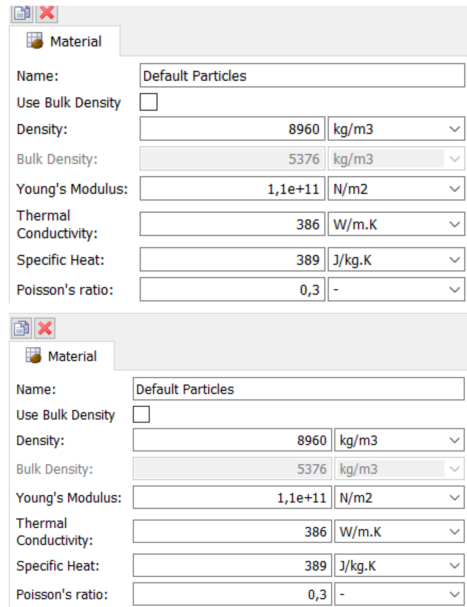


Figure 3.18: Representation of copper material properties

Both the pictures in figure 3.18 represent the material properties for 180-degrees with far-field and 360-degree nozzle-only geometries respectively.

- **Particles**

Specifying the shape and size of particles is done in this section. Rocky is comprised of plenty of different shapes of particles to be chosen from its database. For *CS* applications, sphere-shaped particles are preferred for deposition.

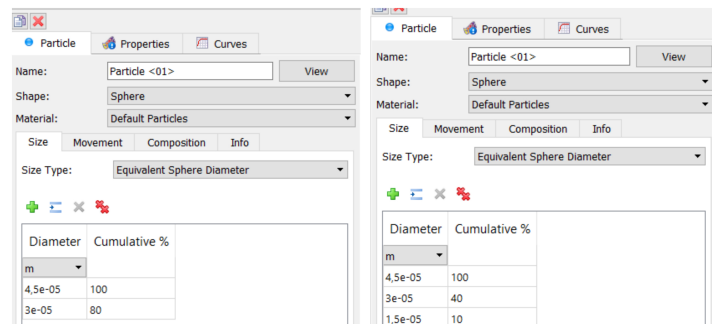


Figure 3.19: Particles dialogue box

The size type is equivalent to sphere diameter, which represents the particle size based on the diameter of a sphere equivalent to volume as the shape being measured, and the desired shapes and materials have been selected from the tab. Based on the presented data, three different particle dimensions are chosen for the CS application: 15  $\mu\text{m}$ , 30  $\mu\text{m}$ , and 45  $\mu\text{m}$ . Cumulative represents the range of sizes used in the simulation, and it should always be in the same order as the particle diameter. If a two-way simulation is performed, the movement choice can be set. A detailed discussion has been made on particles in section 2.5.3.

- **Inputs**

For the simulation to begin, the input option displays the particle's inlet attributes, such as mass flow rate, temperature, and velocity. The boundary conditions used in the Ansys Fluent are identical to this option.

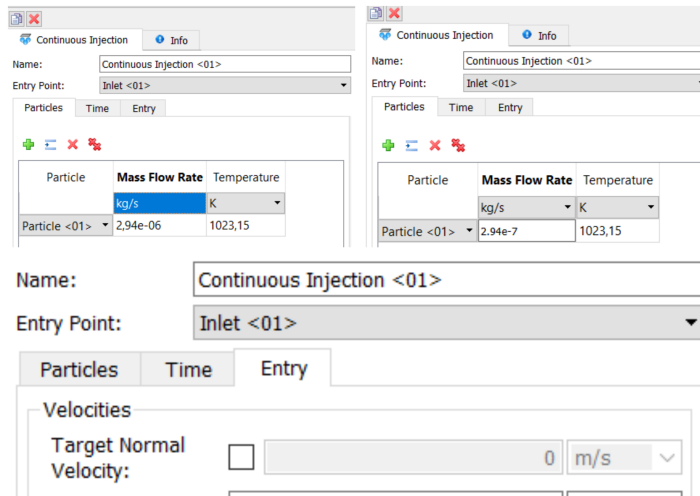


Figure 3.20: Input dialogue box

- **Entry point** indicates the inlet formed by using circular coordinates. The entry point is a crucial aspect of the simulation since even minor changes in the inlet coordinates can result in a catastrophic outcome.
- **Mass flow rate**, the value calculated from section 3.2.1. The mass flow rate can be adjusted according to computer resources, which is why the mass flow rate in the simulation is lower than in the numerical solution.
- **Temperature**, option is enabled only when the thermal model or energy equation is enabled from the steady state simulation. The inlet temperature of gas 1023.15 K has been applied to the particle inlet temperature as they both start at the same inlet point.
- **Target normal velocity**, The normal speed of the particles emitted from the Entry Point can be modified when this option is selected. Speed is calculated using local

coordinates. This option is unchecked because it will supply additional velocity to the particle from the entry location, resulting in an inaccurate solution.

- ***CFD coupling***

When geometry is imported from Ansys Fluent, the *CFD* one-way coupling option shows automatically. When you select this option, a list of parameters emerges, including the heat transfer law and drag law.

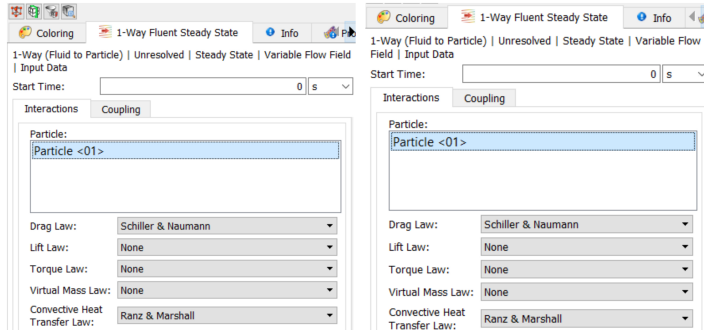


Figure 3.21: One-way coupling dialogue box

Schiller and Naumann provide the drag law, which is important for two-way coupling. These alternatives aren't very useful in one-way coupling because the particle isn't affected by the fluid. The Ranz & Marshall (1952) correlation is useful for measuring heat transfer between a spherical particle and its surroundings. The relationship is as follows:

where  $R_{ep}$  is the relative Reynolds number based on the diameter of the particle and the relative velocity and  $Pr$  is the Prandtl number [12].

- ***Solver***

Unlike most setup settings, which may only be changed before processing, the parameters under Execution on the Solver | General tab, as well as any of the choices on the Solver | Advanced tab, can be changed after processing has started without invalidating the results. Figure 3.22's top two images depict the 180-degree with far-field and nozzle-only

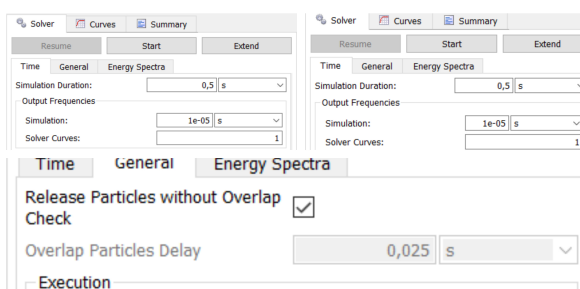


Figure 3.22: Solver dialogue box

geometry, respectively.

- **Simulation duration** indicates the total amount of real-time required to conduct the simulation. Convergence checks for the one-way simulation will be omitted because two-way simulation is not performed.
- **Output frequencies**, For Fluent two-way coupling simulations alone, this value determines the ratio of Rocky files saved to Fluent files saved. The time step size value set in the Fluent scenario determines the latter. Despite applying a variety of output frequencies, the final solution remains unchanged.
- **Release particle without overlap**, when activated for continuous injection inputs only, this overrides the option that prevents particles from discharging from an inlet if they are blocked by other particles or boundaries. When cleared, Rocky will use the Overlap Particles Delay time to delay the release of any overlapped particles. In real-life conditions, the particles will be accelerated one after the other without delay from the powder feeder. Rocky can be used with the multi-GPU option to maximize the simulation efficiency and reduce the total calculation time.



## 4 Results and discussion

This is the most important part of any study because it is here that any unsolved issues can be addressed with convincing proof of remedy. The solution and comparisons of every model available in Ansys Fluent, as well as a final discussion on how to choose appropriate simulation methods, ESSS Rocky, which represents the solution of particle properties, and a scientific question section, which represents the answer to the questions posed in section 1.2's problem statement are all covered in this chapter.

### 4.1 Ansys Fluent

#### 4.1.1 Final solution

The method for configuring the *CS* nozzle simulation was addressed in chapter 3. When the setup is complete, the solution is identified by looking at the residual and convergence message from the console tab, indicating that the simulation has been completed.

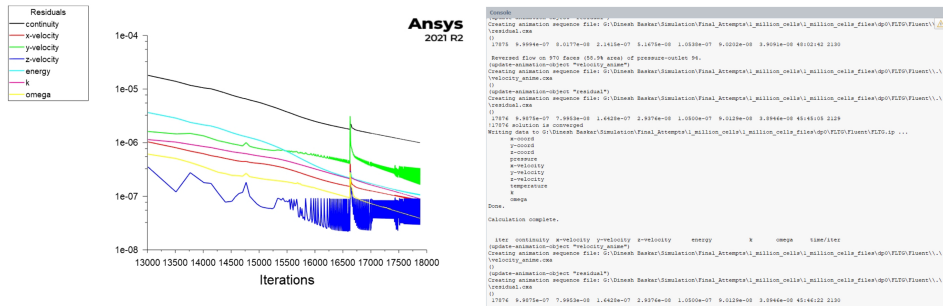


Figure 4.1: Representation of residuals and convergence

The residual and convergence of the simulation are depicted in Figure 4.1. After 15000 iterations, the error values tend to maintain a stable residual for the next 20000 iterations, as shown in the residual graph. The user set  $1e-6$  as the limit in the residual dialog box in the approach section, however, the answer here illustrates that the residual can be further decreased to  $1e^{-7}$  or  $1e^{-8}$  because of the million number of meshing cells offered. The gradients generated by the equations produce less inaccuracy when the simulation is run with the maximum number of cells. As can be seen on the right-hand side of figure 4.1, this shows that the solution has converged.

#### 4.1.1.1 Contour result

The contour option is the next best approach to look at the results visually. The contour can be selected from the outline tree view's solutions tab once the simulation is finished.

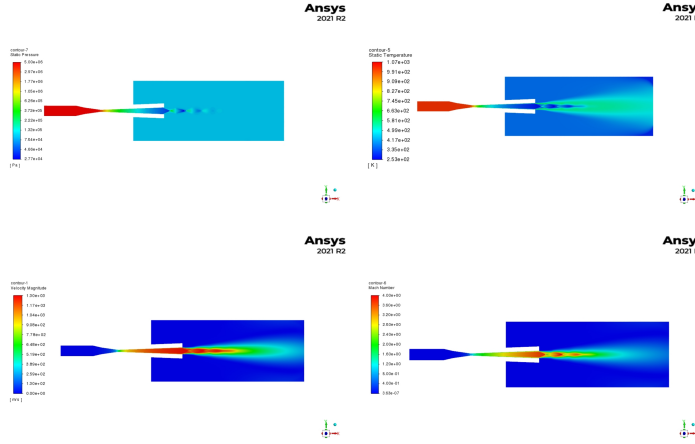


Figure 4.2: Solution contours

Figure 4.2 depicts the various contours obtained by the solution. The top-left and top-right images depict the pressure and temperature contours, respectively, while the bottom-left and bottom-right photographs depict the velocity and Mach number contours. Because the symmetry entities were mirrored to exhibit fully developed diamond shocks, the technique displays a 90-degree model whereas the results display a 180-degree model.

- ***Shock diamonds***

It has been demonstrated that the provided geometry nozzle can reach a supersonic state with the generation of shock diamonds at the exit of the nozzle by maintaining a sonic condition near the throat and lowering the backpressure.

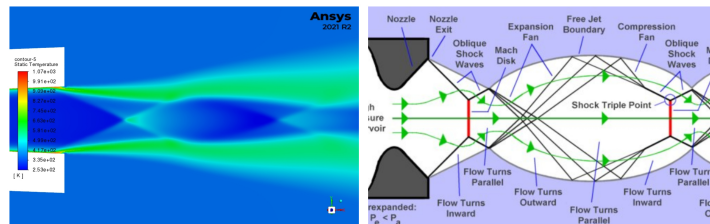


Figure 4.3: Representation of shock wave structure

Figure 4.3 depicts the shock diamonds. The flow near the centerline will be traveling parallel to that centerline when it exits the nozzle. However, beyond the free jet limit, the ambient environment has a higher pressure than the exhaust. As a result of the increased pressure, the exhaust is forced to turn inward toward the centerline. A form of wave known as an oblique shock wave allows for this turning. Any shock wave creates a change in flow pressure, which in this case is an increase. The fact that an oblique shock wave is inclined at an angle to the direction of the flow passing through it gives it its name. A normal shock wave, on the other hand, is a shock wave that is perpendicular to the flow direction. In the picture above, a normal shock occurs when the flow returns to

being parallel to the centerline. In the exhaust flow, this normal shock generates a Mach disk. The temperature of the flow rises as it passes through this typical shock wave, igniting any surplus fuel in the exhaust and causing it to burn. The burning fuel causes the Mach disk to glow and become visible, resulting in the ring pattern. This normal shock wave, like the oblique shock, raises the pressure of the exhaust gases. However, the flow gets so compressed that the pressure exceeds that of the surrounding air. As a result, the flow starts to spin outward, and the exhaust expands to equalize with the outside air. A succession of expansion waves that reflect off the free jet boundary and towards the centerline is used to turn the flow. The flow is turned outward and the pressure is reduced as a result of these waves.

The exhaust pressure is reduced by the expansion fan, but it is now lower than the ambient pressure. When the expansion waves hit the contact discontinuity, they reflect inward, causing compression waves and a compression fan to form. The flow is forced to curve inward and rise in pressure as a result of these compression waves. If the compression waves are strong enough, they will combine to generate an oblique shock wave, which will form a new Mach disk comparable to the one near the nozzle exit. The pressure above the external air rises as a result of this series of compression and shock waves, prompting a new expansion fan to form, and so on [6].

- *K – ω SST*

When the flow is removed from the wall region, this turbulence model is demonstrated to be the best for near-wall and free stream velocity conditions. As a result, there are no variations in the flow field.

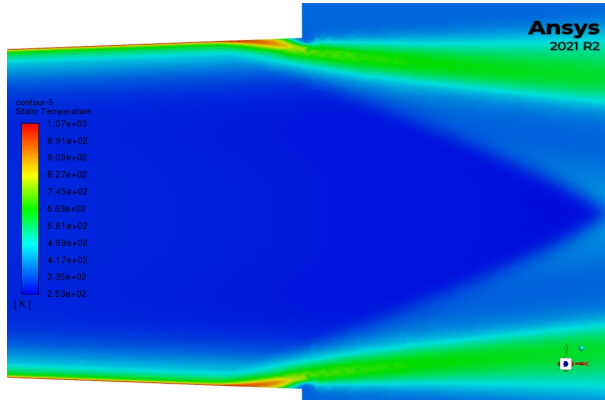


Figure 4.4: Flow separation

Figure 4.4 depicts a close-up picture of flow separation, in which near the wall region the flow is separated without any fluctuations to form shock diamonds at the exit. This is one of the major reasons for choosing the *K – ω SST* turbulence model which provides the best of both worlds.

- *Overexpanded flow*

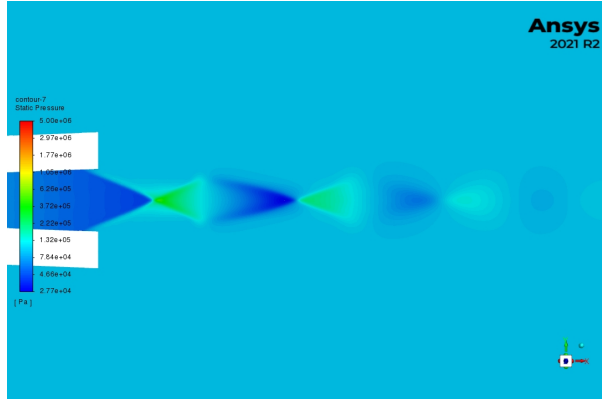


Figure 4.5: Pressure contour representing the over-expanded flow

The velocity magnitude in the picture depicts a linear change in the flow, which is highly useful in particle modeling because the nozzle is operating in overexpanded flow.

Figure 4.5 depicts the linear pressure creation generated by the overexpanded shock diamonds formed at the exit. This demonstrates that particles exiting the diverging section of the chamber tend to travel linearly along the axis as a shock and contact the substrate at maximum velocity.

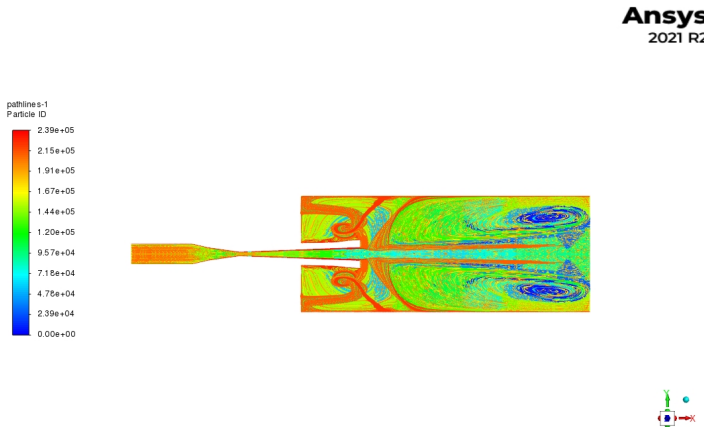


Figure 4.6: Depicts the particle pathline to illustrate the shock-diamond properties

The shape of the particle vector field is depicted in Figure 4.6. The emergence of an extra distant field to the left of the diverging section demonstrates a change in flow parameters on the shock formation's left side. This was discussed in detail in section 2.2.1.2. The flow parameters alter on the left side of the shock diamonds, but there are no obvious changes on the right side, except perhaps the creation of eddies at the far end of the far-field, as seen in the contour figure. Eddies form at the nozzle's far-field as a result of some particles being bounced back from the substrate due to poor adhesion and bow shock creation.

- **Bow shock**

Bow shocks are another important parameters that are being formed for all the supersonic velocity applications which are a necessity to understand the physics behind it. To observe the bow shock in CS application, a substrate should be added to the geometry at the far-field so that the high-velocity fluid when exiting out of the nozzle in supersonic velocity, the bow shock region is formed. The top two images of figure 4.7 represent the

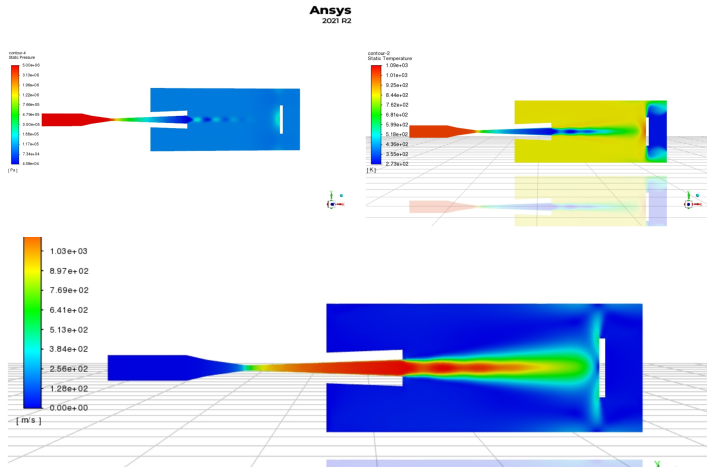


Figure 4.7: Representation of bow-shock

pressure and temperature contour and the below image represents the velocity contour. The hollow gap in the far-field represents the substrate as supposed to mimic the real-life condition. From the top-left image, the pressure contour represents an unusual pressure region forming in front of the substrate where the pressure increases. This vortex region is known as a bow shock. This vortex region can be observed in the velocity contour. Tien-Chein Jen et al [20], conducted a simulation method to understand the bow shock near the substrate. He concluded that there is a steep pressure increase across the bow shock and the pressure in this area closed by bow shock and the substrate is substantially higher than in the region beyond the Mach disk, and the gas flow pattern is also quite different. He also represented that the acceleration of copper particles with diameters greater than  $5\mu m$  is virtually completely unaffected by cone-shaped weak shocks in the nozzle, the Mach disk, and the bow shock outside the nozzle. This proves that the bow shock formed in the simulation does not affect particle acceleration. To have a clear insight, vector field contours are represented below.

The bottom-left image of figure 4.8 shows the formation of eddies before the substrate. This was shown in figure 4.6 and occurs due to the vacuum created when the particles bounce back from the substrate surface and the formation of the bow shock. Bottom-right shows a close-up image of the bow shock. At the substrate, the properties of the fluid change suddenly and this is because a vacuum is created which will affect the particle sizes that are less than  $5\mu m$ .

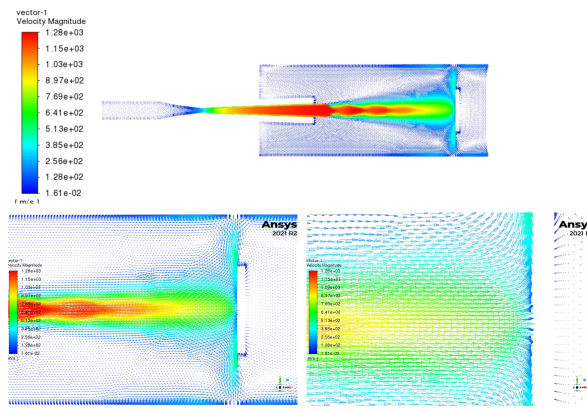


Figure 4.8: Representation of vectors

#### 4.1.1.2 Numerical Vs simulation results

After the contour results have been observed, a plane is generated to determine the exact exit point of the divergence to provide a data point at that precise place. This is done to extract flow parameters at the diverging section so that the findings can be compared to the numerical solution obtained in section 3.1.1.

Flow properties	Numerical results	Simulation results	Error percentage
Mach number (Ma)	3.93	3.9	0.7
Exit Temperature	250.22 K	253 K	1.1
Exit Pressure	0.361 bar	0.322 bar	1.0
Exit velocity	1246.1 m/s	1251.2 m/s	0.4

Table 2: Numerical & simulation results with percentage error

Table 2 shows that the average error percentage of the CS nozzle's exit condition is **0.8**, which is significantly less than the permitted limit of **5%** for *CFD* applications. This error percentage demonstrates that the geometry, physics configuration, meshing properties, boundary conditions, gradients, and residual conditions selected for the CS nozzle simulation are excellent.

#### 4.1.1.3 Plotting solution graphs

The derived answer can be plotted as a graph in the outline view's results tab. Because the node values and gradients that are generated may impact the solution graph, the graph should be seen in a 1-D solution rather than a 3-D solution to get accurate results. As illustrated in figure 4.9, a line is drawn from the front field to the distant field with the use of the surface tab.

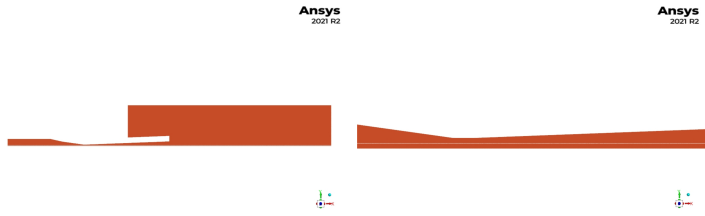


Figure 4.9: Representation of graph line that was created to obtain respective plots

Figure 4.9 depicts a white line that runs from the front field to the far-field. An *xy* plot can be selected from the plots tab to display the desired characteristics at the desired location on the mesh. The graph is examined at the line, which is produced at the symmetry wall.

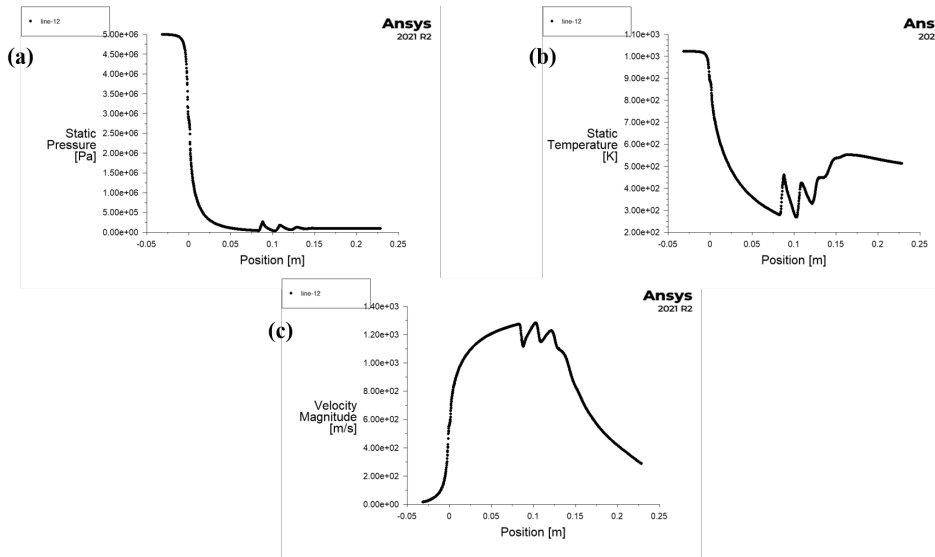


Figure 4.10: Representation of pressure(a); temperature(b); velocity(c) plot

Figure 4.10 represents the pressure, temperature, and velocity magnitude of the *CS* nozzle simulation. The fluctuations in the graph represent the formation of shock regions at the exit of the nozzle. From the pressure graph, it is proven, that as the pressure decreased in the throat region, the velocity of the fluid started to increase from the throat area until it reaches its maximum velocity at the exit of the diverging section.

#### 4.1.1.4 Ansys Fluent Vs KSS (Kinetic Spray Solutions)

KSS is a software product company providing software solutions for many *CFD* applications, and this section deals with the comparison between the results generated from Ansys Fluent and KSS generated results from their software code, where they used the same geometry dimension reference.

- **Pressure plot**

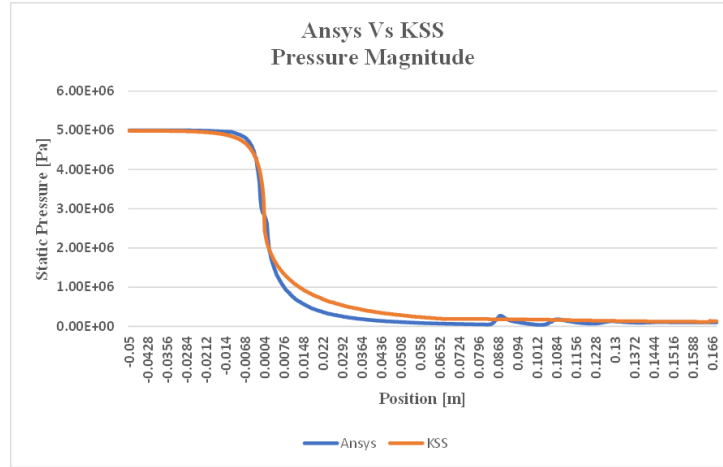


Figure 4.11: Pressure plot

The main aim of this comparison is to demonstrate a better understanding of simulation methods that provide accurate results when compared with the *KSS* software where a 2-D model is used to study the flow properties. The difference between the 2-D model and the 3-D model is that the 2-D model is more suitable for a laminar condition where they do not need to account for transport equations, whereas in the 3-D model transport equations need to be solved accurately so that the transition between the flows from laminar to turbulence will occur smoothly. On any day, a 2-D model does not provide accurate results when compared with a 3-D model. As a result, the orange curve in figure 4.11 represents the *KSS* generated plot which does not contain fluctuation at the exit of the nozzle. Whereas the Ansys generated plot (represented in a blue curve) contains the fluctuation which is a representation of shock formation outside the nozzle.

- **Temperature plot**

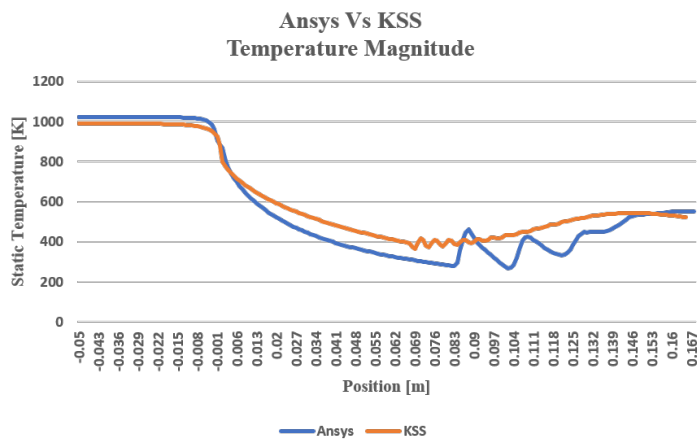


Figure 4.12: Temperature plot

When compared to the *KSS* inlet temperature (orange curve) of roughly 980 K, the inlet temperature for the *CS* nozzle application is 1023.15 K, a difference of 43.15 K in the inlet condition. This is why the *KSS* displays an error, and the formation of a fluctuation in the curve should occur at the nozzle's departure. The fluctuation supplied by the Ansys simulation is around 83 mm, but the fluctuation provided by the *KSS* is approximately 62 mm, presuming the diverging part of the nozzle terminates at 77 mm, as seen in the graph. This demonstrates that the *KSS* simulation permits shock creation to occur inside the diverging part of the nozzle, affecting the flow characteristics and perhaps resulting in a drop in efficiency.

- ***Velocity plot***

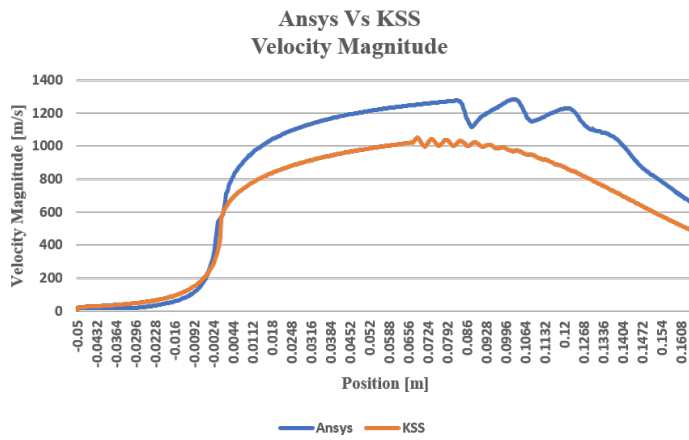


Figure 4.13: Velocity plot

The inlet velocity needs to be calculated from the simulation, and by observing figure 4.13 the *KSS* (orange curve) final velocity is very less when compared to the Ansys simulation. *KSS*'s maximum velocity reached is at 1000 m/s whereas, the Ansys simulation method provides a maximum velocity of around 1250 m/s which is almost equal to the numerical results that have been mentioned in section 4.1.1.2.

The results that are mentioned in this chapter prove that usage of the 3-D model with necessary boundary conditions and inlet conditions will help in producing accurate results corresponding to the numerical simulation results. A list of different turbulence models and solvers has been compared and a final discussion of choosing the best simulation methods is discussed in the upcoming sections.

#### 4.1.2 List of model comparisons

The comparison of several simulation methodologies, turbulence models, solvers, and carrier gas models is covered in this section. All of the models in this section employ the same 90-degree geometry as in section 3.1.2.1, as well as the same boundary condition and mesh sizes

and types. The use of the same meshing properties across all models makes it easier to distinguish between graph fluctuations and make an informed decision about which simulation approach to use.

### 1. Density Vs Pressure based solver

To properly evaluate the findings, the first comparison is between solvers in which the geometry meshing is done with the same accuracy and the same amount of cells. Except for the solver type, which is described below, the simulation setup is the same for both.

- **Solver:** Density-based (blue curve); Pressure-based(orange curve)
- **Time:** Steady-state
- **Model:**  $K - \omega$  SST
- **Material:** Nitrogen (Ideal gas)
- **Boundary conditions:** 50 bar, 1023.15 K
- **Method:** Implicit, least-squares cell-based
- **Residual:**  $1e^{-6}$

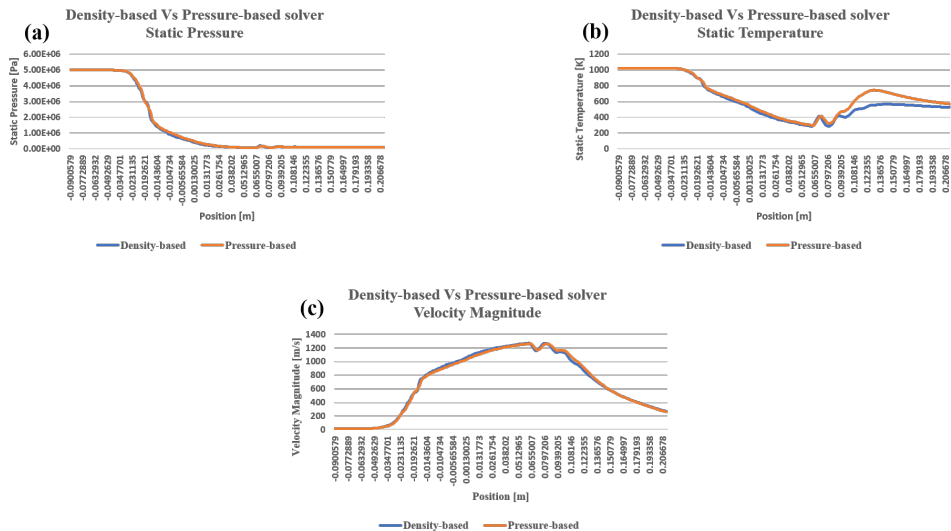


Figure 4.14: Density Vs Pressure based

The pressure and velocity magnitudes of the solver are represented by a and c in the graph, with density and pressure-based solvers having little influence on the solution. Graph b, on the other hand, illustrates the temperature magnitude, in which the pressure-based solver tends to vary from the density-based solver's original answer, which is similar to figure 4.12. This fluctuation is caused by a pressure-based solver's inability to tackle high-compressible flows. This demonstrates that a density-based solution is a better alternative for high-compressible and high-turbulent flows, and the solver was created expressly for this reason. A detailed discussion about the solver has been made in section 2.4.1.

## 2. Steady-state Vs Transient condition

A steady-state simulation differs from marching a transient solution to a steady-state in that the steady-state simulation ignores many of the time-related cross-terms and higher-order terms. In steady-state, all of these variables are zero, hence they do not affect the steady-state result. All of these terms are included in the transient simulation. The steady-state model usually has an easier time converging since there are fewer terms to model and some transitory non-linearities are removed, but in a few models, these non-linearities aid convergence.

- **Solver:** Density-based
- **Time:** Steady-state (blue curve); Transient (orange curve)
- **Model:**  $K - \omega$  SST
- **Material:** Nitrogen (Ideal gas)
- **Boundary conditions:** 50 bar, 1023.15 K
- **Method:** Implicit, least-squares cell-based
- **Residual:**  $1e^{-6}$

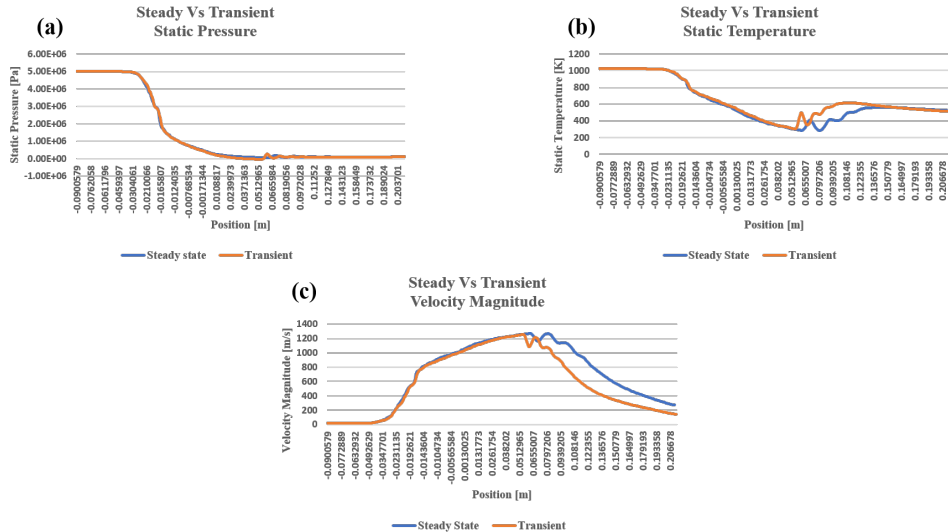


Figure 4.15: Steady-state Vs Transient plot

From figure 4.15, the temperature curve of transient (orange curve) has a sudden rise at the shock region when compared to the steady-state condition. This can also be seen in the velocity magnitude, and when compared with the graph of 4.12 and 4.13, steady-state has the advantage in this application.

## 3. Turbulence models Vs K-omega-SST

Ansys is provided with plenty of turbulence models to choose from, and a handful of models that is suitable for CS nozzle application are compared with the  $K - \omega$  SST model.

- **Solver:** Density-based
- **Time:** Steady-state
- **Model:**  $K - \omega$  SST,  $K - \omega$  standard,  $K - \omega$  GEKO,  $K - \omega$  BSL,  $K - \varepsilon$  standard,  $K - \varepsilon$  RNG, Spalart-Allmaraus, LES
- **Material:** Nitrogen (Ideal gas)
- **Boundary conditions:** 50 bar, 1023.15 K
- **Method:** Implicit, least-squares cell-based
- **Residual:**  $1e^{-6}$

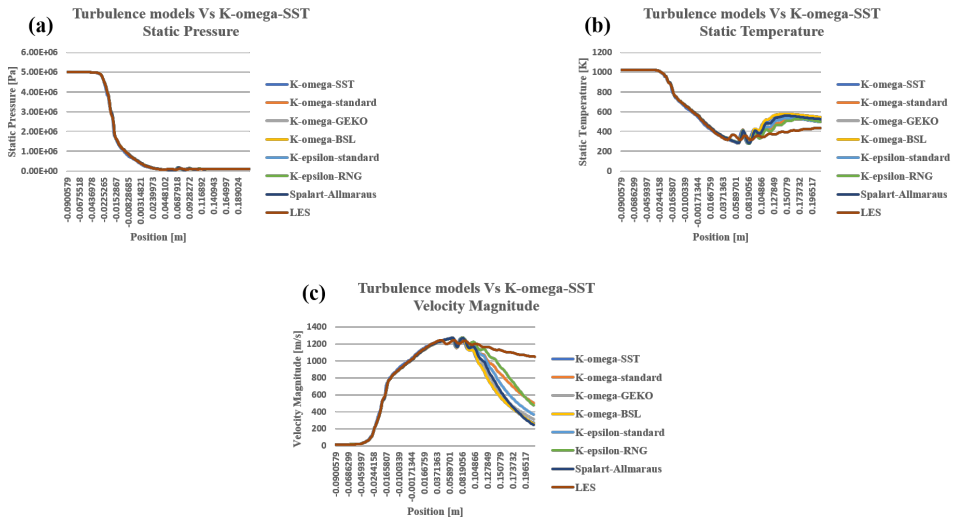


Figure 4.16: Turbulence models Vs  $K - \omega$  SST

The pressure, temperature, and velocity magnitude of the solution are represented by a, b, and c, respectively, in figure 4.16. Because it is designed to be utilized in the presence of eddies, the *LES* model does not produce the predicted findings in all of the photos. On the other hand, Spalart-Allmaraus is more suited to exterior flow applications such as flow over an airfoil.  $K - \varepsilon$  models, as explained in section 2.4.2 of turbulence modeling, are better for free stream velocity applications since they don't capture the flow parameters near the wall. This is why the  $K - \varepsilon$  models produce poor graph results following the shock region, as the temperature and velocity graph values worsen. When looking at the graph attentively, the flow properties are nearly the same until the shock zone is reached, after which the  $K - \varepsilon$ , Spalart-Allmaraus, and *LES* models deviate from the original values.

However, the  $K - \omega$  model on the other hand has 4 different sub-models, in which the  $K - \omega$  standard and  $K - \omega$  GEKO are more likely to be generalized  $K - \omega$  models which use one consolidated equation rather than the two-equation model without any shear stress term to solve the problem. Shear stress term is necessary for separation from the near-wall

region. A detailed discussion has been made on different turbulence models in section 2.4.3.

#### 4. Real Vs Ideal gas

Ansys Fluent is comprised of 4 different real gases that can be chosen from the Fluent database. The boundary condition applied are:

- **Solver:** Density-based
- **Time:** Steady-state
- **Model:**  $K - \omega$  SST
- **Material:** Ideal gas, Real gas-Soave-redlich-Kwong, Real gas-peng-robinson, Real gas-redlich-Kwong, NIST Real gas
- **Boundary conditions:** 50 bar, 1023.15 K
- **Method:** Implicit, least-squares cell-based
- **Residual:**  $1e^{-6}$

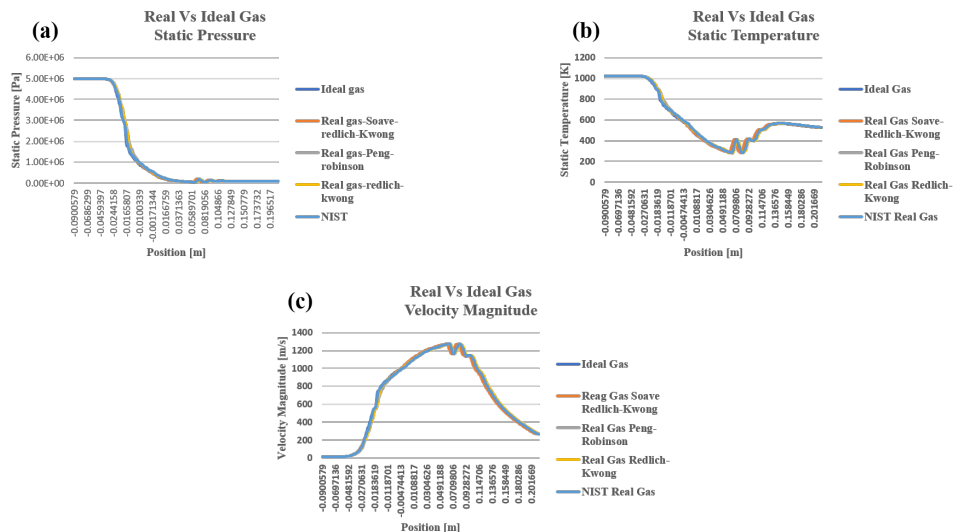


Figure 4.17: Real Vs Ideal gas

There is no major difference between the real gas and ideal gas simulations, as mentioned in section 2.4.4, and this is demonstrated in figure 4.17, where the entire ideal gas and real gas models appear to be tracing the same route.

#### 5. Implicit Vs Explicit method

An explicit scheme is one in which the updating technique is simple and does not rely on other values at the present level, whereas an implicit scheme contains information at the current level and requires simultaneous equations to be solved.

- **Solver:** Density-based
- **Time:** Steady-state
- **Model:**  $K - \omega$  SST
- **Material:** Nitrogen (Ideal gas)
- **Boundary conditions:** 50 bar, 1023.15 K
- **Method:** Implicit (blue curve), explicit (orange curve)
- **Residual:**  $1e^{-6}$

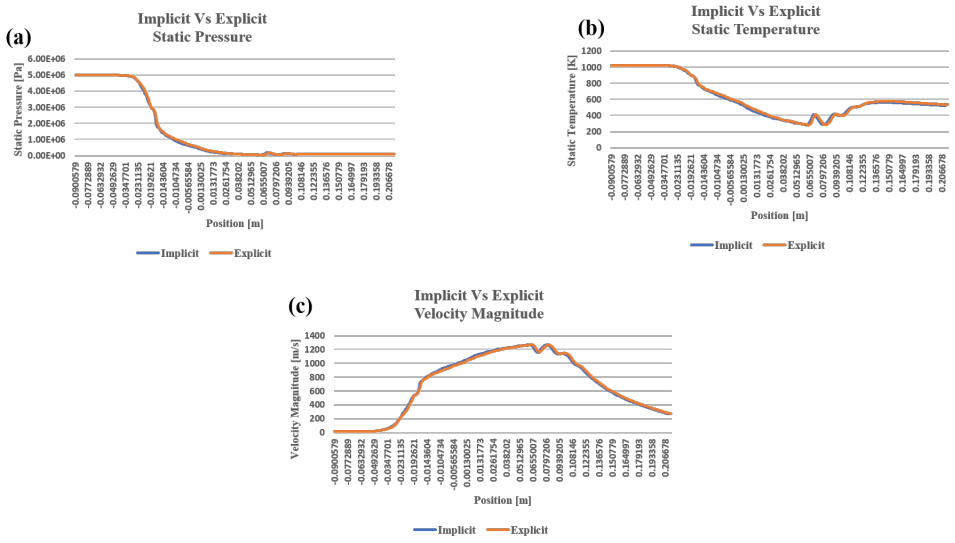


Figure 4.18: Implicit Vs Explicit

The explicit method is less time-consuming to program and calculate. However, because of its limited stability, it's best to select a small enough step size to avoid divergence. The implicit technique, on the other hand, is quite stable and converges when the parameters are specified correctly. The implicit technique is ideal for solving equations that take a long time to solve because it can employ a sufficiently large step size. It's also difficult to forecast the future from the past condition in non-linear equations like contact. In certain circumstances, using the implicit technique rather than the explicit method is suggested.

#### 4.1.3 Final discussion

Figures 4.14 to 4.18 show the various models and solver techniques that can be used to solve the CS nozzle problem. However, most of the models depart from the original unique solution due to the nature of the equations that are specific to a given application. *CFD* is a trial-and-error process, and no one can state with absolute assurance that this is the only model that will generate unique results for various applications. This decision is always based on the needs of the user and the application for which it will be used. However, for the CS nozzle application,

several physical setups were compared to come up with a unique setup that could only operate well for nozzle applications with a certain shape.

- **Density-based:** Figure 4.14 shows that, as compared to a pressure-based solver, density-based solvers produce better results during heat transfer.
- **Steady-state:** Transient method is more suitable for a time marching solution in which the flow properties can be taken at each time step. For the *CS* nozzle, a steady-state should be used because it is being used for the one-way particle simulation in Rocky. Transient simulation can be used for two-way coupling.
- **$K - \omega$  SST:** As previously stated,  $K - \omega$  SST is the best turbulence model for the near-wall and free-stream velocity regions, and no other turbulence model has this property.
- **Ideal gas:** Although there are some discrepancies in the solution when compared to a Real gas simulation, Ideal gas is utilized to make a clear judgment of flow attributes because both gases behave similarly under specific conditions. Under normal circumstances, many real gases behave like ideal gases.
- **Implicit:** When it comes to the stability of the solution, the implicit condition will provide better stability but it takes much time to provide convergence when compared to the explicit condition.
- **Least squares:** As previously said, least-squares tend to square the mistake and average it, resulting in a significantly lower error percentage in geometry with million cells when compared to the other two discretization methods.
- **Residual:** Ansys Fluent guidance recommends a residual value of  $1e^{-3}$  or  $1e^{-4}$  as a safe limit to approach, however for a million-cell application like the *CS* nozzle, a residual value of  $1e^{-6}$  exhibits convergence in the solution while maintaining residual stability, as seen in figure 4.1.

## 4.2 ESSS Rocky

The 180-degree far-field geometry and the 360-degree nozzle geometry have been distinguished in this section. The mechanism for setting up the particle simulation was presented in chapter 3 along with the boundary conditions. As previously mentioned, a steady-state simulation must first be performed before the data can be translated to the Rocky work page for one-way simulation.

#### 4.2.1 180-degree far-field simulation

The one-way simulation must have a steady-state *CFD* solution that may be utilized for coupling with the Rocky before simulating the particle. To begin, the geometry is imported into the Ansys workbench, and the meshing is completed using the Fluent meshing software.

Overall Summary				
name	id	cells (quality < 0.10)	minimum quality	cell count
fluid_domain	897	0	0.10527867	1272683
Overall Summary	none	0	0.10527867	1272683
[Quality Measure : Orthogonal Quality]				
----- 1272683 cells were created in : 0.52 minutes				
----- The mesh has a minimum Orthogonal Quality of: 0.11				
----- The volume meshing of geom-volumenk-rper is complete.				

Skewed-cells (> 0.80)				
name	skewed-cells (> 0.80)	averaged-skewness	maximum-skewness	face count
volumenk-rper	0	0.00919111288	0.5075454	207514
geom-volumenk-rper	0	0.00919111288	0.5075454	207514

----- After Surface mesh, the model consists of 1 fluid/solid regions and 0 voids.  
----- Surface Meshing of Geom complete in 0.72 minutes, with a maximum skewness of 0.51.

Figure 4.19: Mesh metrics

Image (a) of figure 4.19 represents the number of cells formed for the geometry and (b) represents the skewness and orthogonality of the cells.

**Number of cells: 1272683 (1 million)**

After the meshing process, the geometry is set up with the same boundary conditions that is being displayed in section 3.1.2.3.

- **Solver:** Density-based
- **Time:** Steady-state
- **Model:**  $K - \omega$  SST
- **Material:** Nitrogen (Ideal gas)
- **Boundary conditions:** 50 bar, 1023.15 K
- **Method:** Implicit
- **Residual:**  $1e^{-6}$

Figure 4.20 shows the steady-state simulation solution graphs (images a, b, c, and d). The residual shown in the figure indicates that the solution has converged, and the data can be imported into Rocky for particle simulation, in which three types of simulation have been performed to compare particle solutions to make a decision about which simulation method to use.

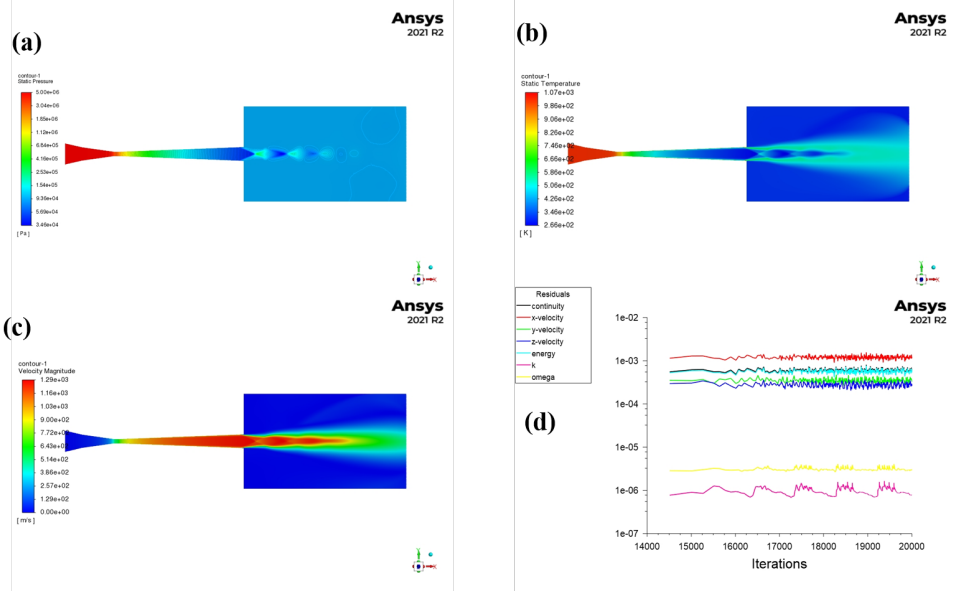


Figure 4.20: Steady-state simulation contours

- **Type – 1:**

The methodology of simulation setup is the same for all three types except the solver time for the simulation. A detailed discussion has been made on the simulation setup in section 3.2.

- **Gravity:** “0” for all coordinates
- **Material:** Copper
- **Particles:**  $45 \mu\text{m}$ ,  $30 \mu\text{m}$
- **Mass flow rate:**  $2.94e^{-6}$
- **No. of particles:** 10629
- **Simulation duration & Frequency:**  $0.5$ ,  $1e^{-5}$

The images "a" and "c" depict the particle's velocity and temperature, respectively, whereas images "b" and "d" depict the graph corresponding to the velocity and temperature contours. The following is a summary of the findings:

- **Average velocity at the far end of far-field:**  $536 \text{ m/s}$
- **Average Temperature at the far end of far-field:**  $826 \text{ K}$

- **Type – 2:**

The particle sizes have been lowered from  $45 \mu\text{m}$ ,  $30 \mu\text{m}$  to  $10 \mu\text{m}$ , and  $15 \mu\text{m}$  in these type – 2 approaches. According to basic theory, as the particle size is lowered, the velocity increases as the temperature rises.

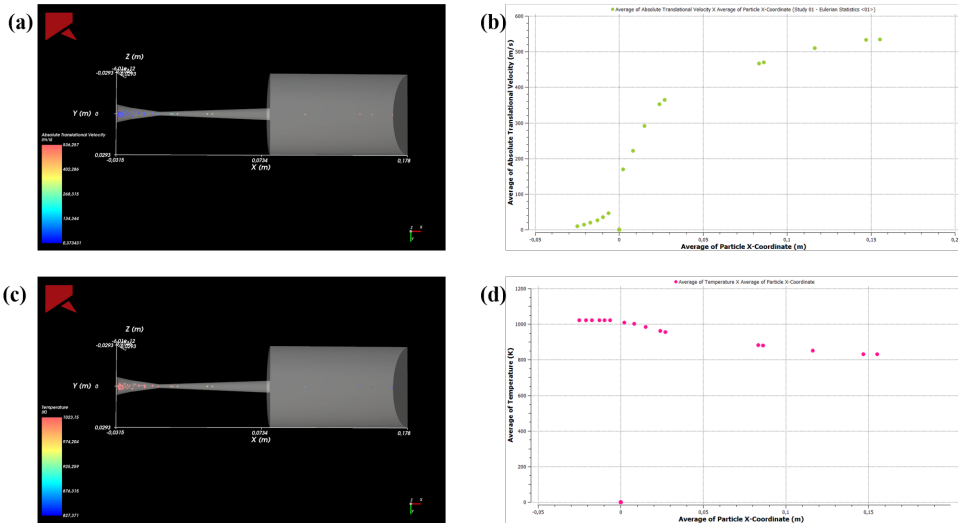


Figure 4.21: Type-1 of 180-degree far-field geometry

- **Gravity:** “0” for all coordinates
- **Material:** Copper
- **Particles:**  $10 \mu\text{m}, 15 \mu\text{m}$
- **Mass flow rate:**  $2.94e^{-7}$
- **No. of particles:** 5212
- **Simulation duration & Frequency:**  $0.1, 1e^{-4}$

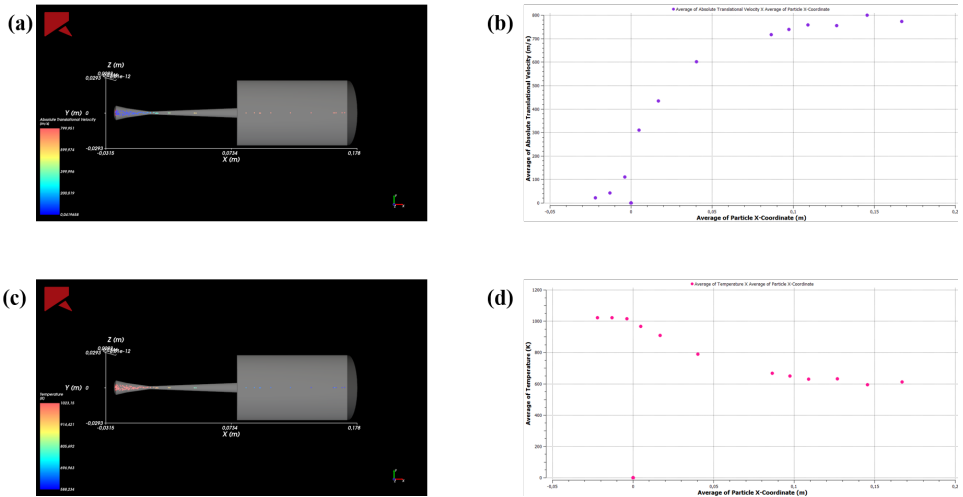


Figure 4.22: Type-2 of 180-degree far-field geometry

- **Average velocity at the far end of far-field:**  $799 \text{ m/s}$
- **Average temperature at the far end of the far-field:**  $590 \text{ K}$

Due to the use of small particle size, the velocity has been enhanced as compared to the type – 1 simulation. Because the mass flow rate is proportional to the number of particles,

distinct mass flow rates in two types are used to lower the overall simulation time. The simulation duration is also modified to demonstrate that it does not affect the flow and particle properties because it is linked directly to the simulation timeline.

- **Type - 3:**

Target normal velocity has been applied to the nozzle's inlet condition in this type of modeling procedure. The target normal velocity will give the particles a normal velocity from the start of the simulation, which may alter the final solution attributes. The target velocity is usually the same as the fluid velocity at the inlet, and the fluid velocity calculated from the *CFD* simulation is 16 m/s.

- **Gravity:** “0” for all coordinates
- **Material:** Copper
- **Particles:** 45  $\mu\text{m}$ , 30  $\mu\text{m}$
- **Mass flow rate:**  $2.94e^{-6}$
- **No. of particles:** 1931
- **Simulation duration & Frequency:** 0.1,  $1e^{-4}$
- **Target normal velocity:** 16 m/s

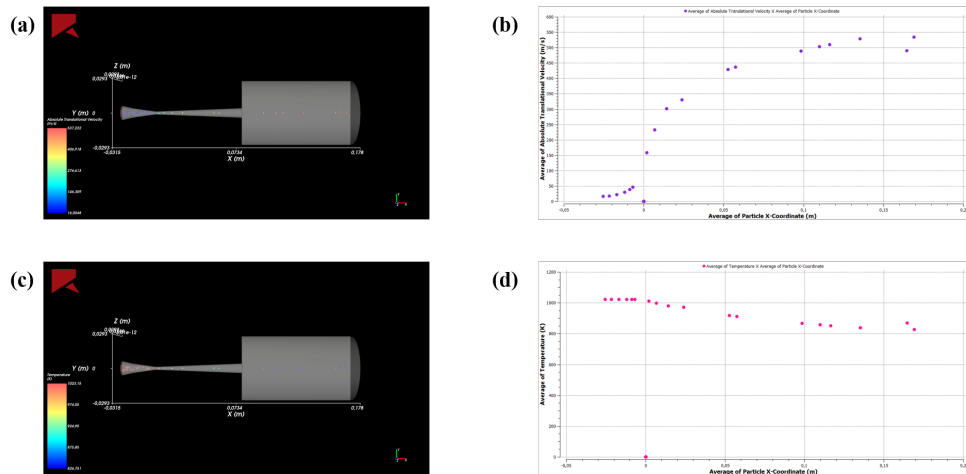


Figure 4.23: Type-3 of 180-degree far-field geometry

- **Average velocity at the far end of far-field:** 537 m/s
- **Average temperature at the far end of the far-field:** 826 m/s

Figure 4.23 shows that the average velocity of a particle has increased by 1%, but the particle values can change because these particles are dynamic and it is difficult to determine their exact velocity position. This shows that even at the target normal velocity, the characteristics did not change much, indicating that it is safe to use in *CS* applications.

#### 4.2.2 360-degree without far-field

This section depicts a 360-degree nozzle without the use of far-field to investigate particle characteristics at the nozzle's diverging end. A steady-state simulation must be run in conjunction with the Rocky simulation, as detailed in section 4.2.1.

(a)

name	id	cells (quality < 0.10)	minimum quality	cell count
fluid_domain	459	1	0.069509066	2388495
Overall Summary	none		1	0.069509066
[Quality Measure : Orthogonal Quality]				
----- 2388495 cells were created in : 0.42 minutes				
----- The mesh has a minimum Orthogonal Quality of: 0.07				
----- The volume meshing of geom-volumenk-rper is complete.				

(b)

name	skewed-cells (> 0.80)	averaged-skewness	maximum-skewness	face count
volumenk-rper	0	0.010771424	0.45457524	125096
geom-volumenk-rper	0	0.010771424	0.45457524	125096
----- After Surface mesh, the model consists of 1 fluid/solid regions and 0 voids.				
----- Surface Meshing of Geom complete in 0.77 minutes, with a maximum skewness of 0.45.				

Figure 4.24: Mesh Metrics nozzle-only

Image (a) of figure 4.24 represents the number of cells formed for the geometry and (b) represents the skewness and orthogonality of the cells.

**Number of cells: 2388495 (2 million)**

After the meshing process, the geometry is set up with the same boundary conditions that is being displayed in section 3.1.2.3.

- **Solver:** Density-based
- **Time:** Steady-state
- **Model:**  $K - \omega$  SST
- **Material:** Nitrogen (Ideal gas)
- **Boundary conditions:** 50 bar, 1023.15 K
- **Method:** Implicit
- **Residual:**  $1e^{-6}$

Figure 4.25 shows the steady-state simulation solution graphs (images a, b, c, and d). The data can now be loaded into the Rocky work area because the residuals have reached a point of convergence. With this model, two types of particle simulations were created and compared, as well as a final discussion to demonstrate the most appropriate particle simulation method.

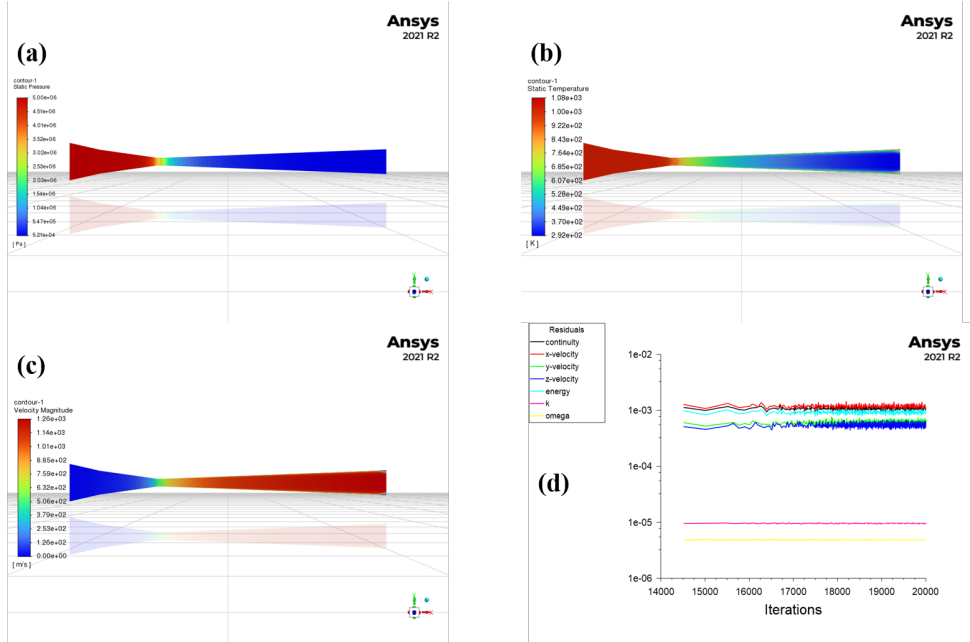


Figure 4.25: Steady-state simulation contours of 360-nozzle

- **Type – 1:**

Type – 1 simulation is made to observe the velocity and temperature at the end of the diverging section of the nozzle as well as to understand how the shock formation in the nozzle is affecting the particle properties.

- **Gravity:** “0” for all coordinates
- **Material:** Copper
- **Particles:**  $45 \mu\text{m}$ ,  $30 \mu\text{m}$
- **Mass flow rate:**  $2.94e^{-5}$
- **No. of particles:** 106273
- **Simulation duration & Frequency:**  $0.5, 1e^{-5}$
- **Average velocity at the diverging section:**  $360 \text{ m/s}$
- **Average temperature at the diverging section:**  $930 \text{ K}$

When compared with 180-degree with far-field geometry, the velocity at the diverging section is 360m/s approximately and due to the shock formation after the diverging section where the pressure and temperature may vary inside each diamond section of the shock increased velocity to 536 m/s approximately.

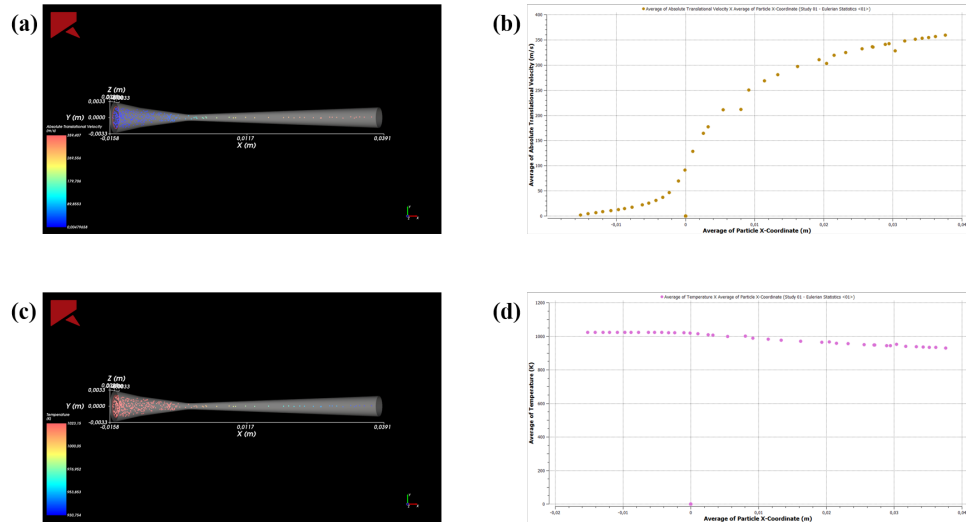


Figure 4.26: Type-1 of 360-degree nozzle without far-field

- **Type – 2:**

Type – 2 simulations are carried out in the hopes of discovering the clogging region that occurs inside the nozzle, which would limit the particle bonding effectiveness to the surface. This effect is observed by simulating a large number of particles inside the nozzle using the same simulation setup as type-1.

- **Gravity:** “0” for all coordinates
- **Material:** Copper
- **Particles:**  $10 \mu\text{m}, 15 \mu\text{m}$
- **Mass flow rate:**  $2.94e^{-6}$
- **No. of particles:** 573871
- **Simulation duration & Frequency:**  $0.5, 1e^{-5}$
- **Average velocity at the diverging section:**  $570 \text{ m/s}$
- **Average temperature at the diverging section:**  $764 \text{ K}$

The simulation results of the type-2 methods are not fully developed. Future studies have to be made to finish this simulation.

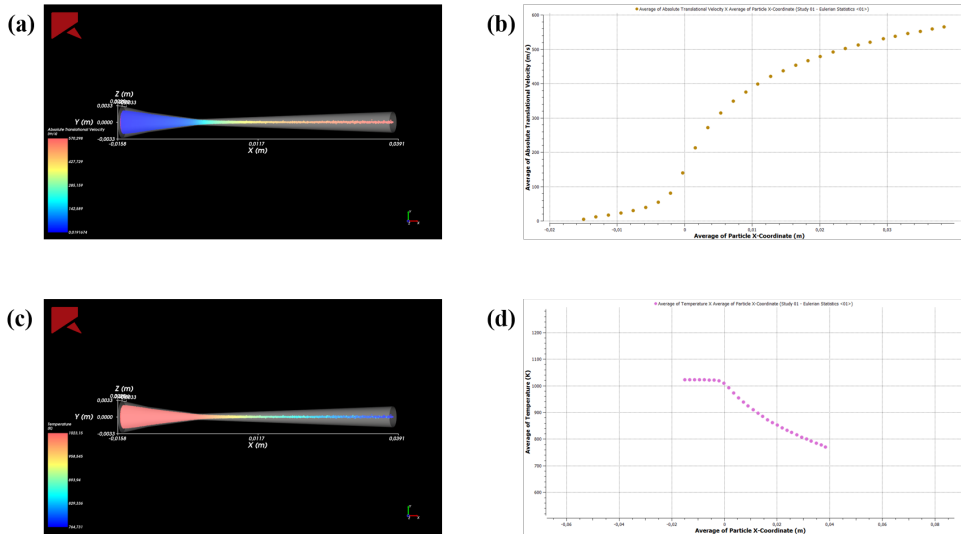


Figure 4.27: Type-2 of 360-degree nozzle without far-field

#### 4.2.3 Final discussion

The solutions in figures 4.19 to 4.27 are based on various simulation methodologies and particle sizes. The whole CFD setup, as well as the particle simulation, is comparable for both geometries. Because of the need to reduce the overall time required to complete the simulation, there are some variances in the mass flow rate. This section is commonly categorized as providing information on selecting the best simulation approach and comparing the outcomes.

- *Choosing the appropriate simulation method*
  - **Gravity** is set to “0” for all coordinates because particles move in the fluid direction without any gravity acting on the particle.
  - **Thermal**, should be enabled if the simulation process consists of heat transfer or if the energy equation is solved from *CFD* simulation.
  - **Material**, copper is chosen as the particle material by applying the copper properties.
  - **Particles**, provided in descending order of their sizes with a cumulative percentage representing their percentage of a particle of each diameter will enter into the simulation.
  - **Mass flow rate**, from the above figures the mass flow rates mentioned for each result, are different from one another, and yet they provide almost similar answers, this is because the mass flow rate of particles is directly influenced by the number of particles and not the simulation results.
  - **Target normal velocity** is more suitable for two-way simulation as they provide an initial velocity for the particles to start the simulation. As in the case of one-way simulation the comparison shows that there is no significant difference in the solution.

- **One-way coupling**, if the thermal model is enabled then a suitable conductive heat transfer law should be chosen. A detailed discussion has been made in section 3.2.2.2.
- **Solver**, from the above graphs and results, each type has its solver parameters, and yet they did not affect the simulation procedure because the solver parameters are useful for providing the total time needed for the simulation, however, the simulation frequency represented above is mainly useful in case of two – way coupling since it uses time marching solution to simulate the problem.

#### 4.2.4 Comparison between the simulation results

To verify that the simulation approach is correct, three primary conditions must be met when comparing simulation results of particle properties: critical velocity, temperature, and deposition window. This section is separated into two sections: 180-degree nozzles with far-field geometry and 360-degree nozzles without far-field geometry.

##### 1. *180-degree with far field*

Particle Properties	Type – 1	Type – 2	Type - 3	KSS (critical values)
Average velocity	536 m/s	799 m/s	537 m/s	328 m/s
Average Temperature	826 K	590 K	826 K	738.15 K

Table 3: Comparison between KSS and Rocky generated solutions

The values shown here are taken from the far end of the far-field, just before the deposition takes place. The simulated values are compared to *KSS* software values, which clearly show that the critical particle velocity recorded by the *KSS* is 328 m/s, and when compared to the simulated values of three types, it is proven that the particles are exceeding the critical velocity, resulting in better bonding to the substrate surface. With a gas inlet pressure of 50 bar and a temperature of 1023.15 K, the critical velocity and temperature specified by the *KSS* are particularly suited for particle sizes in the range of 15  $\mu\text{m}$ , 30  $\mu\text{m}$ , and 45  $\mu\text{m}$ .

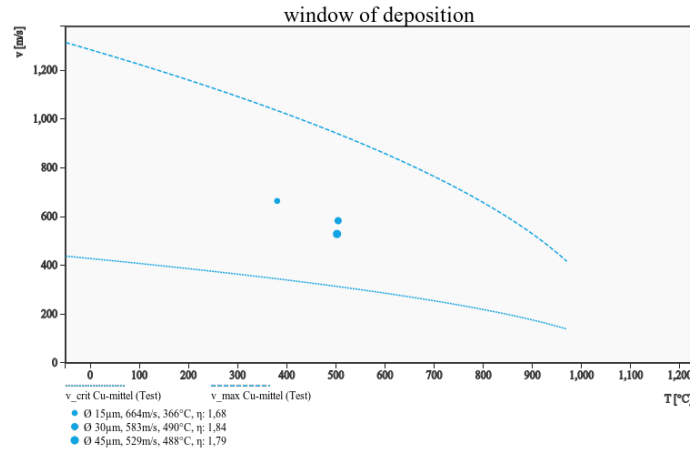


Figure 4.28: Window of deposition by *KSS*

The window of deposition chart from the *KSS* website is shown in Figure 4.28. The critical velocity line is at the bottom, and the erosion line is at the top, with the in-between space representing where the particles tend to deposit. This is referred to as the deposition window. The following are the different particle size values:

- **15  $\mu\text{m}$ :** 664  $\text{m/s}$ , 639.15 K
- **30  $\mu\text{m}$ :** 583  $\text{m/s}$ , 763.15 K
- **45  $\mu\text{m}$ :** 529  $\text{m/s}$ , 761.15 K

These temperature and velocity values represent the properties exactly at the substrate after the deposition. Stoltenhoff et al [3] had made a compressive study of the bonding mechanism that takes place between particles and the substrate. He stated that particles will experience localized heating which will increase the velocity and temperature to an extent at the very point of the particle and substrate. This quick rise in velocity at the particle and substrate surfaces can be used to detect the creation of a jet. This is due to hardening effects at the interface caused by high strains and strain rates. On the other hand, adiabatic heating can cause softening due to significant plastic strain at the interface. At greater velocities, this softening impact might overwhelm the hardening effects, resulting in adiabatic shear instability at the contact. When compared with the velocity and temperature that have been observed from the Rocky simulation:

Particle size	Rocky velocity	KSS velocity	Rocky temperature	KSS temperature
15 $\mu\text{m}$	799 $\text{m/s}$	664 $\text{m/s}$	590 K	639.15 K
30 $\mu\text{m}$	536 $\text{m/s}$	583 $\text{m/s}$	826 K	763.15 K
45 $\mu\text{m}$	536 $\text{m/s}$	529 $\text{m/s}$	826 K	761.15 K

Table 4: Window of deposition comparison

By observing table 4 the temperature of particle size  $30 \mu\text{m}$  and  $45 \mu\text{m}$  has reduced value in the *KSS* temperature, but the temperature of  $15 \mu\text{m}$  has increased compared to the Rocky and this is because of the condition of flattening ratio.

## 2. *360-degree without far-field*

The average velocity and temperature at the diverging section are about  $360 \text{ m/s}$  and  $960 \text{ K}$ . Schmidt et al., [28] experimented to study the particle acceleration at the end of the nozzle, he suggested that increasing the temperature of the gas will result in higher particle impact temperature. Bigger particles tend to have their thermal inertia that will help the particle to maintain the temperature for a better bonding mechanism. This is proved by the 180-degree nozzle and 360-degree nozzle, in which the temperature of the 360-degree nozzle at the diverging section is  $960 \text{ K}$  with the usage of  $45 \mu\text{m}$  size particle, whereas the temperature at the far end of the far-field of the 180-degree nozzle is recorded as  $826 \text{ K}$ . Inspite of traveling of the particles through the shock region, the temperature tends to maintain a higher value before impact.

## 4.3 Scientific answers

This section deals with answering the scientific questions that can be used to understand the whole process of thesis work. Three questions have been displayed in section 1.2

### 1. How does the shock wave produced in the nozzle affect the particle behavior?

Shock waves (or diamond shocks) created in the nozzle are an over-expanded type of wave, and simulation results from section 4.2 show that particles tend to flow linearly, just as shock waves produced outside the nozzle do. From 4.21 to 4.27, this may be seen in the graph. The production of oblique shock at the nozzle's rear exit is the primary cause. In section 4.1, a full study of shock formation was presented.

### 2. Does the particle ever reach critical velocity?

Table 3 shows that the critical velocity of the copper particle was exceeded by particles of various sizes. It's also been proved that after an impact, the particle tends to have a high temperature at the substrate's surface, and that larger particles have higher thermal inertia, which helps them maintain a high temperature during their journey through the nozzle's diverging and far-field sections. In section 4.2.3, the critical velocity has been thoroughly discussed.

### 3. What is the clogging effect and where exactly the clogging will appear in the nozzle and what are the causes and effects?

The clogging effect is a phenomenon that causes particles to stick to the surface of the nozzle wall, lowering the bonding mechanism's efficiency. Wang, X, et al. [29] conducted experiments and reported on the formation of clogging in the throat area of each

nozzle.

The clogging effect will be most noticeable around the throat region at the point where the converging portion meets the throat section, where the area is smallest and the temperature is highest. Figure 4.27 illustrates this point.

The clogging effect in the nozzle can be caused by two factors: particle dispersion and the high temperature of the nozzle wall in the throat region. Particle dispersion refers to the tendency for particles to disperse and collide with one another as well as with the temperature walls, resulting in particles clinging to the surface due to the rising temperature inside the particle. The clogging effect is also caused by particle pre-heating. When operating with the nozzle for an extended period of time, the temperature of the nozzle wall rises dramatically. This can be minimized by installing a cooling system outside the nozzle surface, and it has been demonstrated that the cooling system reduces the inner wall temperature by promoting convective heat transfer.

This temperature rise of the nozzle wall can be seen in figure 4.27, since the usage of maximum number of particles in the simulation, the temperature change near the throat region can be seen clearly. From the figure 4.27 the temperature remains high even when the particle reached half-way through the diverging section of the nozzle. The particle dispersion can also be viewed near the diverging section where some particles tend to move from the line of approach because of their constant collision with other particles and the walls of the nozzle.

- **Purpose of the scientific questions**

The main purpose of any scientific questions formed for a research is to provide a basic idea of the topic that could help to built future contribution for the topic which ultimately help other researchers to use this idea to improve the technology.

These questions provides information for the basis of flow simulation and particle simulation and the simulation setup methods that could bring unique solutions. The future contribution for CS nozzle is to reduce the clogging effect that occurs near the throat region and this report gives a glimpse of the clogging effect in the figure 4.27. This simulation shows that the particle experiences high temperature in the converging and throat section of the nozzle as well as the particle dispersion in the diverging section of nozzle. This can be used as a basis to setup the flow simulation and particle simulation by studying chapter 3 of this report and a two-way simulation can be made by taking the idea of particle temperature and velocity from this report.

For any research work, the final solution is to have a maximum efficiency and the CS nozzle is no stranger to that. Maximum deposition efficiency will be the final solution for CS nozzle and to attain it, the particles need to exceed the critical velocity as well as the particles need to have maximum temperature and velocity inside the nozzle. The

clogging effect, particle-particle and particle-fluid interactions make sure to reduce the velocity and temperature of the particles that leads to poor efficiency.

These questions are linked in a way that once the particle behavior in the shock region is found out, then the particle can exceeds the critical velocity for deposition. The clogging effect happening inside the nozzle will tend to reduce the velocity of neighboring particle by colliding with the other particle, as a result some particles failed to reach its critical velocity and in turn reducing the efficiency of deposition. From this discussion it is clearly confirmed that clogging effect is the reason for reducing the deposition efficiency and a future two-way simulation has to be made with considering a cooling jacket around the nozzle in the interest of reducing the temperature.



## **5 Conclusion**

Comprehensive analyses of the cold spray process were performed with computational methods in the interest of finding the best simulation methods that are suitable for cold spray application as well as the particle simulation that will help in proving the critical velocity of particles which leads to the higher efficiency of bonding between the particles and surface of the substrate. The importance of geometry standards and the computational resources have proven that the solution could attain convergence, and the numerical investigation is compared with the simulation results proves the best way to judge the uniqueness and accuracy of the solution. The simulation setup results of *CFD* use a unique combination of methods that can provide accurate results and the usage of  $K - \omega$  *SST* shows beyond doubt that it is the best turbulence model one can use to study the near-wall region. It is demonstrated that density-based solver, steady-state timeline, and least-squares gradient methods provide a better convergence rate over the solution. The comparison between Ansys Fluent generated results and *KSS* generated results, demonstrates that Fluent generated results with 1 million cells of mesh, provide expected results that are compared with numerical solution exhibit a 0.8% of error which is way below the acceptable value of 5%. The particle simulation on the other hand demonstrated the existence of critical velocity of different sizes of particles and a suitable simulation setup that applies to the cold spray nozzle. It is demonstrated that the comparison made between different types of setup methods, the one without target normal velocity and enabling the thermal mode for one-way coupling provides a suitable solution that exceeds the critical velocity of copper which is the result of a perfect bonding mechanism. The particle movement at the shock region tends to have a linear way of accelerating due to the fact of formation of over expanded shock diamond. This is proven by the velocity of particles that is increased after the diverging section which makes the particles fly at supersonic velocity and adhere to the surface. However, the clogging effect cannot be studied with the one-way coupling as it does not take account of the fluid properties.

### **5.1 Recommendations for future contribution**

Even though the proposed thesis work establishes the presence of critical velocity using the recommended simulation setup, there is one key consequence that many researchers are still unaware of the clogging effect. This study will improve the cold spray application to a higher extent than could be proposed to be used in every industry. A list of recommendations could be followed in future contributions to the simulation.

- Firstly, two-way simulation needs to be done and the fluid properties should be taken into account for simulating with the particle.

- The drag force, lift force, and inter-particle attractions need to be formulated based on the particle and implemented into the simulation.
- Two-way coupling works on transient simulation methods, the needs to be taken with utter care while implementing the time step for each simulation.
- Poly-hedral cells are not supported for Rocky, so the user needs to be careful while choosing the meshing metrics.

These suggestions can be considered when simulating with two-way coupling and a total number of particles; the higher the number of particles, the better the clogging effect inside the cold spray nozzle can be observed.

## References

- [1] AP Alkhimov, VF Kosarev, and SV Klinkov. “The features of cold spray nozzle design”. In: *Journal of thermal spray technology* 10.2 (2001), pp. 375–381.
- [2] John David Anderson and J Wendt. *Computational fluid dynamics*. Vol. 206. Springer, 1995.
- [3] Hamid Assadi et al. “Bonding mechanism in cold gas spraying”. In: *Acta materialia* 51.15 (2003), pp. 4379–4394.
- [4] Gyuyeol Bae et al. “General aspects of interface bonding in kinetic sprayed coatings”. In: *Acta Materialia* 56.17 (2008), pp. 4858–4868.
- [5] Gyuyeol Bae et al. “General aspects of interface bonding in kinetic sprayed coatings”. In: *Acta Materialia* 56.17 (2008), pp. 4858–4868.
- [6] Raman Baidya, Apostolos Pesyridis, and Maxim Cooper. “Ramjet nozzle analysis for transport aircraft configuration for sustained hypersonic flight”. In: *Applied Sciences* 8.4 (2018), p. 574.
- [7] Pasquale Cavaliere, L Cavaliere, and Lekhwani. *Cold-Spray Coatings*. Springer, 2018.
- [8] Yunus A Cengel. *Fluid mechanics*. Tata McGraw-Hill Education, 2010.
- [9] Yunus A Cengel, Michael A Boles, and Mehmet Kanoğlu. *Thermodynamics: an engineering approach*. Vol. 5. McGraw-hill New York, 2011.
- [10] Victor K Champagne et al. “The cold spray materials deposition process: fundamentals and applications”. In: (2007).
- [11] RC Dykhuizen and MF Smith. “Gas dynamic principles of cold spray”. In: *Journal of Thermal spray technology* 7.2 (1998), pp. 205–212.
- [12] ESSS-Rocky. *Rocky-Dem DEM-CFD Coupling Technical Manual*. 2018.
- [13] Ansys Fluent. “12.0 Theory Guide”. In: *Ansys Inc* 5.5 (2009), p. 15.
- [14] Ansys Fluent. “17.0 ANSYS Fluent Meshing User’s Guide”. In: *Canonsburg (PA): ANSYS Inc* (2016).
- [15] Masahiro Fukumoto et al. “Deposition of copper fine particle by cold spray process”. In: *Materials transactions* (2009), pp. 0904200749–0904200749.
- [16] Frank Gärtnner et al. “The cold spray process and its potential for industrial applications”. In: *Journal of Thermal Spray Technology* 15.2 (2006), pp. 223–232.
- [17] Mica Grujicic et al. “Computational analysis of the interfacial bonding between feed-powder particles and the substrate in the cold-gas dynamic-spray process”. In: *Applied Surface Science* 219.3-4 (2003), pp. 211–227.

- [18] Nancy Hall. “Mach Number”. In: *NASA GRC, May* (2015).
- [19] Tien-Chien Jen et al. “Numerical investigations on cold gas dynamic spray process with nano-and microsize particles”. In: *International journal of heat and mass transfer* 48.21-22 (2005), pp. 4384–4396.
- [20] Tien-Chien Jen et al. “Numerical investigations on cold gas dynamic spray process with nano-and microsize particles”. In: *International journal of heat and mass transfer* 48.21-22 (2005), pp. 4384–4396.
- [21] Irina Kharlamova, Alexander Kharlamov, and Pavel Vlasák. “MODEL OF AVERAGED TURBULENT FLOW AROUND CYLINDRICAL COLUMN FOR SIMULATION OF THE SALTATION”. In: *Engineering MECHANICS* 21.2 (2014), pp. 103–110.
- [22] Santosh Kumar et al. “The role of thermal spray coating to combat hot corrosion of boiler tubes: a study”. In: *J Xidian Univ* 14.5 (2020), pp. 229–239.
- [23] Chang-Jiu Li and Wen-Ya Li. “Deposition characteristics of titanium coating in cold spraying”. In: *Surface and Coatings Technology* 167.2-3 (2003), pp. 278–283.
- [24] Roman Gr Maev and Wolf Leshchinsky. *Introduction to low pressure gas dynamic spray: physics and technology*. John Wiley & Sons, 2009.
- [25] RC McCune et al. *An exploration of the cold gas-dynamic spray method for several materials systems*. Tech. rep. ASM International, Materials Park, OH (United States), 1995.
- [26] ESSS Rocky. “Rocky DEM technical manual”. In: (2018).
- [27] H Schlichting et al. “Boundary layer theory springer”. In: *Eighth Revised and Enlarged Edition* (2000).
- [28] Tobias Schmidt et al. “From particle acceleration to impact and bonding in cold spraying”. In: *Journal of thermal spray technology* 18.5 (2009), pp. 794–808.
- [29] Xudong Wang et al. “Investigation on the clogging behavior and additional wall cooling for the axial-injection cold spray nozzle”. In: *Journal of Thermal Spray Technology* 24.4 (2015), pp. 696–701.
- [30] Victor Yakhut and Steven A Orszag. “Renormalization group analysis of turbulence. I. Basic theory”. In: *Journal of scientific computing* 1.1 (1986), pp. 3–51.